SIEMENS

MAGNETOM Flash

The Magazine of MRI

Issue Number 1/2016 | SCMR Edition

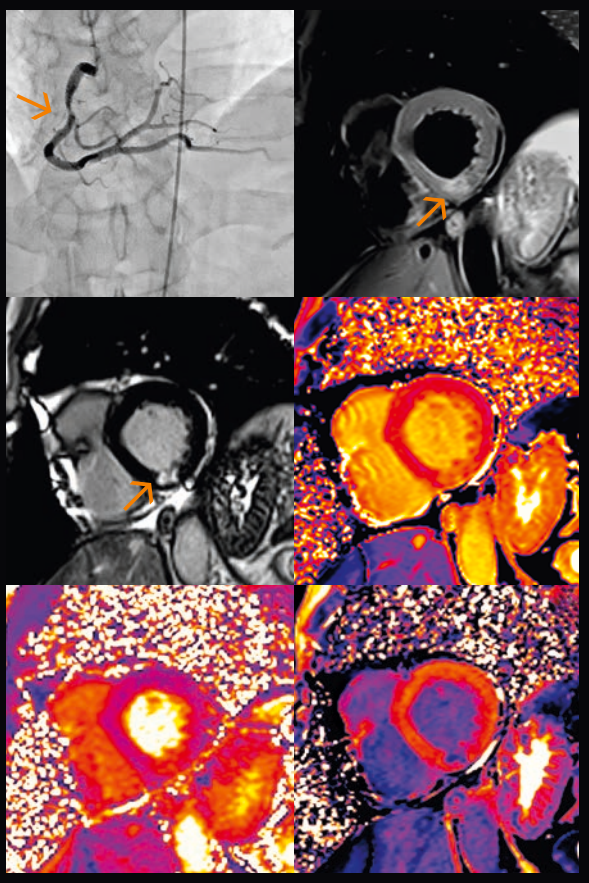

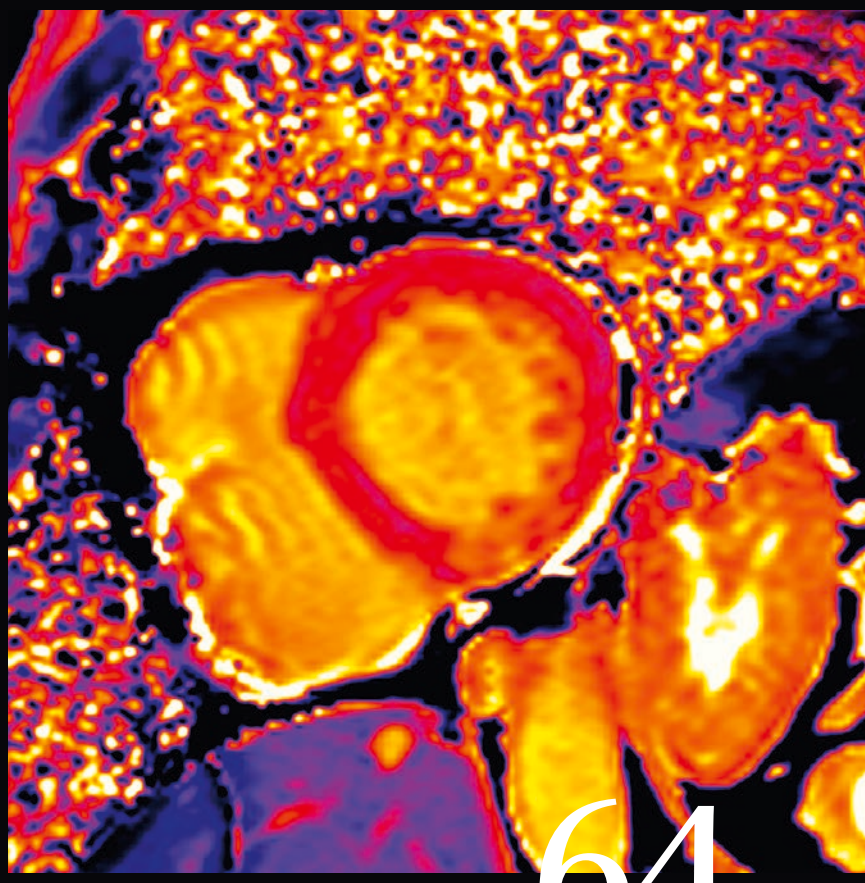

64

Editorial Comment
Eike Nagel
Page 2

CMR Teaching Network
Jeanette Schulz-Menger
Page 8

Cardiac Diffusion Tensor MRI Using SMS Acquisition
Choukri Mekkaoui et al.
Page 38

***syngo*.MR Cardiac 4D Ventricular Function**
Bernd Wintersperger
Page 57

Professor Eike Nagel, M.D., Ph.D. is a world-recognized opinion leader in cardiac imaging. For more than 25 years he has been using cardiovascular magnetic resonance imaging to diagnose problems of the heart or the vessels non-invasively. Professor Nagel has recently been appointed as Chair of Cardiovascular Imaging at the Goethe University Frankfurt, Germany, where he leads a new Cardiovascular Imaging Center equipped with magnetic resonance imaging and computed tomography. He focuses on the translation of new diagnostic tools into clinical routine particularly in the areas of coronary artery disease, cardiomyopathy and heart failure.

The Future of Cardiovascular Magnetic Resonance

This issue of MAGNETOM Flash highlights several developments and advances in the field of cardiovascular magnetic resonance imaging (CMR). They demonstrate the continuing development of this fascinating technique, which looks set to continue. A few general trends can be observed:

Quantification

CMR is becoming fully quantitative, as evidenced by the rapid development of mapping techniques quantifying T1 and T2 relaxation and allowing calculating extracellular volume. Several cases demonstrating its clinical value are shown in this issue. This development is a revolution in CMR imaging as we move away from black, white and grey values, visual assessment and contrast differences to fully quantifiable data approximating to physiology. While the development of these technologies is ongoing, we can already appreciate their value in the detection of early changes [1], assessment of underlying pathophysiology rather than its consequences [2] or quantification of alterations in absolute terms [3, 4]. Novel data also demonstrates that these quantifiable measures are superior to classic markers such as volumes, ejection fraction and even late gadolinium enhancement in predicting cardiovascular events in patients with, for example, non-ischemic cardiomyopathies [5] or informing on the acuity of inflammation (myocarditis) [6]. Similar changes are imminent in perfusion analysis and flow imaging.

Speed

Today's CMR is fast and continues to accelerate. The increase in speed is due to two changes. Firstly, with increasing capabilities of navigator sequences data acquisition has become less dependent on breath holding. Navigator sequences used to be slow, unpredictable and frequently of low quality. This was mainly due to the imperfect estimation of cardiac displacement based on measurements of the right hemidiaphragm and – as a result of the suboptimal correction of breathing motion – the rejection of a large proportion of the data acquired. Novel image navigators use the true position of the heart, yielding a much better correction for cardiac displacement during breathing allowing to increase scan efficiency to nearly 100% [7]. This efficiency may make navigator sequences faster and more patient friendly than breath holding for routine scanning in the very near future.

Secondly, the amount of redundant data acquisition is reduced. Changes such as parallel imaging have altered cardiac imaging strategies dramatically, as they allow a majority of acquisitions to be performed within a single breath hold rather than requiring long scans averaged over multiple breathing cycles. Compressed sensing now allows squeezing 3D volumes into a single breath hold or a short navigator scan, finally making CMR a truly 3D (or 4D) method.

New applications

Novel abilities continue to emerge. This is partially a consequence of an increase in speed and the development of novel sequences. The greater speed allows transferring imaging methods to the heart, which were previously reserved for non-moving structures. An example is diffusion tensor imaging, which has been successfully used in the brain and other structures and starts to emerge as a cardiac option [8]. Novel sequences utilize contrast better than previous

Previously Professor Nagel was Chair of Clinical Cardiovascular Imaging, Head of the Department of Cardiovascular Imaging and Deputy Head of the Division of Imaging Sciences and Medical Engineering at King's College London as well as Honorary Consultant Cardiologist at Guy's and St. Thomas' Trust, London, UK. He has developed and tested new methods for improved diagnoses and has developed stress tests for magnetic resonance imaging, which are now in use worldwide. He holds several patents on imaging methods, and has authored more than 250 publications and 25 book chapters. Professor Nagel is known worldwide for his teaching abilities.

methods, as highlighted by the articles on QISS MRA, which generates unprecedented contrast in non CE MRA [9]. I am sure that coronary MRA will also challenge CTA in the next few years.

CMR in 2030

The trends described above are only a small proportion of the opportunities that will open up to us in the near future. Our approach to imaging will change drastically. Whilst an accurate prediction of the future is almost impossible, I'd like to present my vision of CMR in 2030. A glance back 15 years will remind us of the speed of change. In 2000, the newly-launched iMac boasted a quarter of RAM, a CPU with half the speed and about the same display matrix as a 2010 iPhone. And at about the same time in CMR we were replacing Turbo Gradient Echo with SSFP, testing the first perfusion sequences (with a single shared prepulse) and using large external optical disks to store the data. So, how do I think the next 15 years may pan out?

In my vision, diagnostic tools will have immediate public access. Medical care will be much less confined to hospitals or require doctors. People will be able to scan their hearts (function, structure, blood flow, synchrony, coronary arteries, contractility, cardiac efficiency, cell size) in public diagnostic centres without referral. They will be checked for contraindications by an artificial intelligence (AI) robot. Additional modules can be added based on the findings. The data will be automatically analysed and compared to a large database of age-gender-ethnicity-height-weight-matched controls, people with similar co-morbidities as well as the person's own previous scans. The results will be available immediately and if any therapy is needed a further meeting with an AI robot will assess possible contraindications and co-morbidities. The person will then be issued with the ingredients for his home-based pill-printer: a software update will provide the correct medication on a daily basis. Some patients will still need to see a doctor, as the AI robot has not yet been FDA cleared for certain diseases where information remains insufficient for adequate algorithms.

Of course, all therapy will require accurate, quantifiable and reproducible diagnostics before approval by health insurers. Continuation of therapy will be only reimbursed if a therapeutic effect can be demonstrated by imaging. As an example, a quantitative analysis of myocardial ischemia will be required before any anti-anginal therapy or even revascularization is approved. Interventionalists will be required to follow the imaging guidance. More expensive drugs will only be reimbursed if shown to be effective in the specific patient.

Trials will require full phenotypisation of participants before, during, and at the end of the study. Endpoints will increasingly be based on the underlying pathophysiology rather than symptoms, outcomes or consequences of disease.

These are just some examples of what may lie ahead. Does CMR have a role here? It's hard to tell, but to remain at the heart of developments in 15 years' time we need to pursue the following five strategies.

Firstly, we must continue the drive for speed. Speed reduces costs, provides access, generates large numbers and creates the convenience required for success.

Institute for Experimental and Translational Cardiovascular Imaging, DZHK Centre for Cardiovascular Imaging, University Hospital Frankfurt, Germany (Goethe CVI)

This new institute will provide a platform for interdisciplinary multimodality cardiovascular research. The institute is equipped with a state-of-the-art 3T MAGNETOM Skyra MR and a SOMATOM Force CT exclusively for cardiovascular research. It is situated on the campus of the University Hospital within the European Cardiovascular Science Centre, which also houses several excellent groups in basic cardiovascular science. The Institute is embedded in and supported by the German Centre for Cardiovascular Research (DZHK), a cluster of 28 members with outstanding cardiovascular research capacities.

Strong connections with the clinical partners in the university hospital namely Prof. Dr. Andreas Zeiher (Cardiology, Angiology, Nephrology) and Prof. Thomas Vogl (Interventional and Diagnostic Radiology) provide access to patients, practical know-how, clinical equipment and support.

Secondly, we must become fully quantitative. This may not require everything to be measured in signal intensity units, but it does require everything to be measured in units that are reproducible, have normal ranges with small standard deviations and relate to the severity and extent of the abnormality. Quantification enables comparability, follow-up, assessment of therapeutic needs and success and replaces the human eye with all its limitations by a reliable system. This will require standardization, reduction of freedom in parameters and massive improvement in postprocessing software.

Thirdly, we must strive for evidence-led approaches and overcome the battles of turf and power for access and reimbursement. We need to bring highly qualified teams together to push the borders of technology and knowledge. Failing this, other techniques, markers or groups will provide the services that we could lead on.

Fourthly, we must share knowledge and empower the next generation [10]. Our strength will depend on our ability to provide rapid services to large populations.

Lastly, we must not think in silos. I believe that CMR has all the advantages required to be a core modality in the type of diagnostic center I have described above (no ionizing radiation, 3D coverage, high spatial and temporal resolution, excellent soft tissue contrast, endless possibilities). However, there are other techniques and blood markers that may provide similar information. We should embrace these techniques to allow for true comparison of their relative values, strengths and weaknesses, and also to remain at the forefront of this knowledge. We need to ensure that we are the ones to train the AI robots, not the other way round.

Our goal remains to reduce the burden of cardiovascular disease. I believe that advanced imaging can play a major role in this goal. Together, we will be strong enough to make sure the therapies of the future (cardiac regeneration, cardiac rejuvenation, printable electronic membranes) will be based on diagnostic imaging before, during and after therapy, thus ensuring maximal benefit for our patients while remaining within the given financial framework.

I wish you an exciting and inspiring SCMR 2016.

With best regards

References

1 Case Report: Detection of Myocardial Changes in a Patient Undergoing Chemotherapy, Steve W. Leung, et al., University of Kentucky Medical Center, Lexington, KY, USA [in this issue].

2 Case Report: Myocardial Fibrosis in a Non-Ischemic Cardiomyopathy, Jeremy D. Collins, et al., Feinberg School of Medicine, Northwestern University, Chicago, IL, USA [in this issue].

3 Case Report: Clinical Usability of MyoMaps in Myocardial Infarction, Masashi Nakamura, Saiseikai Matsuyama Hospital, Matsuyama, Ehime, Japan [in this issue].

4 Case Report: Acute Myocardial Syndrome in a 37-Year-Old Patient with Severe Renal Impairment, Anna S. Herrey, et al., The Barts Heart Centre, London, UK [in this issue].

5 Puntmann et al., JACC Cardiovascular Imaging 2016, in press.

6 Hinojar R, Foote L, Arroyo Ucar E, Jackson T, Jabbour A, Yu C-Y, et al. Native T1 in discrimination of acute and convalescent stages in patients with clinical diagnosis of myocarditis: a proposed diagnostic algorithm using CMR. JACC Cardiovasc Imaging. 2015 Jan;8(1):37–46.

7 Self-Navigated Free-Breathing High-Resolution 3D Cardiac Imaging: A New Sequence for Assessing Cardiovascular Congenital Malformations, Pierre Monney, M.D. Division of Cardiology and Cardiac MR Center, University Hospital of Lausanne (CHUV), Lausanne, Switzerland [in this issue].

8 Cardiac Diffusion Tensor MRI Using SMS Acquisition with a Blipped-CAIPIRINHA Readout, Choukri Mekkaoui, et al., Massachusetts General Hospital, Harvard Medical School, Boston, MA, USA [in this issue].

Prof. Nagel also leads the new Clinical Interdisciplinary Cardiovascular Imaging Service provided by the Institute of Interventional and Diagnostic Radiology and the Clinic for Cardiology, Angiology and Nephrology. This interdisciplinary service allows for rapid translation of research findings into clinical routine and the transfer of clinical questions into research, and also provides a platform for truly interdisciplinary clinical training and service.

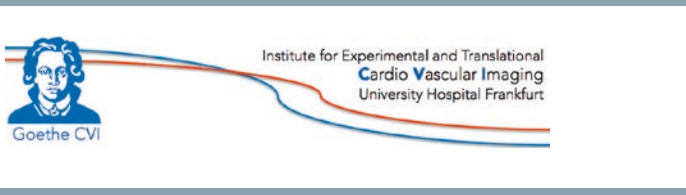

9 – Quiescent Interval Single-Shot (QISS) Lower Extremity MRA for the Diagnosis of Peripheral Artery Disease: Case Presentations, Akos Varga-Szemes, et al., Medical University of South Carolina, Charleston, SC, USA.
– Case Report: QISS MRA at 3T, Anna-Maria Lydon, et al., University of Auckland, New Zealand
[both in this issue].

10 Cardiovascular Magnetic Resonance Teaching Network. Requirements for Simplified Distribution and Sustained Quality, Jeanette Schulz-Menger, et al., Charité Medical Faculty and HELIOS Clinic Berlin-Buch, Germany
[in this issue].

Content

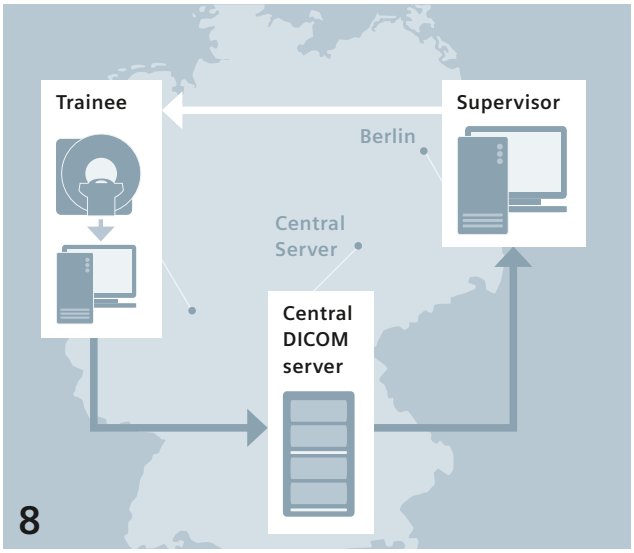

CMR Teaching Network

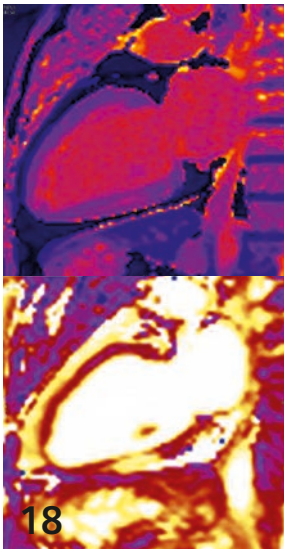

Non-contrast tissue characterization with T1 and T2 mapping

Learn from the experience of other MAGNETOM users

The MAGNETOM World is the community of Siemens MR users worldwide, providing you with relevant clinical information. Here you will find application tips and protocols to optimize your daily work. Lectures and presentations from experts in the field will allow you to be exposed to new ideas and alternative clinical approaches.

Put the advantages of the MAGNETOM World to work for you!

www.siemens.com/magnetom-world

2 The Future of Cardiovascular Magnetic Resonance
Eike Nagel, DZHK Centre for Cardiovascular Imaging, University Hospital Frankfurt/Main, Germany

8 Cardiovascular Magnetic Resonance Teaching Network. Requirements for Simplified Distribution and Sustained Quality
Jeanette Schulz-Menger, et al., Charité Medical Faculty and HELIOS Clinic Berlin-Buch, Germany

18 Case Report: Acute Myocardial Syndrome in a 37-Year-Old Patient with Severe Renal Impairment
Anna S. Herrey, et al., The Barts Heart Centre, London, UK

20 Case Report: Detection of Myocardial Changes in a Patient Undergoing Chemotherapy
Steve W. Leung, et al., University of Kentucky Medical Center, Lexington, KY, USA

22 Case Report: Myocardial Fibrosis in a Non-Ischemic Cardiomyopathy
Jeremy D. Collins, et al., Feinberg School of Medicine, Northwestern University, Chicago, IL, USA

26 Case Report: Clinical Usability of MyoMaps in Myocardial Infarction
Masashi Nakamura, Saiseikai Matsuyama Hospital, Matsuyama, Ehime, Japan

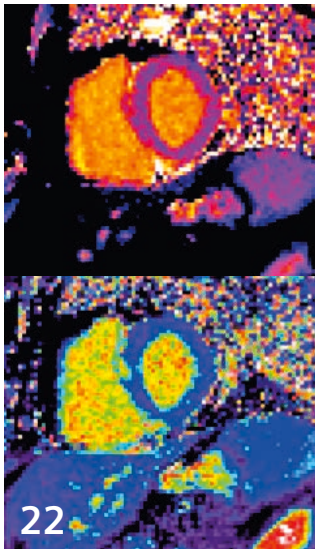

Myocardial Fibrosis in a Non-Ischemic Cardiomyopathy

QISS lower extremity MRA

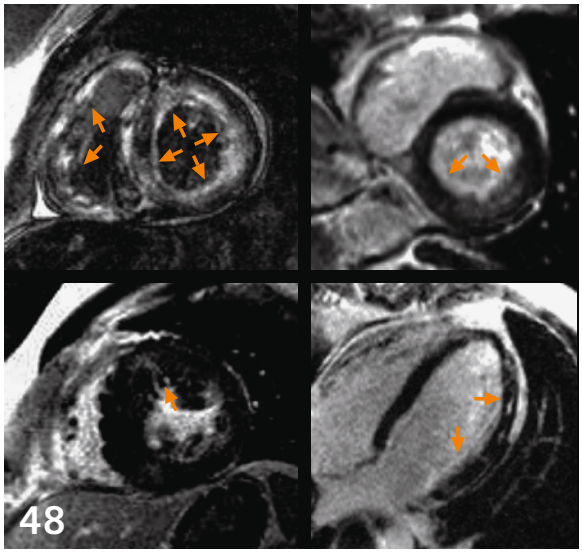

Delayed Enhanced Cardiac MRI in the Assessment of Cardiomyopathies

30 Quiescent Interval Single-Shot (QISS) Lower Extremity MRA for the Diagnosis of Peripheral Artery Disease: Case Presentations
Akos Varga-Szemes, et al., Medical University of South Carolina, Charleston, SC, USA

36 Case Report: QISS MRA at 3T
Anna-Maria Lydon, et al., University of Auckland, New Zealand

38 Cardiac Diffusion Tensor MRI Using SMS Acquisition with a Blipped-CAIPIRINHA Readout
Choukri Mekkaoui, et al., Massachusetts General Hospital, Harvard Medical School, Boston, MA, USA

41 Self-Navigated Free-Breathing High-Resolution 3D Cardiac Imaging: A New Sequence for Assessing Cardiovascular Congenital Malformations
Juerg Schwitter, et al., University Hospital of Lausanne (CHUV), Lausanne, Switzerland

48 Utility of Delayed Enhanced Cardiac MRI in the Assessment of Cardiomyopathies
Dipan J. Shah, et al., Houston Methodist Hospital, Houston, TX, USA

52 **How-I-do-it:** Reconstructing synthetic MOLLI and PSIR images
Magalie Viallon, et al., Université de Lyon, France

57 *syngo*.MR Cardiac 4D Ventricular Function
Bernd J. Wintersperger, et al., University Health Network, University of Toronto, Canada

Cardiovascular Magnetic Resonance Teaching Network

Requirements for Simplified Distribution and Sustained Quality

Fabian Muehlberg, M.D.; Edyta Blaszczyk, M.D.; Jeanette Schulz-Menger, M.D.

Working Group Cardiac MRI, Experimental and Clinical Research Center, a joint cooperation between the Charité Medical Faculty and the Max-Delbrück Center for Molecular Medicine und HELIOS Clinic Berlin-Buch, Department of Cardiology and Nephrology, Berlin, Germany

Background

Cardiovascular Magnetic Resonance (CMR) is an accepted method for various clinical indications, i.e. assessment of coronary artery disease (CAD), cardiomyopathies, inflammatory disease as well as valvular disorders [1-3]. Particularly its unique capability to detect and differentiate myocardial injury helps to establish a new understanding of diseases. For over 10 years CMR has been used for therapy guiding in different indications such as revascularization therapy in CAD or chelate therapy in iron overload [4, 5]. The latter has also influenced patient outcome significantly. Whilst CMR plays an important role in a growing number of guidelines and position papers, its use in daily clinical routine should be accelerated. There are several obstacles hampering wide distribution of CMR. It once had the reputation of being difficult and time consuming. However, modern techniques allow faster and more robust scans. There is no doubt that training as well as dedicated teaching is needed, similar to any other specialized methods [6, 7]. In our opinion referring doctors as well as CMR performing doctors need to be educated in the effective use of CMR in clinical routine.

Recently, we published a paper introducing a novel teaching approach allowing time-effective teaching as well as an ongoing quality control [8]. Our aim is to enable CMR in all settings – hospitals of different sizes as well as in outpatient departments. CMR should be offered not only in a dedicated, stand-alone setting but also as part of a routine MR facility covering extra-cardiac indications. In this article, we aim to explain more details of the published approach and highlight the opportunity of remote scanning.

Spectrum of CMR indications

CMR is integrated in the work-up of different diseases as published regularly. Our teaching program includes all current clinical indications and can state that this goal is achievable with high quality standards even in small hospitals. In this chapter we give an overview of the main CMR requests in adult cardiology. We assume that the same setting is also applicable in congenital heart disease (CHD), but usually patients with CHD should be referred to dedicated centers. Table 1 illustrates the main indications including average scan time in a routine setting. The broad number of indications beyond the capability of other imaging modalities has led to the growing interest in CMR and the consecutive interest in time-effective teaching opportunity.

Assessment of coronary artery disease is a major indication for CMR. Stress testing (Fig. 1) and assessment of viability (Fig. 2) cover up to 40% of referrals as shown in different registries [9, 10]. CMR is leading us to new insights as depicted in the case with a chronic myocardial infarction and fatty degeneration, which is also known from autopsy studies. The current clinical impact is not systematically evaluated, as the differentiation applying fat/water separated images is currently not given at all scanners [11]. Another unique capability of CMR is the identification of microvascular obstruction (MVO) in acute myocardial infarction (Fig. 3). MVO is accepted as

Table 1

Indication	Average scan time in minutes
Left and right ventricular function	3-10
Adenosine perfusion	20-40
Viability assessment	20
Inflammatory disease	30
Cardiomyopathies	20-40
Valvular disorders	10-30 (depending on need for contrast-media)
Masses	10-60
Iron overload	10
Angiography	10

Routine CMR indications and average scan time.

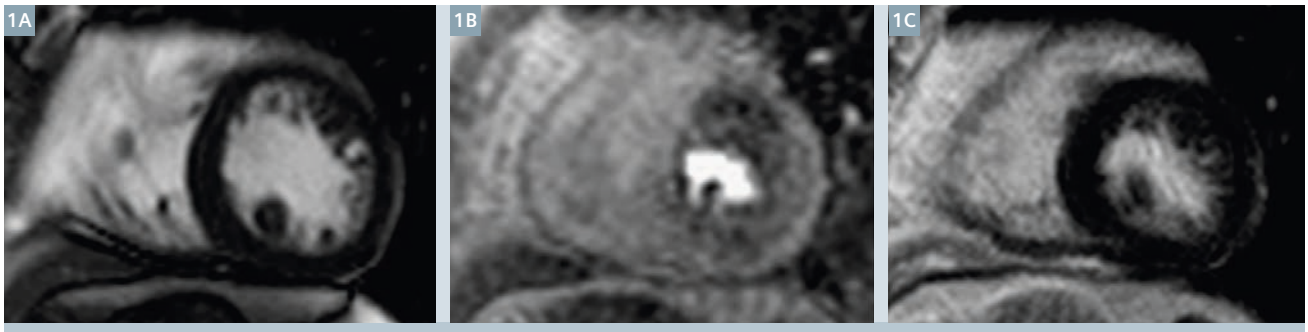

1 76-year-old woman with atypical chest pain and preserved left ventricular ejection fraction (LVEF 75%). CMR with adenosine stress perfusion. Midventricular short axis view shows: **(1A)** SSFP cine short axis in end-diastole, **(1B)** adenosine stress perfusion with predominantly anterior and inferior perfusion defect and **(1C)** fibrosis imaging with late gadolinium enhancement (LGE) with no evidence for myocardial scar.

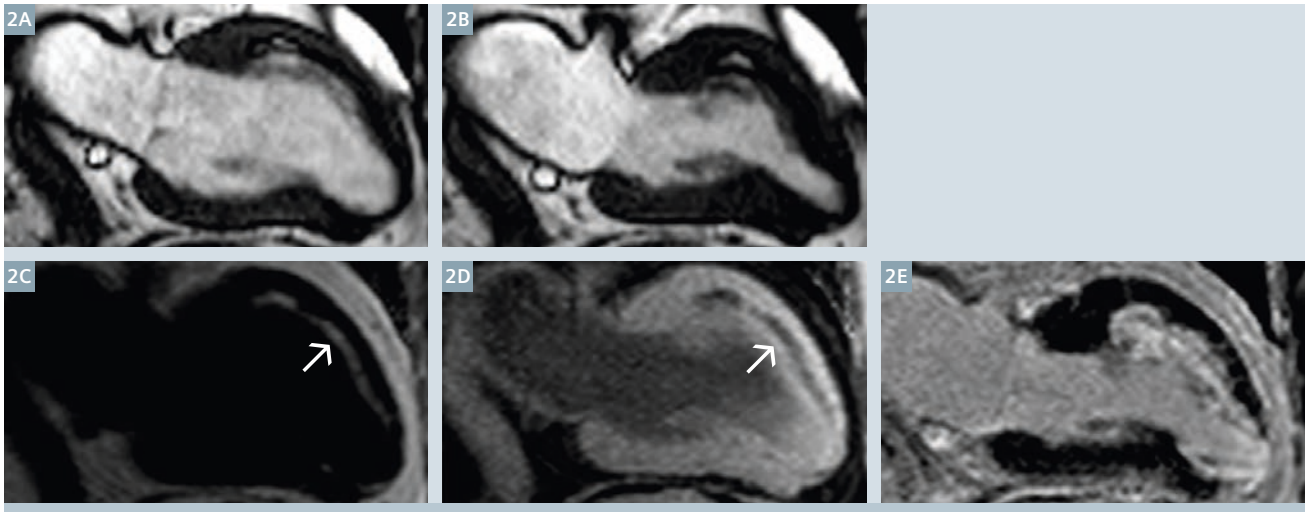

2 71-year-old patient with chronic myocardial infarction and slightly reduced LV function (LVEF 50%). All images are given in a two-chamber view. SSFP cine imaging in **(2A)** end-diastole and **(2B)** end-systole showing the anterior hypokinesia and the apical dyskinesia. Fat/water imaging showing fatty replacement (arrow) of the anterior wall (bright in **2C** and dark signal in **2D**) [9]. **(2E)** Fibrosis imaging (LGE) showing a bright signal – indicating scar and fatty replacement. The combination of scar imaging and fat imaging allows the differentiation of tissue composition. This chronic myocardial infarction shows fatty degeneration of the scar.

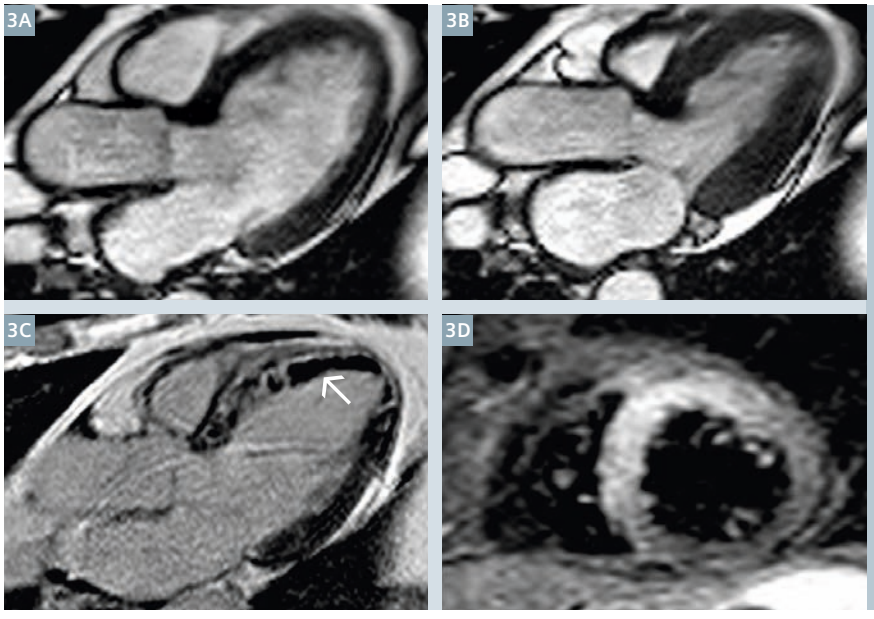

3 56-year-old man with an acute anterior myocardial infarction and preserved ejection fraction (LVEF 54%). Main information are given in a three-chamber view. **(3A)** SSFP cine imaging in diastole and **(3B)** in systole showing mild anterior hypokinesia. **(3C)** Fibrosis imaging (LGE) showing large area of micro-vascular obstruction (dark signal, arrow), surrounded by bright signal indicating fibrosis. **(3D)** Edema imaging (T2-weighted, short axis view) indicating corresponding anterior edema.

being relevant to prognosis even despite impairment of the left ventricular ejection fraction [12].

Furthermore, CMR is uniquely capable of assessing inflammatory reaction including differentiation of reversible injury (Fig. 4). This is also a part of other clinical recommendations, including the assessment of different pathological mechanisms such as edema, hyperemia and fibrosis [11]. Parametric mapping techniques are adding further information and we assume that they will even replace some of current conventional techniques [14, 15].

Interestingly, recent AHA-guidelines for eligibility and disqualification of athletes highlighted the role of CMR for assessment of myocarditis as well as its role in other cardiomyopathies [16]. Differentiation of cardiomyopathies including inflammatory disease is a major indication for CMR, often stated to be 40% of all patients [9, 10].

Diseases with left ventricular hypertrophy (LVH) are playing a major role in cardiology, as i.e. arterial hypertension is often characterized by increased wall thickness. The differentiation of the underlying injury in LVH has changed the daily clinical work-up in several centers. Differentiation of tissue composition can be performed based on quantitative mapping techniques. These novel parametric techniques allow the detection of fatty infiltration, as described in Fabry's disease as well as in amyloidosis (Fig. 5) [17]. Hypertrophic cardiomyopathy has a major impact for the patient due to its sensible risk profile for sudden cardiac death. CMR is well established for phenotyping and adding information about patient's risk (Fig. 6). A worldwide NIH-sponsored study is ongoing to evaluate the impact of different risk-markers or its combination. This also includes several CMR biomarkers such as fibrosis imaging [18].

Staging of valvular disease is often a challenge in cardiology. Routinely, transthoracic echocardiography is used, but it may fail due to impaired ultrasound conditions. In these cases CMR can be applied for assessment.

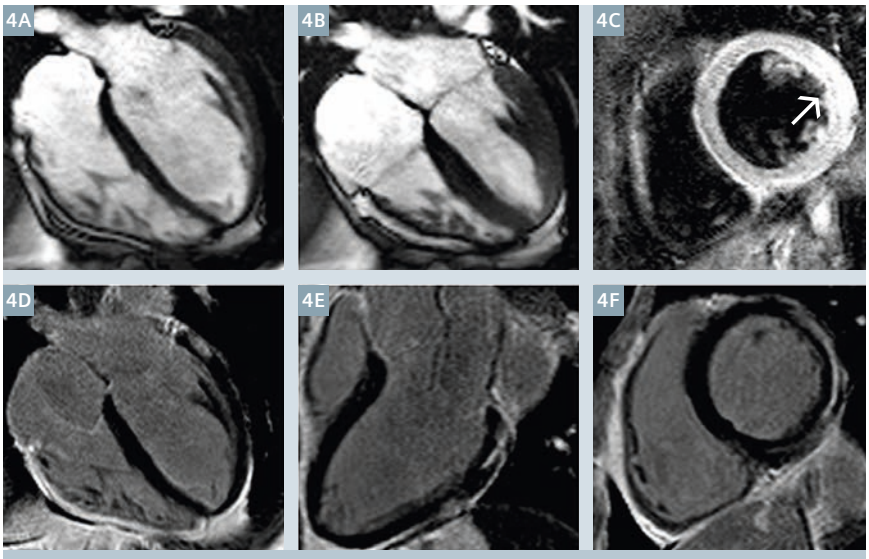

4 34-year-old man with acute myocarditis and preserved LV-function (LVEF 55%). SSFP cine in four-chamber view in end-diastole **(4A)** and end-systole **(4B)** with no wall motion abnormality. **(4C)** Edema imaging (T2-weighted, short axis view) showing large area of edema (arrow). Fibrosis imaging with LGE with typical pattern for acute myocarditis: **(4D)** Four-chamber view, lateral-basal subepicardial LGE, **(4E)** three-chamber view, inferolateral–basal LGE, and **(4F)** short axis view with subepicardial inferolateral and lateral LGE.

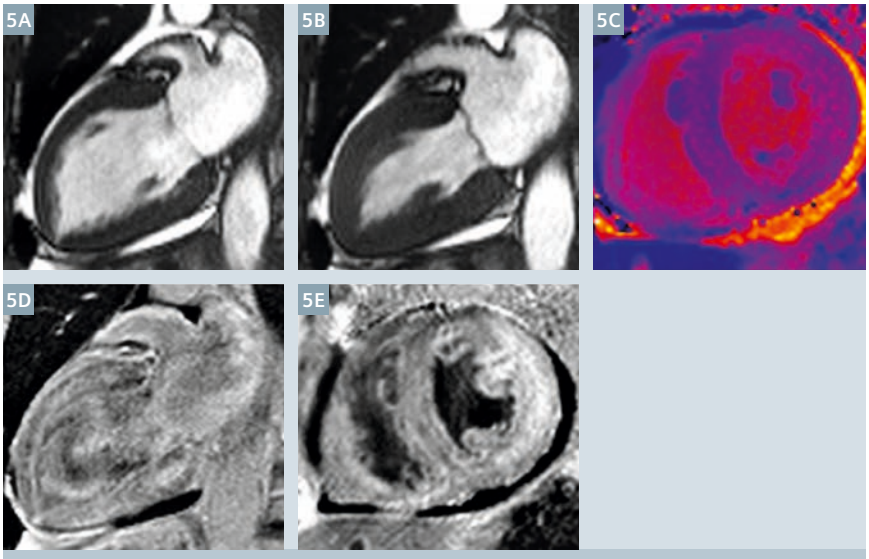

5 75-year-old patient with amyloidosis with preserved LV function (LVEF 52%) and marked left ventricular hypertrophy. SSFP-cine in two-chamber view in end-diastole **(5A)** and end-systole **(5B)**. Minimal pericardial effusion. **(5C)** T1-mapping (midventricuar short axis) max. T1 1186 ms. LGE-imaging in two-chamber view **(5D)** and short axis view **(5E)** showing unusual enhancement with an inhomogenous pattern of myocardium. This finding is pathognomonic for amyloidosis.

Furthermore CMR can be utilized to avoid transesophageal echocardiography e.g. in aortic stenosis (Fig. 7), which is published for the quantification of native valves as well as bioprothesis [19, 20]. Quantification of regurgitation (Fig. 8) as well as application of phase-contrast measurements for shunt quantification are established as well. The diagnostic work-up of valvular disease especially aortic stenosis should also include an angiography, as concomitant abnormalities of the large thoracic arteries

6 30-year-old patient with hypertrophic cardiomyopathy, preserved LV function (LVEF 62%) and asymmetric hypertrophy of the septal wall. Furthermore the papillary muscles are hypertrophied and their insertion is atypically located in the apical region. SSFP cine imaging in the four-chamber end-diastolic view **(6A)** shows a maximal wall thickness of 26 mm, end-systolic view **(6B)**. **(6C)** exemplary post-contrast SSFP cine short axis view with already depicted signs of fibrosis in the inferior insertion point of the right ventricle. Fibrosis imaging (LGE) in a four-chamber view **(6D)** showing intramyocardial fibrosis in the septal wall and basal lateral (arrow). Fibrosis imaging (LGE) in a short axis view **(6E)** showing fibrosis in the inferior insertion point of the right ventricle and less intensive anterior (arrow).

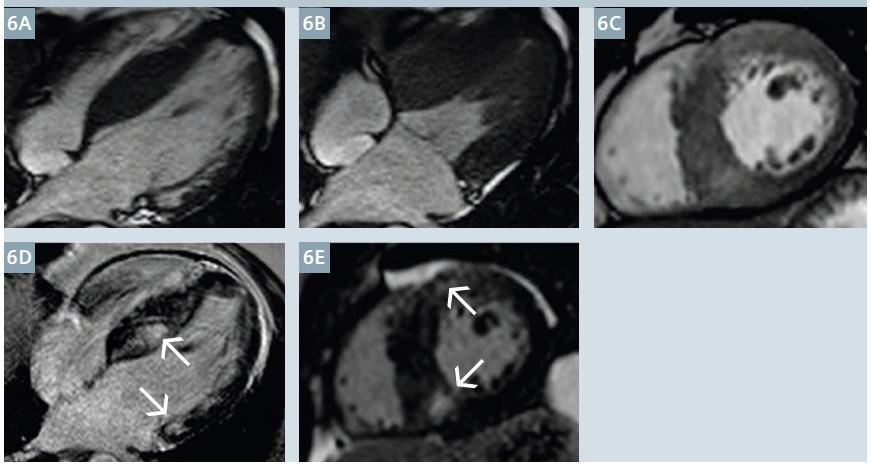

7 56-year-old patient with aortic stenosis based on a congenital bicuspid valve. **(7A)** SSFP cine in diastole: bicuspid aortic valve between LCC and RCC-type 1LR. **(7B)** SSFP cine in systole: valve area 1.2 cm² (opening index 0.6 cm²/m²). **(7C)** Contrast-enhanced 3D angiography showing of the aorta thoracalis with normal diameters.

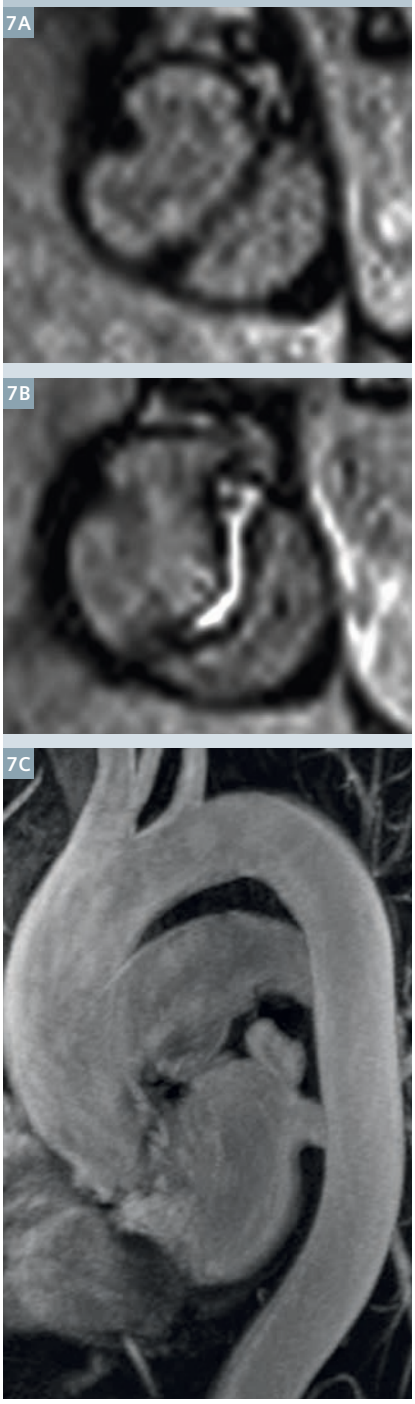

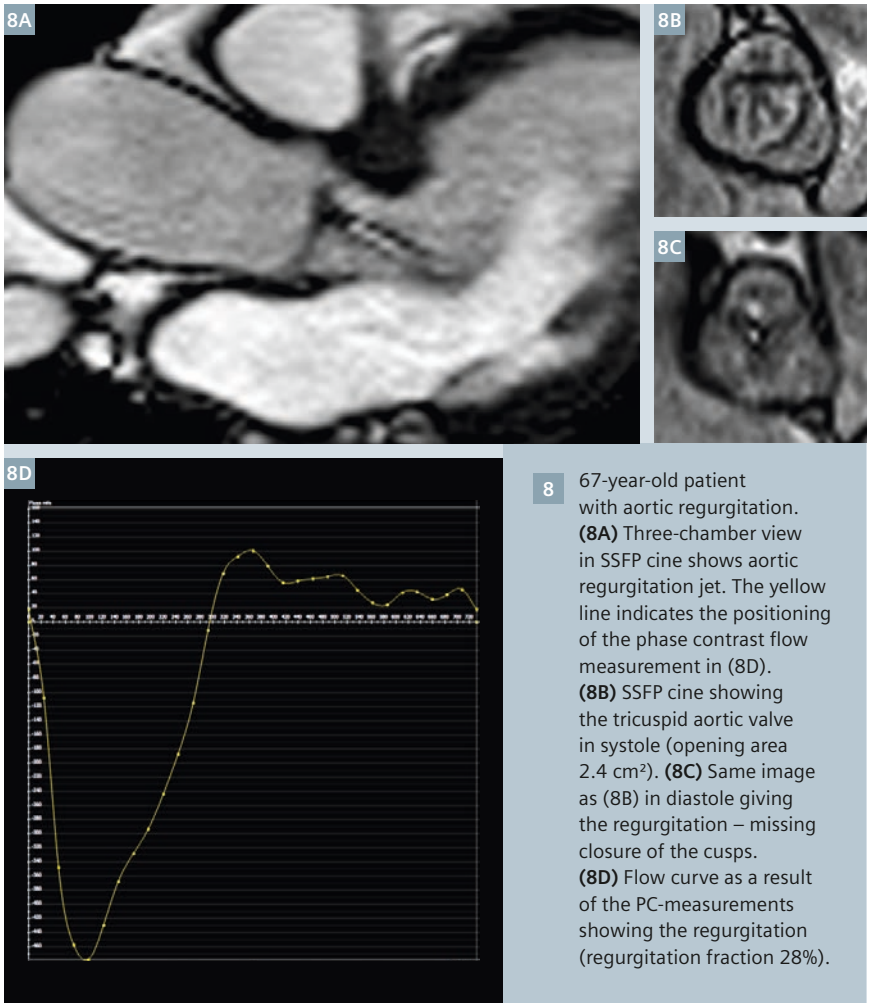

8 67-year-old patient with aortic regurgitation. **(8A)** Three-chamber view in SSFP cine shows aortic regurgitation jet. The yellow line indicates the positioning of the phase contrast flow measurement in (8D). **(8B)** SSFP cine showing the tricuspid aortic valve in systole (opening area 2.4 cm²). **(8C)** Same image as (8B) in diastole giving the regurgitation – missing closure of the cusps. **(8D)** Flow curve as a result of the PC-measurements showing the regurgitation (regurgitation fraction 28%).

are common. The enhanced distribution of CMR leads to a growth in this application as well.

Since the early years of CMR differentiation of masses has been a major indication. Using different CMR techniques it is possible to differentiate the tissue composition of a mass as well as to find signs for malignant growth pattern (Figs. 9, 10).

This short overview of CMR indications is not exhaustive, but it reflects the width of indications driving the intention to offer CMR in hospitals of all sizes.

Current CMR teaching modes

For standardization of CMR certification dedicated teaching systems have been defined by different radiology (i.e. American College of Radiology (ACR)), cardiology (i.e. European Society of Cardiology (ESC)) and interdisciplinary societies (i.e. Society for Cardiovascular Magnetic Resonance Imaging (SCMR)).

These guidelines require a multimodal teaching system with lectures, seminars and case studies, as well as a dedicated teaching center providing the necessary volume of CMR scans. In order to meet these requirements, training courses typically require periods of off-site training of a potential trainee in a high-volume CMR center such as ours.

There exist several teaching modalities for CMR, i.e. in our institution we offer four different types of CMR courses. As illustrated in Figure 11, weekend courses provide basic CMR knowledge whereas three in-depth courses with different features enable participants to acquire advanced skills in CMR interpretation.

In traditional fellowship teaching, trainees typically spend several weeks in an experienced CMR center. Teaching is provided by experienced CMR supervisors, sometimes on a one-on-one basis, and structured along daily clinical cases. However, this teaching mode requires significant times away from the individual home facility, typically six to twelve weeks.

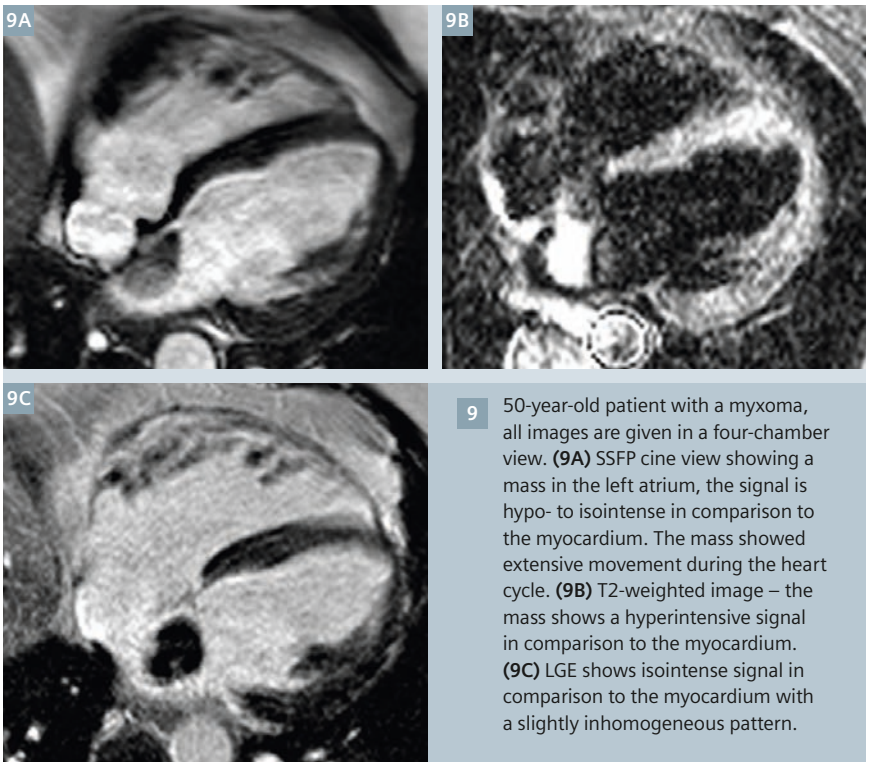

9 50-year-old patient with a myxoma, all images are given in a four-chamber view. **(9A)** SSFP cine view showing a mass in the left atrium, the signal is hypo- to isointense in comparison to the myocardium. The mass showed extensive movement during the heart cycle. **(9B)** T2-weighted image – the mass shows a hyperintensive signal in comparison to the myocardium. **(9C)** LGE shows isointense signal in comparison to the myocardium with a slightly inhomogeneous pattern.

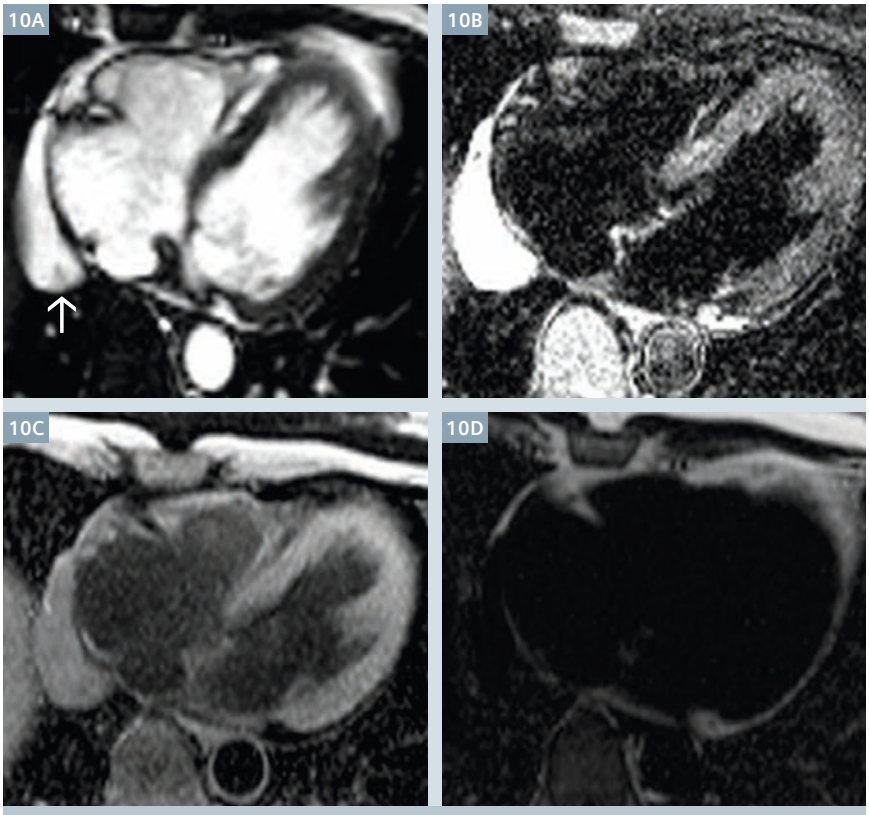

10 49-year-old patient with a pleuropericardial cyst adjacent to the right atrium (arrow), all images are given in an atypical four-chamber view (adapted to delineate the extracardiac mass). **(10A)** SSFP cine imaging showing a well-defined structure without any infiltration of cardiac structures. Signal intensity is hyperintense in comparison to the myocardium **(10B)** T2-weighted image, signal intensity is hyperintense in comparison to the myocardium **(10C+D)**. Fat/water imaging excluded fat component within the mass [9].

Basic CMR knowledge	Advanced CMR knowledge	
Weekend CMR courses • lectures (6 hours) • seminars (3 hours) • hands-on CMR cases (6 hours)	**Module-based network teaching** • 5 weeks one-on-one case-guided teaching in our CMR center (module I/III) • 4-8 months flexible self-guided CMR training in home facility with remote co-evaluation/supervision by our CMR center within one working day (modules II/IV) **Fellowship teaching** • 8-12 weeks one-on-one case-guiding teaching in our CMR center **Laptop teaching** • 6 weeks one-on-one case-guided teaching in our CMR center • 4-8 months flexible virtual CMR training in home facility with 150 pre-defined CMR cases on laptop (incl. regular review/ correction by level II/III expert in our center)	**All advanced CMR training courses include** • >30 hours lectures on physical and clinical CMR prinicples • >150 self-conducted CMR evaluations • all topics required by SCMR certification guidelines

11 Overview of CMR teaching options. *Adapted from [3].*

Our center also offers a laptop-based teaching course, which requires less time off-site in our facility where basic standard CMR protocols and evaluation tools are introduced. Afterwards trainees return to their individual home facility, equipped with a laptop containing selected CMR cases for self-interpretation. Participants evaluate all cases and discuss results with an expert in the teaching center upon completion. Additionally, if needed, ad hoc discussions on a particular case are arranged via telephone or web conference.

CMR teaching network

The HELIOS CMR network consists of a central DICOM server and several clients in hospitals throughout Germany (Fig. 12).

The CMR network has three major objectives:

Firstly, it is used for remote teaching purposes. Trainees who have been educated in basic CMR evaluation in our center return to their individual home facility and self-interpret CMR cases using their individual scan environment and staff. Afterwards, facilitating the network, DICOM files and reports are uploaded onto a central DICOM server and remotely co-evaluated by SCMR level II/III supervisors within one working day. This enables remote guidance of a trainee in their home facility, where they are faced with their own interpretational errors and technical hurdles arisen in their working environment – but with the backup of an experienced teaching center.

Secondly, it is used as an expert platform even beyond training courses. This ranges from simple

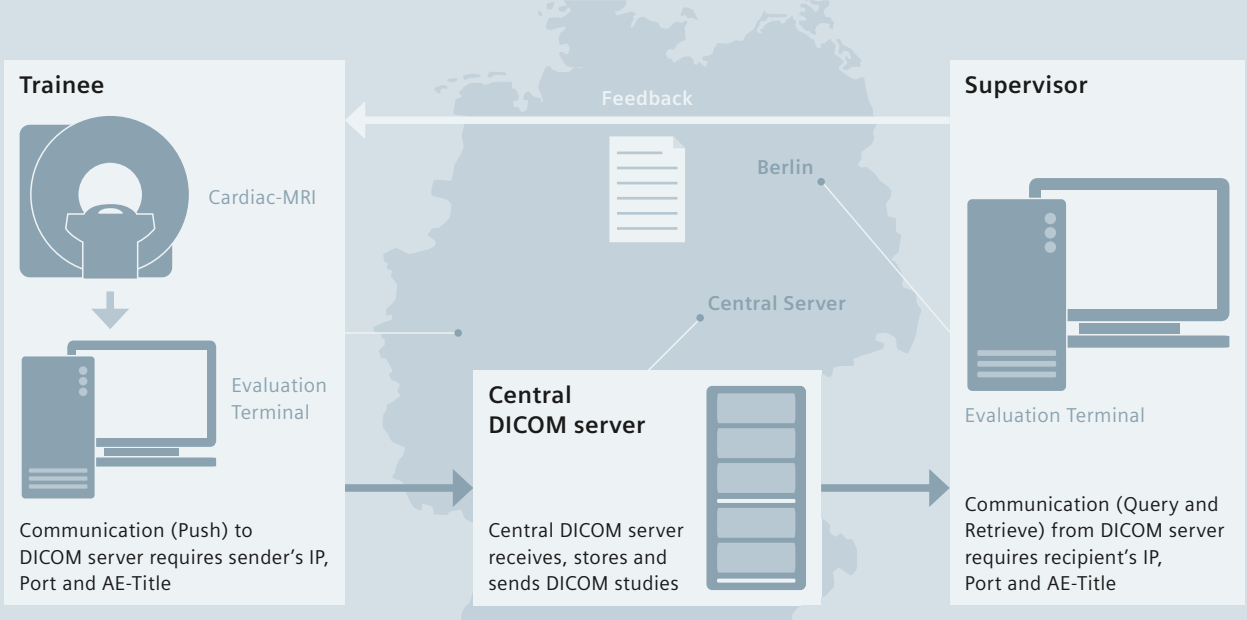

12 HELIOS CMR network structure.

second expert evaluation of a scan transmitted to the CMR expert center, up to the development of case databases for rare findings, common errors and image artifacts.

Thirdly, it is utilized for real-time remote scan control. Having established a full two-way connection between two MRI workstations, Expert-i software (Siemens Healthcare, Erlangen, Germany) enables supervisors and technical assistants to remotely control and conduct a CMR scan elsewhere. Over recent years, members within our CMR network have leveraged this capability and contacted our center to obtain remote assistance in the event of technical CMR issues or an inconclusive CMR finding (Fig. 13). If necessary, the remote supervisor in our center is able to actively adjust CMR sequence parameters and even conduct the entire scan remotely in real-time.

Since its first initialization in 2009 our CMR teaching network expanded from initially five sites to fourteen sites by September 2015. These 14 sites consist of five small hospitals (<400 beds), five medium sized hospitals (400-1,000 beds) and four large hospitals (>1,000 beds). Accordingly, our CMR network has enabled even small institutions to acquire CMR expertise, which has enhanced the portfolio of medical care in these institutions – something that would have been much more challenging outside a network structure.

Comparison to other imaging networks

Tele-learning modalities were introduced in response to advances in technology and the increasing demand for flexible learning opportunities that are not time- and location-dependent [21].

At the same time there is an increasing demand for expert networks in a number of medical fields, particularly due to centralization of expertise in larger institutions and an increasing degree of sub-specialization in medicine [22]. Most networks mainly concentrate on facilitation of communication, knowledge exchange and research collaboration between institutions [23, 24]. Particularly knowledge exchange and real-time expert advice were studied in neurology, i.e. in so-called 'tele-stroke networks' enabling remote clinical stroke evaluation and therapy guidance [25]. A combination of time pressure and incomplete national and global coverage with neurologic expertise has supported the introduction of telemedicine especially in rural areas and was demonstrated by several prospective studies to be cost effective and quality improving [26, 27].

Even cost savings can be expected due to earlier diagnosis and treatment as well as through the avoidance of referrals to larger centers, if imaging networks enable even small hospitals to conduct a broader portfolio of imaging modalities. This has also been proven for telemedicine in stroke patients [24-26] and is of utmost importance when it comes to rural areas where the next available specialized imaging center might be hundreds of miles away.

Furthermore, studies have shown, i.e. for CT colonoscopy, that especially in complicated cases, good detection rates are achieved only if state-of-the-art protocols and experienced readers are directly involved [27]. Hence, high quality imaging networks should be built not only for basic educational purposes but also function as platforms for continuous expert access.

One particular area of concern in remote networks arises from data safety and legal issues, especially in case of potential cross-border networks. While these hurdles may be difficult to overcome in general, there are examples for bilateral agreements between countries as potential means

13

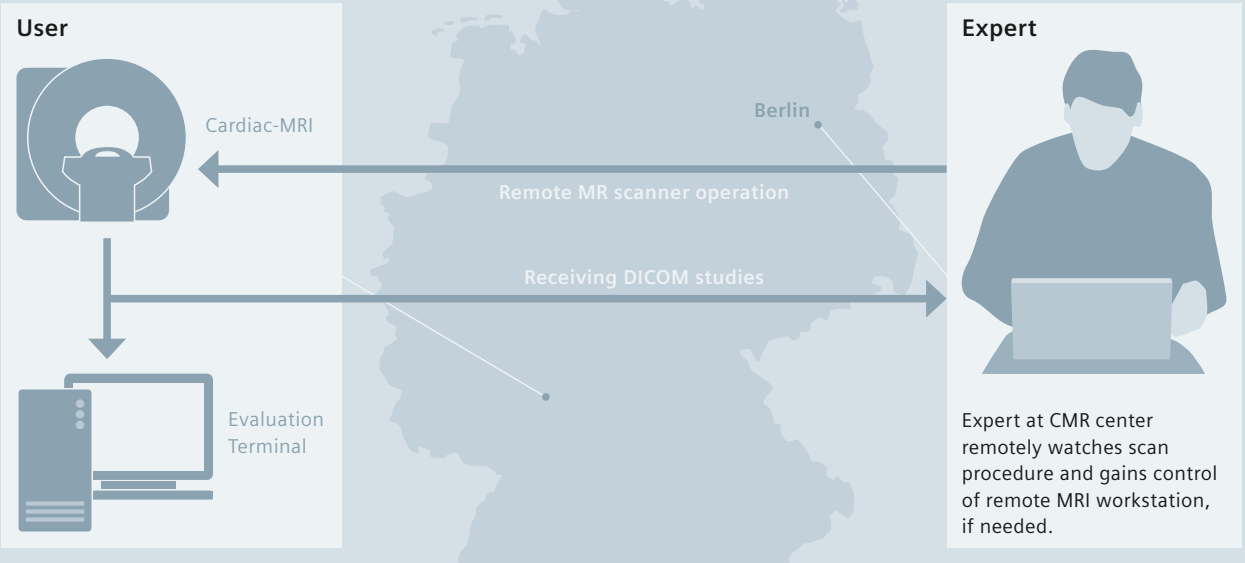

13 Real-time remote CMR scan control and supervision.

to overcome legal barriers as they regulate the distribution of responsibility, i.e. in a German-Estonian partnership for congenital heart disease [28]. In our network, data safety issues were less problematic as the network is national and firm-owned with an intranet connection for all clinics that has ensured consistently high data security standards.

Remote scanner access

In a subgroup of sites Expert-i was applied. The remote scanner access was used to supervise the new center during their first own MR-scan experience. An active interaction was only used in case of major difficulties and ceased to be necessary after fewer than 10 scans. The implementation was fast and uneventful. It was usually done by an experienced CMR-technician. In our experience, that back-up was well received and shortened the scan time, as small optimization could be operated immediately. Furthermore, we have also operated own scans from outside the hospital to test the capability of remote scanning. The only potential obstacle is the available bandwidth of the network itself. The procedure is illustrated in Figure 13.

In the case of pharmacological stress or unstable patients, a medical doctor has to be onsite as well, but a dedicated CMR experience must not be given. That setting enables sites without CMR-specialists to run a CMR. But it provides also the possibility to teach potential CMR users, as an enabling seems to be preferable. Meanwhile, CMR is robust enough to perform basic protocols worldwide also in small sites. Standard protocols, reporting- and post-processing guidelines are published and will be updated regularly [29].

Future perspectives

CMR has a growing acceptance as indicated in different guidelines, but for different reasons the use is limited in different regions of the world. One obstacle is a missing reimbursement in several countries that should be faced by local authorities but needs a joint effort. Knowledge of CMR has to be disseminated and teaching plays a key role. Referring doctors have to be educated worldwide using conferences as well as educational papers. Fortunately, it is only a matter of time as CMR is today part of the teaching at medical schools. Another crucial point is the hands-on teaching at the scanner as well as image-interpretation. Our introduced setting will help to accelerate the distribution of knowledge and is applicable in different settings.

References

1 Garbi M, McDonagh T, Cosyns B, et al. Appropriateness criteria for cardiovascular imaging use in heart failure: report of literature review. Eur Heart J Cardiovasc Imaging. 2015 Feb;16(2):147-53.

2 Wolk MJ, Bailey SR, Doherty JU, et al. ACCF/AHA/ASE/ASNC/HFSA/HRS/SCAI/SCCT/SCMR/STS 2013 multimodality appropriate use criteria for the detection and risk assessment of stable ischemic heart disease: a report of the American College of Cardiology Foundation Appropriate Use Criteria Task Force, American Heart Association, American Society of Echocardiography, American Society of Nuclear Cardiology, Heart Failure Society of America, Heart Rhythm Society, Society for Cardiovascular Angiography and Interventions, Society of Cardiovascular Computed Tomography, Society for Cardiovascular Magnetic Resonance, and Society of Thoracic Surgeons. J Card Fail. 2014 Feb;20(2):65-90.

3 Muehlberg F, Toepper A, Prothmann M, et al. MRI applications on infiltrative cardiomyopathies. J Thorac Imag. 2015 [in press].

4 Kim RJ, Wu E, Rafael A, et al. The use of contrast-enhanced magnetic resonance imaging to identify reversible myocardial dysfunction. N Engl J Med. 2000 Nov 16;343(20):1445-53.

5 Anderson LJ, Holden S, Davis B, et al. Cardiovascular T2-star (T2*) magnetic resonance for the early diagnosis of myocardial iron overload. Eur Heart J. 2001 Dec;22(23):2171-9.

6 Kim RJ, de Roos A, Fleck E, et al. Guidelines for training in Cardiovascular Magnetic Resonance (CMR). J Cardiovasc Magn Reson. 2007;9(1):3-4.

7 Weinreb JC, Larson PA, Woodard PK, et al. American College of Radiology clinical statement on noninvasive cardiac imaging. Radiology. 2005;235(3):723-7.

8 Muehlberg F, Neumann D, von Knobelsdorff-Brenkenhoff F, et al. A multicenter cardiovascular MR network for tele-training and beyond: setup and initial experiences. J Am Coll Radiol. 2015 Aug;12(8):876-83.

9 Bruder O, Wagner A, Lombardi M, et al. European Cardiovascular Magnetic Resonance (EuroCMR) registry--multinational results from 57 centers in 15 countries. J Cardiovasc Magn Reson. 2013 Jan 18;15:9.

10 von Knobelsdorff-Brenkenhoff F, Bublak A, El-Mahmoud S, et al. Single-centre survey of the application of cardiovascular magnetic resonance in clinical routine. Eur Heart J Cardiovasc Imaging. 2013 Jan;14(1):62-8.

11 Kellman P, Hernando D, Shah S, et al. Multiecho dixon fat and water separation method for detecting fibrofatty infiltration in the myocardium. Magn Reson Med. 2009 Jan;61(1):215-21.

12 Wu KC, Zerhouni EA, Judd RM, et al. Prognostic significance of microvascular obstruction by magnetic resonance imaging in patients with acute myocardial infarction. Circulation. 1998 Mar 3;97(8):765-72.

13 Friedrich MG, Sechtem U, Schulz-Menger J, et al. Cardiovascular magnetic resonance in myocarditis: A JACC White Paper. J Am Coll Cardiol. 2009 Apr 28;53(17):1475-87.

14 Bohnen S, Radunski UK, Lund GK, et al. Performance of t1 and t2 mapping cardiovascular magnetic resonance to detect active myocarditis in patients with recent-onset heart failure. Circ Cardiovasc Imaging. 2015 Jun;8(6).

15 Ferreira VM, Piechnik SK, Dall'Armellina E, et al. T(1) mapping for the diagnosis of acute myocarditis using CMR: comparison to T2-weighted and late gadolinium enhanced imaging. JACC Cardiovasc Imaging. 2013 Oct;6(10):1048-58.

16 Maron BJ, Udelson JE, Bonow RO, et al. Eligibility and Disqualification Recommendations for Competitive Athletes With Cardiovascular Abnormalities: Task Force 3: Hypertrophic Cardiomyopathy, Arrhythmogenic Right Ventricular Cardiomyopathy and Other Cardiomyopathies, and Myocarditis: A Scientific Statement From the American Heart Association and American College of Cardiology. J Am Coll Cardiol. 2015 Oct 27. pii: S0735-1097(15)06571-7.

17 Sado DM, White SK, Piechnik SK, et al. Identification and assessment of Anderson-Fabry disease by cardiovascular magnetic resonance noncontrast myocardial T1 mapping. Circ Cardiovasc Imaging. 2013 May 1;6(3):392-8.

18 Kramer CM, Appelbaum E, Desai MY, et al. Hypertrophic Cardiomyopathy Registry: The rationale and design of an international, observational study of hypertrophic cardiomyopathy. Am Heart J. 2015 Aug;170(2):223-30.

19 John AS, Dill T, Brandt RR, et al. Magnetic resonance to assess the aortic valve area in aortic stenosis: how does it compare to current diagnostic standards? J Am Coll Cardiol. 2003 Aug 6;42(3):519-26.

20 von Knobelsdorff-Brenkenhoff F, Rudolph A, Wassmuth R, Schulz-Menger J. Assessment of mitral bioprostheses using cardiovascular magnetic resonance. J Cardiovasc Magn Reson. 2010 Jun 23;12:36.

21 Tomlinson J, Shaw T, Munro A, et al. How does tele-learning compare with other forms of education delivery? A systematic review of tele-learning educational outcomes for health professionals. N S W Public Health Bull. 2013;24(2):70-5.

22 Kirsh SR, Ho PM, Aron DC. Providing specialty consultant expertise to primary care: an expanding spectrum of modalities. Mayo Clin Proc. 2014;89(10):1416-26.

23 Latifi R, Weinstein RS, Porter JM, et al. Telemedicine and telepresence for trauma and emergency care management. Scand J Surg. 2007;96(4):281-9.

24 Weinstein RS, Lopez AM, Joseph BA, et al. Telemedicine, telehealth, and mobile health applications that work: opportunities and barriers. Am J Med. 2014;127(3):183-7.

25 Rubin MN, Wellik KE, Channer DD, et al. A systematic review of telestroke. Postgrad Med. 2013;125(1):45-50.

26 Schenkel J, Reitmeir P, Von Reden S, et al. [Cost analysis of telemedical treatment of stroke]. Gesundheitswesen. 2013;75(7):405-12.

27 Lauridsen C, Lefere P, Gerke O, et al. Effect of a tele-training programme on radiographers in the interpretation of CT colonography. Eur J Radiol. 2012;81(5):851-6.

28 Kohler F, Schierbaum C, Konertz W, et al. Partnership for the heart. German-Estonian health project for the treatment of congenital heart defects in Estonia. Health Policy. 2005;73(2):151-9.

29 Schulz-Menger J, Bluemke DA, Bremerich J, et al. Standardized image interpretation and post processing in cardiovascular magnetic resonance: Society for Cardiovascular Magnetic Resonance (SCMR) board of trustees task force on standardized post processing. J Cardiovasc Magn Reson. 2013 May 1;15:35.

Fabian Muehlberg

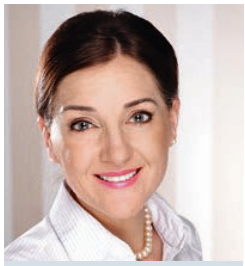

Edyta Blaszczyk

Jeanette Schulz-Menger

Contact

Prof. Dr. Jeanette Schulz-Menger, M.D.
University Medicine Berlin
Charité Campus Buch, ECRC
HELIOS Clinics Berlin-Buch
Department for Cardiology and Nephrology
Schwanebecker Chaussee
13125 Berlin, Germany
Phone: +49 30 9401153536
jeanette.schulz-menger@charite.de

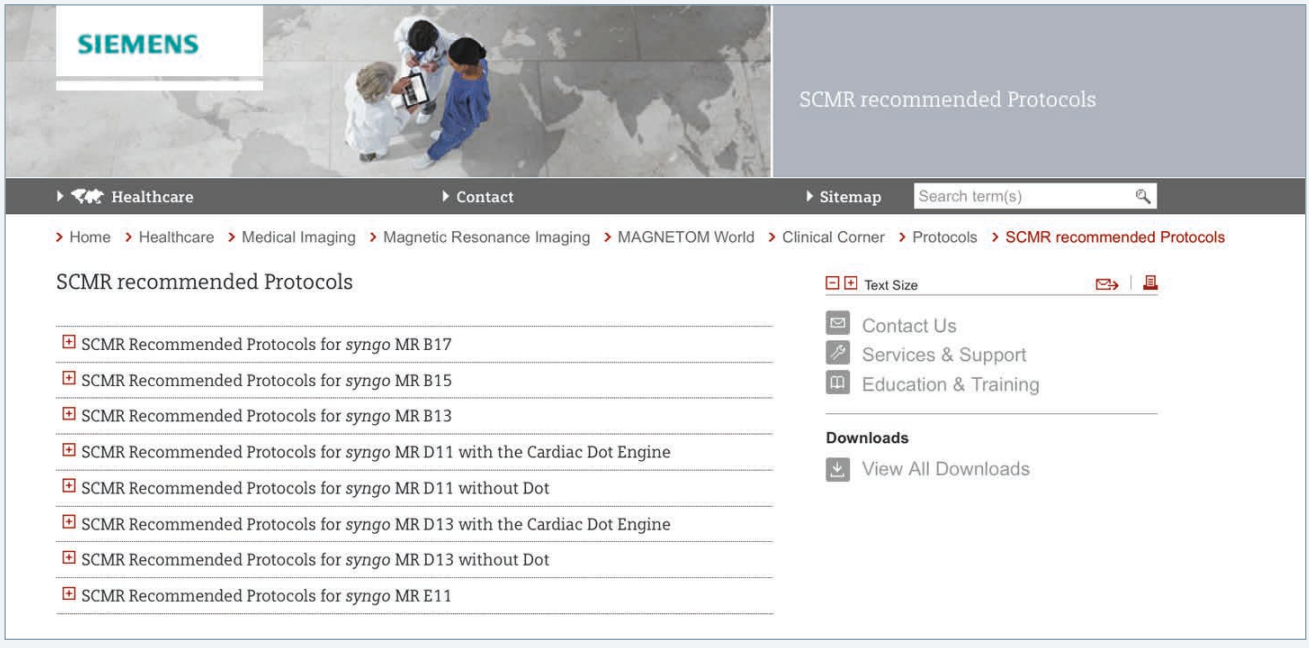

www.siemens.com/magnetom-world

Go to
Clinical Corner > Protocols

SCMR recommended protocols available for Cardiac Dot Engine

To aid standardization of CMR, the Society for Cardiovascular Magnetic Resonance (SCMR) released CMR exam protocol recommendations for the most frequent CMR procedures. In a collaborational effort Siemens Healthcare and the SCMR prepared clinically optimized exam protocols in accordance to the SCMR recommendations for the Siemens MAGNETOM family of MRI scanners, including 3T MAGNETOM Skyra, Skyra^{fit}, Prisma and Prisma^{fit} as well as 1.5T MAGNETOM Aera and Avanto^{fit}, with software *version syngo* MR E11, MAGNETOM ESSENZA and MAGNETOM Amira.

The following SCMR Cardiac Dot protocols are available:

- Acute Infarct Dot
- Adenosine Stress Dot
- Aorta Dot
- Arrhythmic RV Myopathy Dot
- Chronic Ischemia Dot
- Coronaries Dot
- Hypertrophic LV Dot
- Myocarditis Dot (1.5T only)
- Tumor & Thrombus Dot
- Nonischemic Myopathy Dot
- Pericarditis Dot
- Pulmonary Vein Dot
- Valves Dot
- Library Breath-Hold Dot
- Library Free-Breathing Dot

Please contact your Siemens Application Specialist for the exar 1 files of these protocols.

Acknowledgement:
We would like to thank all SCMR members who were on the guidelines committee Christopher M. Kramer *(University of Virginia, Charlottesville, VA, USA);* Jörg Barkhausen *(University Hospital, Lübeck, Germany);* Scott D. Flamm *(Cleveland Clinic, Cleveland, OH, USA);* Raymond J. Kim *(Duke University Medical Center, Durham, NC, USA);* Eike Nagel *(University Hospital, Goethe University, Frankfurt, Germany)* as well as Gary R. McNeal *(Senior CMR Application Specialist; Siemens Healthcare, USA)* for their tremendous efforts and support.

Myocarditis Dot

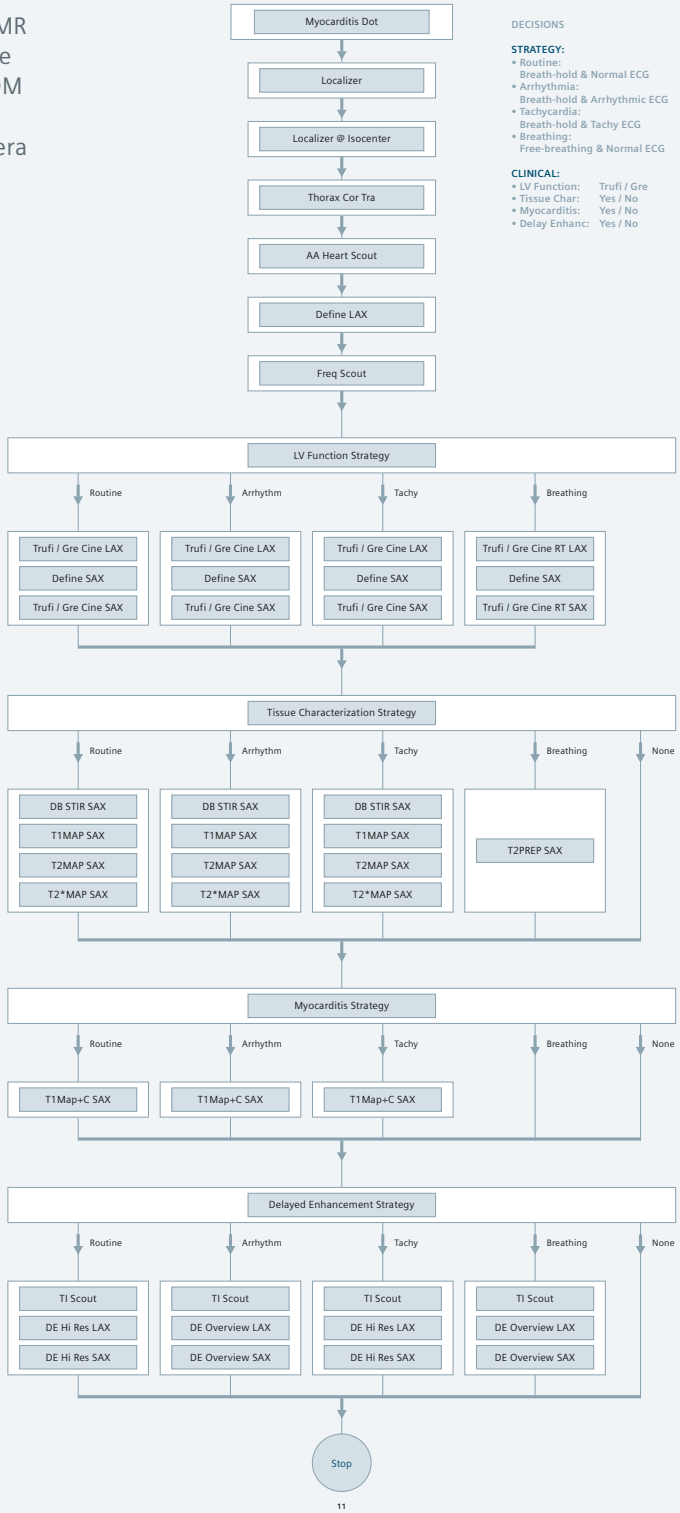

Case Report: Acute Myocardial Syndrome in a 37-Year-Old Patient with Severe Renal Impairment

S. A. Mohiddin; A. S. Herrey

Institute of Cardiovascular Science, University College London;
The Inherited Cardiovascular Diseases Unit and Cardiac Imaging Department, The Barts Heart Centre, London, UK

A 37-year-old lady was admitted to our institution with chest pain and pain in her left arm, but no shortness of breath. Preceding the admission she had experienced symptoms of an acute upper respiratory tract infection.

Her past medical history included hypertension, hypothyroidism, hyperprolactinaemia, focal sclerosing glomerulosclerosis with stage IV chronic kidney disease, eGFR 17 ml/min, treated tuberculosis and three first trimester miscarriages.

On admission, her hs- troponin T was > 7,000 ng/L (normal < 30 ng/L). Her ECG was largely unchanged from a previous one taken in 2013 meeting LVH criteria, but otherwise unremarkable.

Her echocardiogram showed low-normal left ventricular systolic function with akinesis of the mid inferior and mid infero-septal segments with an estimated EF of 55%.

On coronary angiography, her coronary arteries were unobstructed.

To confirm the working diagnosis of myocarditis, she underwent Cardiovascular Magnetic Resonance (CMR) imaging on our MAGNETOM Aera 1.5T (Siemens Healthcare, Erlangen, Germany). In view of her severe renal impairment, no gadolinium contrast was given.

This was reported as showing normal biventricular size, mild systolic impairment with hypokinesis of the antero-septum, infero-septum and inferior wall. Non-contrast tissue characterisation with T1 and T2 mapping identified markedly increased T1 and T2 values matching (and extending beyond) the regional wall motion abnormalities, confirming the diagnosis of florid acute myocarditis.

Subsequently, her troponin levels were falling and she was discharged pain free a few days later.

A month later, her EF on echo had normalised with mild residual inferior hypokinesis and her troponin was normal at 18 n/L. Her repeat CMR, however, showed persistent myocardial inflammation, but with falling T2 values.

In summary, non-contrast myocardial mapping in this case was used to establish and confirm a diagnosis of myocarditis and also to monitor progress.

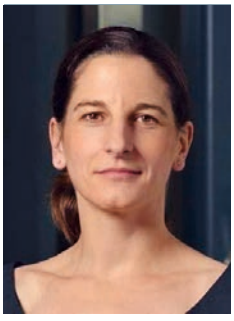

Contact

Anna S. Herrey
Institute of Cardiovascular Science
University College London
The Barts Heart Centre
16-18 Westmoreland Street
London W1G 8PH
UK
anna.john@doctors.org.uk

Reprinted from MAGNETOM Flash 3/2015

Panel 1

The T1 maps (MOLLI) show extensive interstitial expansion in the septum and the inferior wall on the first scan. On the second (F_UP) scan, there is incomplete resolution in the inferior wall and limited change in the septum.

a) On the two-chamber view (T1_MOLLI_2cha and F_UP_T1_MOLLI_2cha) there is increased signal in the inferior wall.

b) In a four-chamber orientation (T1_MOLLI-4cha and F_UP_T1_MOLLI_4cha), there is increased signal in the septum.

c) In the short axis views (T1_MOLLI_mid-SAX and F_UP_T1_MOLLI_mid_SAX), both increased signal can be seen in the septum and the inferior wall.

Panel 2

The matching T2 maps confirm myocardial oedema matching the areas of high native T1 values. The florid changes seen in the initial scan are less impressive at follow-up (F_UP), but still present.

a) High T2 signal is seen in the two-chamber view in the inferior wall (T2-4cha and F_UP_T2_4cha).

b) In the four-chamber orientation, there is increased signal in the mid septum.

c) The short axis view confirms similar changes in septum and inferior wall compared to the T1 maps.

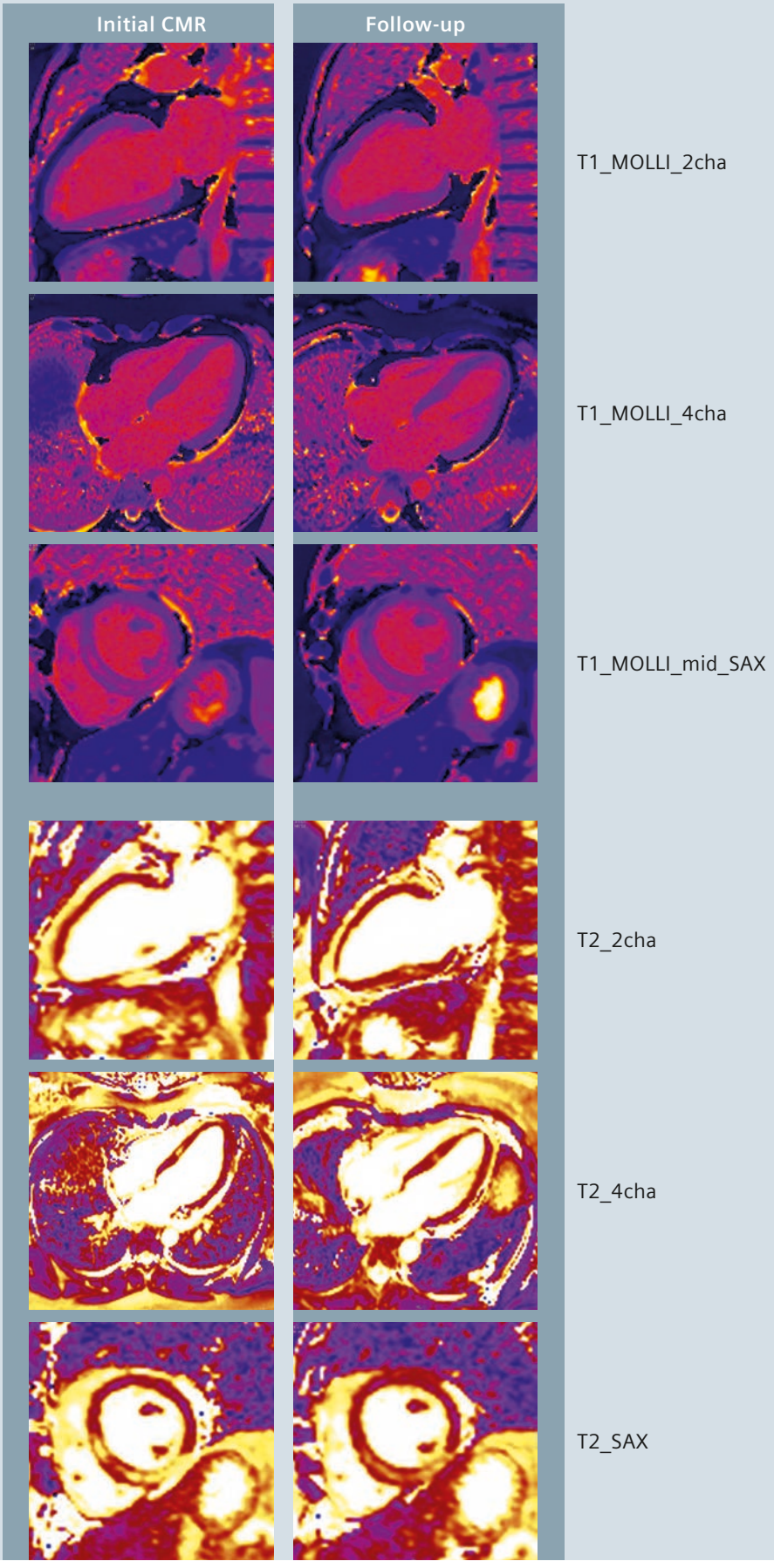

Case Report: Detection of Myocardial Changes in a Patient Undergoing Chemotherapy

Arash Seratnahaei, M.D.; Vincent L. Sorrell, M.D., FACP, FACC, FASE; David Powell, Ph.D.; Peter A. Hardy, Ph.D.; Bruce Spottiswoode, Ph.D.; Steve W. Leung, M.D., FACC

University of Kentucky Medical Center, Gill Heart Institute, Lexington, KY, USA

Patient history

46-year-old female presented with progressive dyspnea on exertion. She was found to have acute myeloid leukemia, and underwent 7+3 chemotherapy induction with daunorubicin. The initial chemotherapy was not effective, and thus re-induction with high dose cytarabine and idarubicin was given. Prior to chemotherapy, she had a normal left ventricular ejection fraction (LVEF) (>55%) by echocardiography. Three weeks after chemotherapy, her repeat LVEF by echo was reduced to 40-50% with a possible thrombus in the LV apex. She underwent cardiac magnetic resonance (CMR) imaging for the assessment of left ventricular function and apical thrombus.

Sequences details

All images have been acquired using a MAGNETOM Aera 1.5T scanner with software version *syngo* MR D13 (Siemens Healthcare, Erlangen, Germany). Mid-ventricular short axis MOdified Look Locker Inversion Recovery (MOLLI) images were acquired during diastole for T1 determination using an 11 heart-beat, 5(3)3, SSFP readout sequence. Imaging parameters were: Field-of-view 300 mm, slice thickness 8 mm, TR 335.62 ms, TE 2.7 ms, matrix 256 × 168 pixels resulting in a resolution of 1.2 x 1.2 mm, TI start = 130 ms, TI increment = 80 ms.

Then, a total dose of 0.2 mmol/kg gadopentetate dimeglumine (MAGNEVIST, Bayer HealthCare Pharmaceuticals, Leverkusen, Germany) was injected at 4 ml/second. Ten minutes after contrast injection,

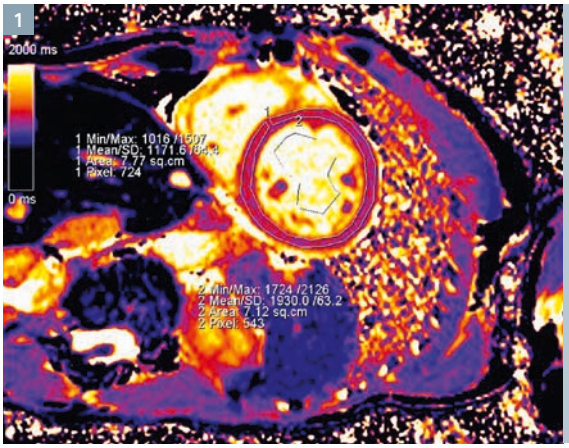

1 Native T1 mapping (MOLLI 5(3)3) in the mid-ventricular short axis demonstrating an elevated native T1 time in the myocardium.

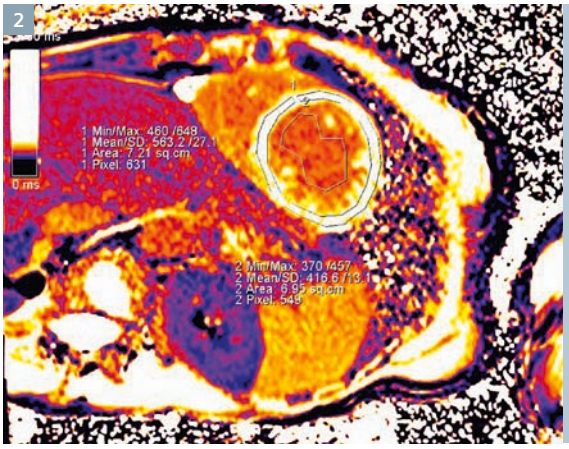

2 Post contrast T1 mapping (MOLLI 4(1)3(1)2) in the mid-ventricular short axis was used for calculation of extracellular volume fraction.

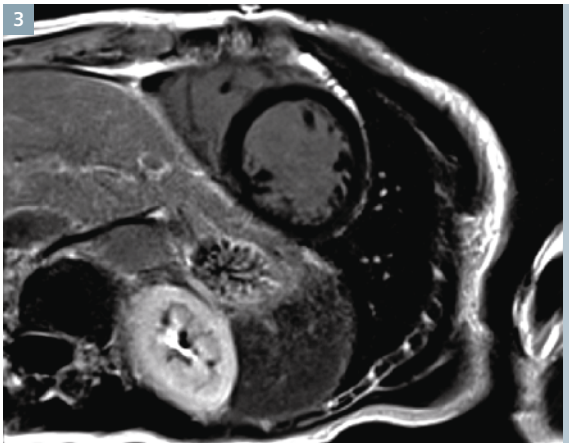

3 Late gadolinium enhancement phase-sensitive inversion recovery mid-ventricular short axis image demonstrating no enhancement.

late gadolinium enhancement (LGE) images were acquired with a phase-sensitive inversion recovery gradient-echo imaging sequence for the assessment of focal myocardial fibrosis. Finally, 18 minutes after contrast injection, post-contrast MOLLI T1 mapping 4(1)3(1)2 was repeated in identical prescription as native T1 mapping.

Native and post-contrast blood T1 times were measured on a region-of-interest manually drawn in the center of the blood-pool. Native and post-contrast T1 times were measured on the T1 maps as shown in figures 1 and 2.

The partition coefficient lambda (λ) and extracellular volume fraction (ECV) were calculated in the following manner:

$$\lambda = \frac{1/T1\,\text{myocardium postcontrast} - 1/T1\,\text{myocardium precontrast}}{1/T1\,\text{blood postcontrast} - 1/T1\,\text{blood precontrast}}$$

$$ECV = \lambda\,(1\text{-Hematocrit})$$

Imaging findings

CMRI confirmed the LVEF was reduced at 40% with global hypokinesis. LGE images did not demonstrate any focal fibrosis or left ventricular thrombus. Native myocardial T1 time was 1171 ms, and 1930 ms for the blood-pool. Post-contrast myocardial T1 was 563 ms, and 417 ms for the blood-pool. Hematocrit, on the morning of the scan, was 26.9%. Calculated ECV was 35.9%, which is elevated. Heart rate was 65 bpm during native T1 mapping and post-contrast T1 mapping. Based on the T1 mapping, the patient appears to have edema or acute inflammatory response that was not detected with traditional CMR imaging.

The quantitative analysis of native T1 mapping (Fig. 1) shows higher T1 value, while the quantitative analysis of the post-contrast T1 mapping (Fig. 2) shows shorter T1 value. LGE (Fig. 3) shows no evidence of fibrosis or scar.

Comments (Discussion)

Endomyocardial biopsy is the 'gold' standard for myocardial disease evaluation. However, this is an invasive procedure and its accuracy is limited by sampling error and carries a risk of morbidity and mortality. Therefore, non-invasive testing is the preferred technique for myocardial tissue evaluation. CMR provides several methods for non-invasive myocardial tissue characterization. For evaluation of the myocardial ECV, T1 mapping before and after gadolinium-based contrast administration has become an emerging technique. Native T1 mapping reveals acute myocardial inflammation, while the combination of native and post-contrast T1 mapping provides information regarding expansion of the myocardial extracellular volume fraction. Increased ECV is seen in focal or diffuse fibrosis/scar or edema [1].

Anthracycline-based chemotherapy has a well-documented history of causing cardiac dysfunction, which limits its use. Both short-term and long-term cardiac dysfunction has been described [2]. Long-term effects are cumulative dose dependent and include irreversible LV systolic dysfunction. In contrast, short-term effects have been described in small case series. These effects can occur immediately or within a few weeks of chemotherapy administration and include pericarditis, arrhythmias, and acute LV systolic dysfunction [2, 3]. In this patient, the native T1 is elevated indicating acute myocardial edema. If the native T1 time was within the normal range, the calculated ECV would have been within the normal range as well. The elevated ECV appears to be driven mainly by the edema, rather than diffuse fibrosis. This case highlights the ability of CMR with T1 mapping to identify acute myocardial edema in a patient who had recently received anthracycline-based chemotherapy. Although the patient's LGE images appear normal, the overall extracellular volume fraction is elevated.

References

1 White SK, Sado DM, Flett AS, Moon JC. Characterising the myocardial interstitial space: the clinical relevance of non-invasive imaging. Heart 2012;98:773–9.

2 Dazzi H, Kaufmann, Follath. Anthracycline-induced acute cardiotoxicity in adults treated for leukaemia. Analysis of the clinico-pathological aspects of documented acute anthracycline induced cardiotoxicity in patients treated for acute leukaemia at the University Hospital of Zurich, Switzerland, between 1990 and 1996. Ann Oncol 2001; 12(7): 963-6.

3 Bristow MR, Thompson PD, Martin RP, et al. Early anthracycline cardiotoxicity. Am J Med 1978; 65(5): 823-32.

Contact

Steve W. Leung, M.D., FACC
University of Kentucky Medical Center
Division of Cardiovascular Medicine
Gill Heart Institute
326 Charles T. Wethington Building
Lexington, KY 40536
USA
Phone: +1 859-323-8040
steve.leung@uky.edu

Case Report: Myocardial Fibrosis in a Non-Ischemic Cardiomyopathy

Jeremy D. Collins, M.D.[1]; Bruce Spottiswoode, Ph.D.[2]; James C. Carr, M.D.[1]

[1] Feinberg School of Medicine, Department of Radiology, Sections of Cardiovascular Imaging and Interventional Radiology, Northwestern University, Chicago, IL, USA
[2] Cardiovascular MR R&D, Siemens Healthcare, Chicago, IL, USA

Patient history

49-year-old male with a history of congestive heart failure for seven years, managed medically, who self-referred for a second opinion regarding management of presumed hypertensive heart disease. About four months prior to referral the patient stopped working due to progressive dyspnea. One month prior to referral he noted acute worsening of his dyspnea and dizziness, and underwent left heart catheterization which was negative for coronary artery disease. At presentation the patient reports orthopnea and paroxysmal nocturnal dyspnea, with persistent dyspnea, lower extremity edema, and a cough. The patient denied recent fevers, chills, headaches, changes in vision, dizziness, weakness, or arthralgias. Past medical history was notable for hypertension, diabetes mellitus – type II, obstructive sleep apnea, obesity, and atrial fibrillation. The patient denies prior or current tobacco use or significant alcohol intake. Family history was negative for premature heart disease. On physical exam the heart rate was regular at 70 beats per minute with a blood pressure of 130/80 mmHg and notable for a split S2, without S3 or S4. S1 was normal. The cardiac apex was non-displaced. Laboratory analysis demonstrated an

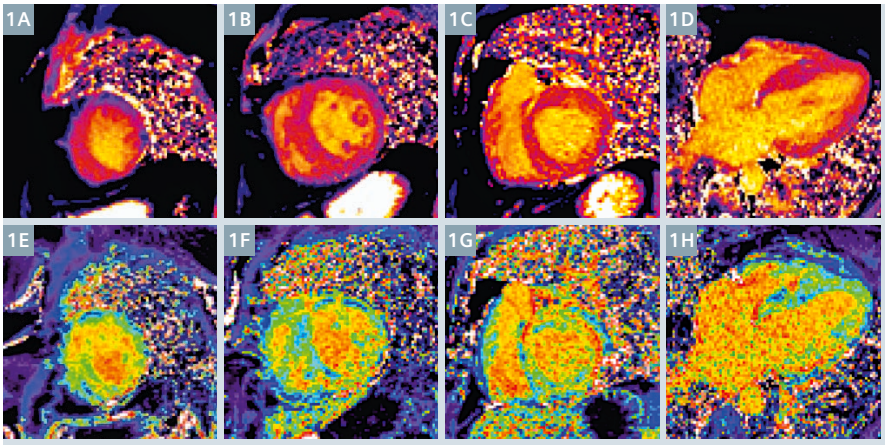

1 Native T1 and Gadolinium extracellular volume (ECV) fraction maps demonstrate marked elevation of myocardial T1 values with corresponding diffuse elevation of the Gadolinium ECV fraction.

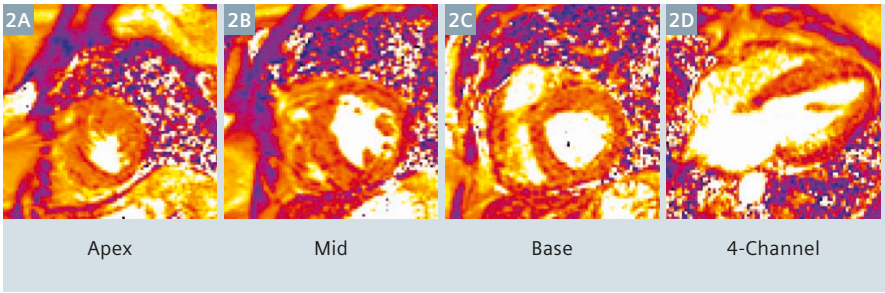

2 T2 maps demonstrate diffuse elevation of myocardial T2 values, indicative of myocardial edema.

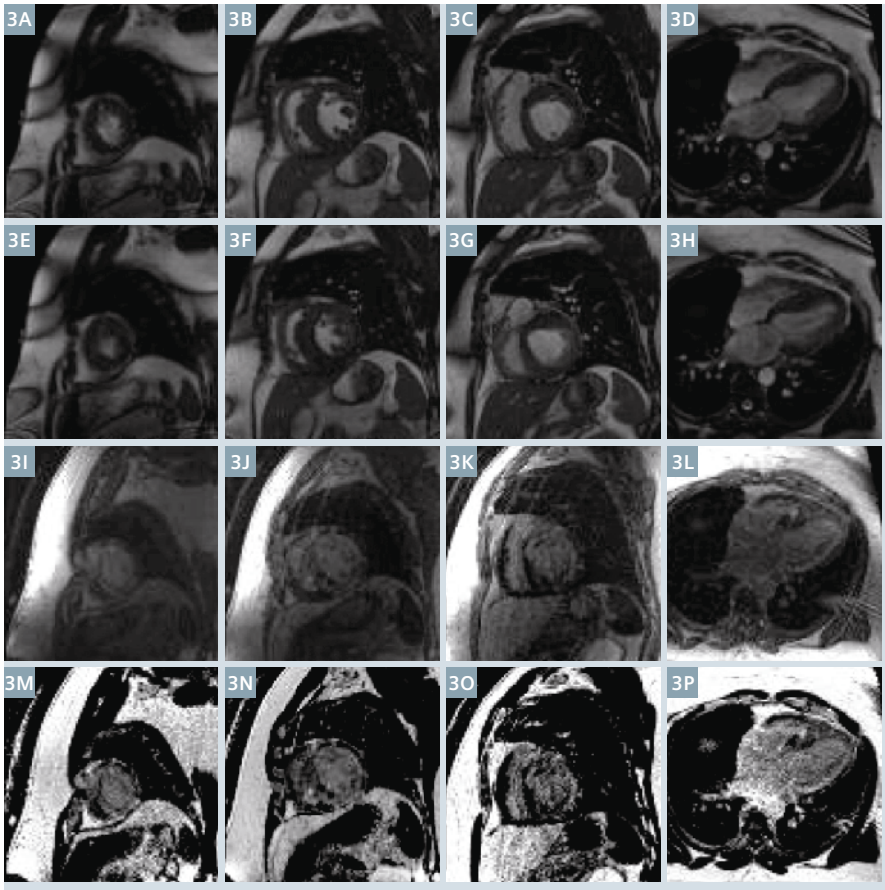

3 End-diastole and end-systole still frames from cine SSFP images demonstrate severe global biventricular systolic dysfunction. Corresponding delayed enhance-ment imaging demonstrates reduced contrast between the myocardium and the blood pool, with suggestion of diffuse pre-dominantly subepicardial and mesocardial scarring.

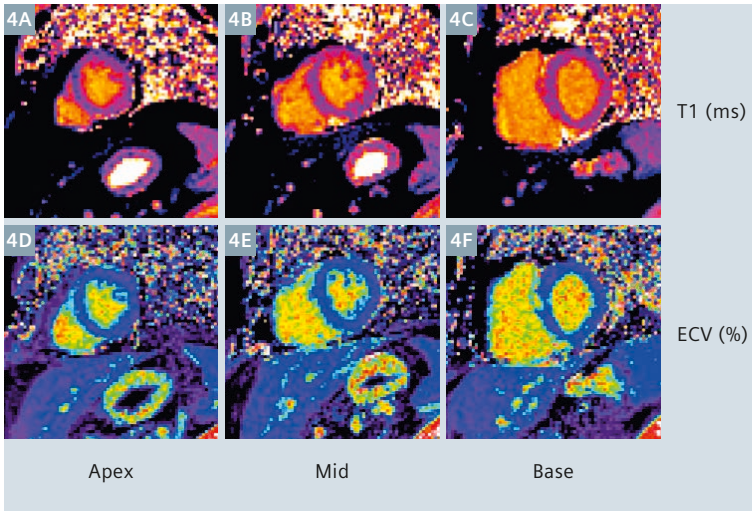

4 Native T1 and Gadolinium extra-cellular volume (ECV) fraction maps from a 64-year-old male patient without diffuse fibrosis, demon-strating normal values. Apparent increased signal along the epicardial anteroseptum was seen to represent volume averaging with the right ventricular blood pool.

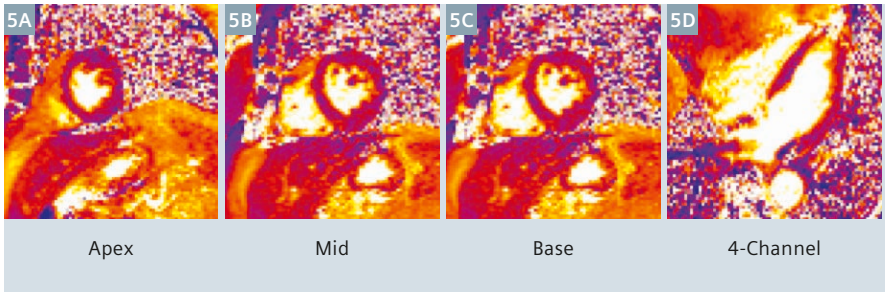

5 T2 maps from a 64-year-old male patient without myocardial edema, demon-strating normal values.

elevated b-type natriuretic peptide at 817 pg/ml.

As part of his work-up to evaluate for an etiology of his non-ischemic cardiomyopathy, the patient was referred for cardiac MRI to evaluate for an infiltrative process and assess biventricular systolic function and scar.

Sequence details

All images were acquired on a MAGNETOM Aera 1.5T scanner with an 18-channel phased array body coil and software version *syngo* MR E11 (Siemens Healthcare, Erlangen, Germany). T1 and T2 mapping was done using MyoMaps (Siemens Healthcare, Erlangen, Germany), which includes inline non-rigid motion correction and pixelwise fitting.

Pre-contrast T1 mapping uses a single shot inversion recovery TrueFISP readout with a 5(3)3 scheme, i.e. an inversion followed by 5 acquisition heartbeats, then 3 recovery heartbeats, and a further inversion with 3 acquisition heartbeats. Post-contrast T1 mapping uses a 4(1)3(1)2 scheme. Other parameters for T1 mapping include: TE 2.7 ms, TR 386 ms, TI start 110 ms, TI increment 80 ms, FOV 380 mm, matrix size 256 × 170, flip angle 35 degrees, bandwidth 1085 Hz/pixel. Pixelwise extracellular volume (ECV) maps were generated using investigational prototype software* with automated image co-registration and blood segmentation.

T2 mapping uses 3 single shot TrueFISP images with T2 preparation times of 0 ms, 25 ms and 55 ms, and 3 recovery heartbeats between each acquisition. Other parameters for T2 mapping include: TE 2.7 ms, TR 250 ms, FOV 360 mm, matrix size 192 × 146, flip angle 70 degrees, and bandwidth 1185 Hz/pixel.

*WIP, the product is currently under development and is not for sale in the US and in other countries. Its future availability cannot be ensured.

Imaging findings

Cardiac MRI was notable for moderate right atrial and severe left atrial enlargement without significant mitral or tricuspid valve disease. There was asymmetric septal hypertrophy in the basal and mid chamber measuring up to 1.7 cm in the mid-chamber inferoseptum. Biventricular systolic function was severely reduced with calculated right and left ejection fractions of 22% and 22%, respectively. The right ventricle was normal in size; the left ventricle was borderline enlarged with an end-diastolic volume index of 92 ml/m^2. Native T1 values were abnormally elevated ranging from 1200-1230 ms indicative of myocardial fibrosis. Native T2 values were elevated ranging from 66-67 ms consistent with myocardial edema. The Gadolinium extracellular volume fraction (ECV) was markedly elevated, at 58% based on a measured hematocrit of 41.8%. Delayed enhancement images were of limited diagnostic value due to the similar myocardial and blood T1 values post-contrast, but suggested diffuse predominantly mesocardial scar extending to involve the subepicardial myocardium. There was relative sparing of the subendocardium, consistent with a non-vascular etiology. Cardiac MRI findings were consistent with ongoing myocardial inflammation and fibrosis in a non-ischemic cardiomyopathy. The scar pattern was considered atypical for amyloidosis given subendocardial sparing.

Additional laboratory analysis was performed to evaluate for a monoclonal gammopathy. Although there was a mild hypergammaglobulinemia, there were no clear bands at serum immunofixation electrophoresis.

The patient was referred for right heart catheterization and biopsy. Right ventricular endomyocardial biopsy demonstrated myocyte hypertrophy with interstitial fibrosis. The mean pulmonary arterial pressure was 37 mmHg, diagnostic of pulmonary hypertension. Congo red staining was negative for apple green birefringence. The diagnosis of non-specific, non-amyloid myocardial fibrosis was made.

Discussion

This case demonstrates the utility of quantitative T1 and T2 myocardial imaging in the evaluation of patients with suspected infiltrative heart disease. Delayed enhancement imaging with phase sensitive inversion recovery has reduced the importance of careful time-to-inversion selection for patchy myocardial scar, such as that seen with focal infiltrative processes or myocardial infarction. However, delayed enhancement imaging is limited in patients with diffuse fibrosis, where regions of normal myocardium are not clearly visualized. In these subjects, there is often little contrast difference between the T1 values of the blood pool post-Gadolinium administration and the fibrotic myocardium. Hence delayed enhancement images of such patients can appear non-diagnostic. Review of images from the TI scout may suggest altered Gadolinium kinetics with T1 shortening of the myocardium compared to the blood pool; however, this is not consistently identified even in significant myocardial fibrosis and is dependent on the Gadolinium kinetics in a particular patient.

It is increasingly recognized that *in vivo* quantitative T1 and T2 parametric mapping with calculation of the ECV is useful in the assessment of infiltrative and inflammatory myocardial disease [1-3]. Native myocardial T2 values are elevated in acute inflammatory states, such as myocarditis, and are useful to assess the extent of ongoing inflammation. Native myocardial T1 values have been suggested as an alternative technique to delayed enhancement imaging to evaluate for myocardial fibrosis [1]. Although dependent on the T1 mapping technique utilized, elevated native T1 values generally greater than 980 ms are considered abnormal at 1.5T, although the influence of other parameters including myocardial iron, blood plasma volume, and myocardial edema have not been fully elucidated. Normal myocardial T1 ranges as well as the extent of elevation in different disease states remain to be determined. The Gadolinium ECV fraction uses pre- and post-contrast myocardial T1 values to determine the gadolinium

distribution into the myocardium, generating a partition coefficient, with ECV values > 30% considered abnormal [4].

In our case the combination of diffuse myocardial T2 elevation, native T1 elevation, and a markedly elevated ECV fraction was indicative of a diffuse fibrotic process with myocardial edema. As indicated by the blood protein analysis and concordant with biopsy findings, the lack of a T1 gradient extending from the subendocardium to the subepicardium made myocardial amyloidosis a less likely diagnosis.

References

1 Bulluck H, Maestrini V, Rosmini S, et al. Myocardial T1 mapping. Circulation journal : official journal of the Japanese Circulation Society. 2015;79(3):487-494.

2 Roller FC, Harth S, Schneider C, Krombach GA. T1, T2 Mapping and Extracellular Volume Fraction (ECV): Application, Value and Further Perspectives in Myocardial Inflammation and Cardiomyopathies. RoFo : Fortschritte auf dem Gebiete der Rontgenstrahlen und der Nuklearmedizin. Sep 2015;187(9):760-770.

3 Varga-Szemes A, van der Geest RJ, Spottiswoode BS, et al. Myocardial Late Gadolinium Enhancement: Accuracy of T1 Mapping-based Synthetic Inversion-Recovery Imaging. Radiology. Jul 30 2015:150162.

4 Barison A, Del Torto A, Chiappino S, et al. Prognostic significance of myocardial extracellular volume fraction in nonischaemic dilated cardiomyopathy. Journal of cardiovascular medicine (Hagerstown, Md.). Oct 2015;16(10):681.

Contact

Jeremy D. Collins, M.D.
Feinberg School of Medicine
737 N. Michigan Ave Ste 1600
Chicago, IL 60611
USA
Phone: +1 (312) 695-2422
jercolli@nm.org

Case Report: Clinical Usability of MyoMaps in Myocardial Infarction

Masashi Nakamura, M.D.

Diagnostic Radiology, Saiseikai Matsuyama Hospital, Matsuyama, Ehime, Japan

Introduction

Cardiac magnetic resonance (CMR) imaging offers a lot of information about myocardial tissue characterization with high spatial resolution, high-quality imaging and contrast. In the past, the key sequences for tissue characterization have been T1-weighted imaging for scar (late gadolinium enhancement: LGE) and T2-weighted imaging for edema. However, because with these two methods clinical cases are evaluated by visual interpretation of relative signal intensities in relation to normal myocardium (no quantification), there has been no agreement on a specific definition of 'abnormal signal'. Recent advances in CMR allow measurement and quantification of myocardial T1, T2, or T2* values (in ms) using short breathhold mapping sequences [1, 2]. The results are displayed in color-coded pixel maps where each pixel represents a physical estimate for T1, T2, or T2* in milliseconds. If the clinical context is known, T1, T2 and T2*mapping can provide useful information. Pre-contrast T1 (native T1) generally increases in conditions that increase total myocardial water, such as acute myocardial infarction (AMI), myocarditis, or stress cardiomyopathy. In addition, the myocardial extracellular volume (ECV) can be calculated from pre- and post-contrast T1 values of myocardial tissue and the blood pool together with the patients' hematocrit [1, 3]. It can quantify the myocardial extracellular space essentially without dependence on magnetic field intensity, amount of contrast medium and imaging parameters. T2 mapping depicts myocardial edema of acute myocardial infarction or myocarditis, while T2*mapping allows early detection of iron overload as in thalassemia.

MyoMaps is a new approach for quantification of myocardial tissue characteristics by Siemens Healthcare. Based on HeartFreeze Inline Motion Correction, MyoMaps provides pixel-based myocardial quantification for T1, T2 and T2*, on the fly [4, 5]. Pixel-based myocardial quantification and color mapping techniques enable a more accurate diagnostic characterization of cardiac territories.

CMR sequences

CMR imaging was performed at 3T (MAGNETOM Skyra, Siemens Healthcare, Erlangen, Germany) with an 18-element surface coil.

After the acquisition of scout images, Dark Blood T2w short axis images were obtained of the left ventricle using a Turbo SE sequence. Imaging parameters were as follows: TR 800 ms, TE 50 ms, flip angle 180°, slice thickness (SL) 6 mm, field-of-view

Case 1

Patient history

A 58-year-old male patient presented to our emergency department with chest pain and clammy sweat. ST-elevation of II, III, aVF was seen. Emergency invasive coronary angiography was performed, 90% stenosis was detected in right coronary artery (RCA) segment #2 (Fig. 1A). Percutaneous coronary intervention was performed in segment #2.

Imaging findings

CMR was performed for comprehensive myocardial assessment 6 days following onset. Short axis Dark Blood T2w (Fig. 1B) and LGE images (Fig. 1C) clearly demonstrate the presence of localized high intensity in inferior segment. With MyoMaps (Figs. 1D-F), the affected regions clearly demonstrate increased native T1 (1550 ms) and T2 (54 ms) values. Additionally, ECV was calculated for the same area as 67.6% compared to 25.2% for normal myocardium (T1 1210 ms, T2 36 ms).

Discussion

Imaging findings (Dark Blood T2w, LGE images) well agree with clinical course for inferior AMI (day 6 from onset, culprit vessel: RCA #2). Color images of T1 and T2 map clearly demonstrate the lesion. This case is a relatively localized lesion, where the native T1 maps demonstrate equivalent visual diagnostic capability to delayed-enhancement images. In addition, quantitative assessment (T1, T2 map and ECV) suggests edematous change and myocardial fibrosis in the area of the lesion. Thus, for this relatively localized lesion, the quantitative assessment allowed an accurate evaluation of myocardial tissue characteristics to support the diagnosis.

370 mm, matrix size 256 x 75%, voxel size 1.4 x 1.4 x 6 mm³, parallel imaging acceleration factor 2, ECG trigger pulse 2; turbo factor 13, fat sat, SPAIR. A gadolinium-based contrast agent (gadopentetate dimeglumine, Magnevist; Schering, Berlin, Germany) was administered intravenously at 0.1 mmol/kg body weight. LGE images were obtained using a TrueFISP IR single-shot and phase sensitive inversion recovery (PSIR) sequence about 10 min after the administration of contrast. The imaging parameters were as follows: TR 852 ms, TE 1.26 ms, echo spacing 3 ms; inversion time, measured by TI scout, flip angle 55°, SL 6 mm, FOV 350 mm, matrix size 224 x 65%, voxel size 1.6 x 1.6 mm, iPAT 2, ECG trigger pulse 2.

Pre-contrast T1 maps were obtained from three short-axis images (basal, mid, and apical) of the left ventricle using single shot TrueFISP based on modified look-locker inversion-recovery (MOLLI) sequence. The imaging parameters were as follows: TR 280.56 ms, TE 1.12 ms, echo spacing 2.7 ms, flip angle 35°, SL 8 mm, FOV 360 mm, matrix size 256 x 66%, voxel size 1.4 x 1.4 x 8 mm³, iPAT 2; MOLLI type 5(3)3 for long T1. Post-contrast T1 maps were obtained in the same locations as the pre-contrast T1 maps. The imaging parameters were as follows: TR 360.56 ms, TE 1.12 ms, echo spacing 2.7 ms, flip angle 35°, SL 8 mm, FOV 360 mm, matrix size 256 x 66%, voxel size 1.4 x 1.4 x 8 mm³, iPAT 2, MOLLI type 4(1)3(1) for short T1.

Pre-contrast T2 maps were obtained in the same locations as the pre-contrast T1 maps using a FLASH sequence with T2 preparation pulses. The imaging parameters were as follows: TR 207.39 ms, TE 1.32 ms, echo spacing 3.1 ms, FA 12°, SL 8 mm, FOV 360 mm, matrix size 192 x 75%; voxel size 1.9 x 1.9 x 8 mm³, iPAT2, T2 prep., duration 0, 30, 55 ms.

Conclusion

T1 and T2 mapping not only enables visual diagnosis but also offers pixel-based physical quantification of myocardial tissue characteristics in myocardial infarction. Thus, in our institutions, the number of MyoMaps examinations has increased over the recent months. Some of the reasons for this are:

1. Few burdens on patients (a single, short breathhold)
2. Non-contrast imaging for renal failure patients (Native T1 or T2 map)
3. Diagnosis of non-ischemic cardiomyopathy (assessment of minute lesions based on pixel-based color mapping)
4. Diagnosis of diffuse myocardial impairment (quantification)
5. Supporting MR image interpretation (objectivity vs quantification)

Current advances in T1- and T2-mapping and ECV quantification might have the potential to improve the diagnosis of cardiovascular disease, refine myocardial risk stratification and guide patient personalized therapeutic strategies.

References

1 Lundin M, Ugander M. Clinical Utility of Cardiac T1- and Extracellular Volume (ECV) Mapping. A Brief Review. MAGNETOM Flash 1/2015: 18-20.

2 Maestrini V, Abdel-Gadir A, Herrey AS, Moon JC. New Generation Cardiac Parametric Mapping: the Clinical Role of T1 and T2 Mapping. MAGNETOM Flash 5/2013: 104-107.

3 Schelbert EB, Wong TC. Clinical Benefits of T1 and ECV Mapping. MAGNETOM Flash 1/2015: 12-17.

4 Xue H, Greiser A, Zuehlsdorff S, Jolly MP, Guehring J, Arai AE et al. Phase-Sensitive Inversion Recovery for Myocardial T1 Mapping with Motion Correction and Parametric Fitting. Magn Reson Med. 2013 May; 69(5): 1408-1420.

5 Girl S, Shah S, Xui H, Chung YC, Pennell ML, Guehring J et al. Myocardial T2 Mapping With Respiratory Navigator and Automatic Nonrigid Motion Correction. Magn Reson Med. 2012 November; 68(5): 1570-1578.

Continued on page 30.

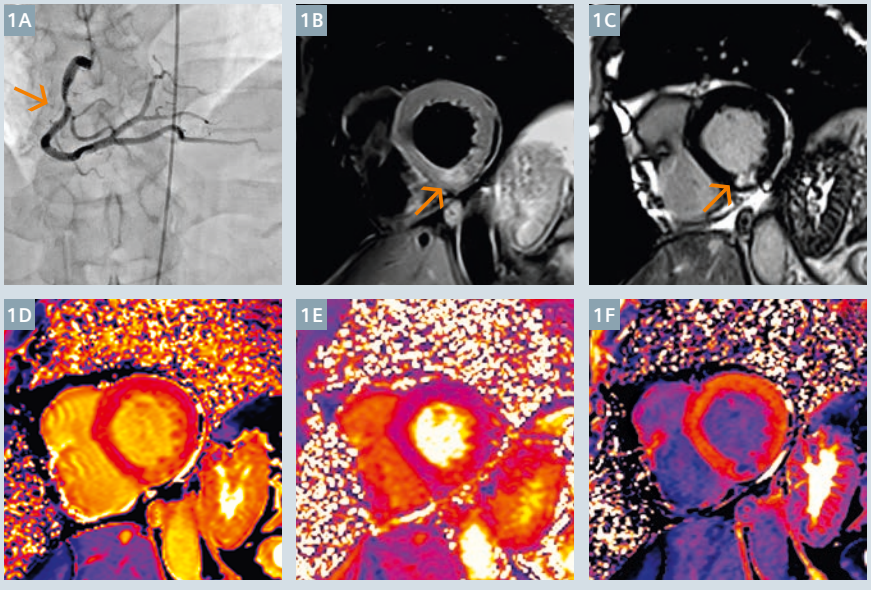

1 A 58-year-old male patient, inferior acute myocardial infarction. **(1A)** Right coronary artery (RCA) segment #2. **(1B)** Dark Blood T2w image with fat saturation. TSE_ELT 13, slice thickness (SL) 6 mm, FOV 312 x 370 mm, matrix 162 x 256, TR 800 ms, TE 50 ms. **(1C)** Late gadolinium enhancement (LGE), Tfi_segment 67, SL 6 mm, FOV 337 x 370 mm, matrix 133 x 224, TI 400 ms, TR 852, TE 1.26 ms. **(1D)** Native T1 map. Inversion recovery (IR) Tfi with motion correction (MOCO) and iPAT2. **(1E)** Native T2 map. T2prep Tfi with MOCO and iPAT2. **(1F)** Post-contrast T1 map. IR Tfi with MOCO and iPAT2.

Case 2

Patient history

A 66-year-old male patient presented to our emergency department with chest pain. High serum levels of CK (303 IU/L) and CK-MB (19.0) were seen. Acute myocardial infarction was suspected and emergency invasive coronary angiography was performed. 99% stenosis was detected in left coronary artery (LAD) segment #6 (Fig. 2A). Percutaneous coronary intervention was performed in segment #6.

Imaging findings

CMR was performed for myocardial viability assessment after 10 days of onset. Dark Blood T2-weighted imaging (Fig. 2B) shows slow moving blood signal (slow flow artifacts) in anterior-septal segments. LGE image (Fig. 2C) demonstrates transmural enhancement in the same segments, and subendocardial low intensity in the septal region. In MyoMaps (Figs. 2D-F), slow flow artifacts are not found in T2 map, and mild myocardial T2 prolongation is shown in anterior-septal segments. The enhanced regions demonstrate increased native T1 (1633 ms) and ECV (55.1%) compared to normal myocardium (native T1 1180 ms, ECV 25.7%). On the other hand, native T1 of subendocardial low intensity area (1200 ms) is approximately equivalent to normal myocardium.

Discussion

The findings on the Dark Blood T2w images are consistent with anterior and septal subacute myocardial infarction (culprit vessel: LAD #6). However, we may overestimate an edematous region due to slow flow artifacts by the cardiac hypofunction in Dark Blood T2w images. T2 map images do not show this artifact and are thus valuable for the correct diagnosis of the edematous region. In quantitative assessment, increased native T1 and ECV suggest myocardial fibrosis and edema. A subendocardial linear area of low signal intensity is shown within the delayed enhanced lesion, suggesting microvascular obstruction (MO). T1 is generally lower in hemorrhage or iron accumulation, but in this case, native T1 value of MO is approximately equivalent to normal myocardium (1200 ms and 1180 ms). It seems that simultaneous occurrence of both fibrosis and iron deposition offset each T1 prolongation effect and T1 shortening effect. In this patient emergency stent insertion was performed. Nonetheless, findings of not only transmural infarction but also MO in this case suggest myocardial viability of infarcted segment to be poor.

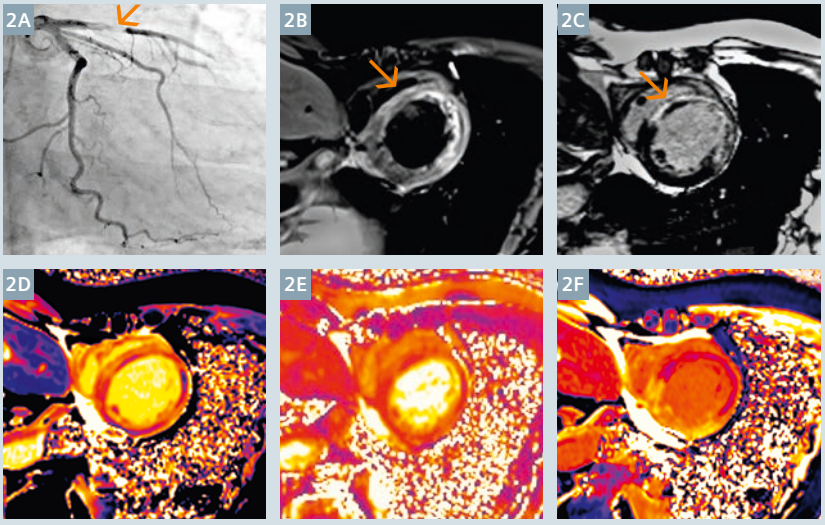

2 A 66-year-old man, septal subacute myocardial infarction. **(2A)** Left coronary artery (LAD) segment #6. **(2B)** DB T2w with fat sat. TSE_ELT 13, SL 6 mm, FOV 312 x 370 mm, matrix 162 x 256, TR 800 ms, TE 50 ms. **(2C)** LGE image. Tfi_segment 67, SL 6 mm, FOV 319 x 350 mm, matrix 133 x 224, TI 400 ms, TR 852 ms, TE 1.26 ms, TR/TE 2RR/1.3 ms. **(2D)** Native T1 map. IR Tfi with MOCO, SL 6 mm, FOV 307 x 360 mm, matrix 144 x 256. **(2E)** Native T2 map. T2prep Tfi with MOCO. SL 6 mm, FOV 289 x 360 mm, matrix 116 x 192. **(2F)** Post-contrast T1 map. IR Tfi with MOCO, SL 6 mm, FOV 307 x 360 mm, matrix 144 x 256.

Contact

Masashi Nakamura, M.D.
Saiseikai Matsuyama Hospital
Diagnostic Radiology
880-2, Yamanishi, Matsuyama
Ehime, 791-8026
Japan
Phone: +81-89-951-6111
m.nakamura1230@gmail.com

A smart addition to your team

Make a smart move with Bayer's new MR SMART Injection System.

The Medrad® MRXperion™ MR Injection System delivers improved efficiencies, personalized care and reproducible quality... all backed by on-site field service and VirtualCare® Remote Support for maximum uptime and patient throughput.

- Automated fluid delivery and streamlined workflow
- Modality worklist* connectivity and protocol storage/retrieval
- Accurate procedure data recording and reporting

Learn more and schedule a personalized demo today!

radiology.bayer.com

*Requires Certegra® @ Point of Care software.

MEDRAD® MRXperion™
MR Injection System

PP-MRX-US-0021 October 2015

Quiescent Interval Single-Shot (QISS) Lower Extremity MRA for the Diagnosis of Peripheral Artery Disease: Case Presentations

Akos Varga-Szemes[1]; Thomas M. Todoran[2]; Shivraman Giri[3]; Stephen R. Fuller[1]; U. Joseph Schoepf[1]

[1] Division of Cardiovascular Imaging, Department of Radiology and Radiological Science, Medical University of South Carolina, Charleston, SC, USA
[2] Division of Cardiology, Department of Medicine, Medical University of South Carolina, Charleston, SC, USA
[3] Siemens Healthcare, Chicago, IL, USA

Introduction

Peripheral artery disease (PAD) affects 12%–14% of the general population and its prevalence increases with patient age [1]. While segmental Doppler pressures and pulse volume recording are the most appropriate techniques for screening symptomatic patients, more sophisticated non-invasive imaging techniques may be necessary for further anatomic evaluation and treatment planning, especially before revascularization [2, 3]. The American College of Radiology (ACR) rates both CT angiography (CTA) and MR angiography (MRA) as "usually appropriate" diagnostic approaches for claudication with suspected vascular etiology [2]. Because many patients with PAD suffer from several comorbidities including renal insufficiency, the administration of either iodinated or gadolinium-based contrast media may be of concern given the increased risk of contrast-induced nephropathy or nephrogenic systemic fibrosis (NSF), respectively [4, 5].

These concerns with the risks of contrast media administration in combination with recent technical advances have led to an increased interest in non-contrast MRA techniques. Although many approaches to non-contrast MRA have been evaluated [6], most of them have limited clinical utility in patients with PAD due to either technical issues (e.g. long acquisition time) or overestimation of mild to moderate stenosis [7, 8].

Quiescent-interval single-shot (QISS) MRA is a recently introduced, robust non-contrast MRA technique [9]. QISS MRA at 1.5 and 3T has shown promising results with reported diagnostic accuracies close to or equal to contrast-enhanced MRA [10-14]. Here, we illustrate some of the benefits of QISS MRA over other modalities through two clinical cases and also provide a brief overview of the literature available for this technology.

Discussion

These cases demonstrate certain benefits of QISS MRA over CTA. As emphasized by ACR guidelines, the two major shortcomings limiting image interpretation of CTA in PAD patients are the relatively difficult acquisition timing following contrast administration due to reduced flow in the stenotic vessels and reduced lumen visibility due to heavily calcified atheromatous lesions [2]. As we have shown, QISS MRA is able to overcome both of these limitations to provide reliable findings comparable to invasive DSA.

The QISS MRA technique was first introduced in 2010 by Edelman et al. [9]. This ECG-triggered technique employs initial saturation pulses followed by a 2D single-shot balanced steady-state free precession readout with a quiescent interval between them.

Case 1

A 55-year-old male was referred for evaluation and treatment of intermittent claudication despite adherence to a regular walking program. The patient was a former smoker and his medical history included hyperlipidemia, hypertension, coronary artery disease, PAD, and ANCA-positive vasculitis. Physical examination revealed diminished femoral and popliteal pulses bilaterally. Posterior tibial and dorsalis pedis pulses were Dopplerable. His ankle-brachial index (ABI) was 0.78 in the right leg and 0.91 in the left leg at rest, while ABI severely decreased post exercise (0.53 and 0.52, respectively). In preparation for revascularization the patient was referred for a lower extremity run-off CTA. CTA demonstrated moderate to severe bilateral iliac and superficial femoral artery stenosis. The evaluation of calf vessels was inconclusive as the slower flow in the stenotic vessels delayed the arrival of contrast and thus acquisition occurred before peak enhancement was reached in these vessels. Prior to intervention, the patient underwent a non-contrast QISS MRA on a 1.5T MAGNETOM Avanto scanner. QISS MRA successfully visualized each arterial segment, including those poorly visualized on CTA. In addition to visualizing the stenosis already found on CTA, QISS MRA was able to delineate infrapopliteal run off to the feet. There was total occlusion of the right peroneal artery and total occlusion of the left anterior tibial and posterior tibial arteries. These findings were confirmed by invasive digital subtraction angiography (DSA).

Reprinted from MAGNETOM Flash 3/2015


CTA
QISS
DSA

Two saturation pulses are used: one to suppress the background signal, and one applied inferior to the slice to suppress the venous blood signal. The quiescent interval before the readout allows the inflow of unsaturated arterial spins into the imaging plane. Due to its design, the flow sensitivity of QISS MRA is negligible compared to other non-contrast techniques such as time-of-flight, 3D fast spin echo based approaches, and

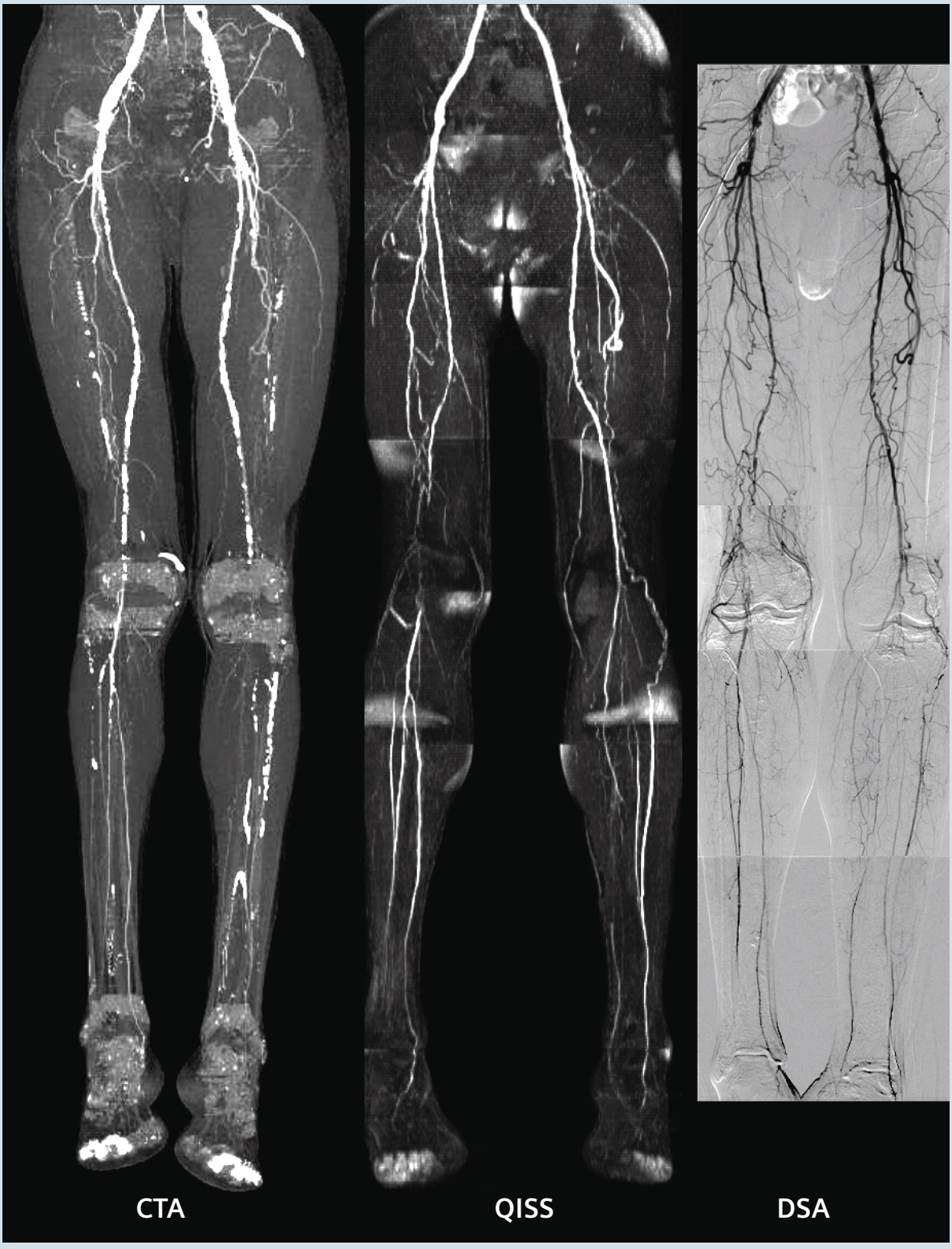

Reprinted from MAGNETOM Flash 3/2015

ungated ghost MRA [10]. Additionally, single-shot 2D TrueFISP acquisition makes this technique relatively insensitive to patient motion.

Novel technological innovations in development promise to further facilitate the clinical implementation of QISS MRA. QISS MRA can be performed without ECG gating by employing prospective self-navigation based on the detection of the acceleration of blood flow during systole with a reference-less phase contrast navigator [15]. Highly undersampled radial *k*-space readout enables the acquisition of multiple 2D slices in a single cardiac cycle shortening the acquisition time of a complete lower extremity runoff MRA to about 2 minutes [16]. High-resolution QISS MRA provides 1.5 mm section thickness and thus more detailed visualization of the vascular anatomy [17]. Quiescent interval low angle shot MRA provides superior image quality for the external carotid arteries compared to 2D time-of-flight with an average acquisition time of less than 6 minutes [18].

The diagnostic accuracy of non-contrast QISS MRA has been evaluated with non-invasive contrast-enhanced MRA as a reference standard, showing a segment-based sensitivity and specificity of 89.7% and 96.5%, respectively [11]. A subgroup analysis in patients who also underwent DSA showed substantial agreement between QISS MRA and DSA [12]. Similarily high sensitivity (98.6%) and specificity (96%) were reported for QISS MRA versus contrast-enhanced MRA in patients with PAD by Klasen et al. [13]. QISS MRA demonstrated superior specificity for detecting hemodynamically significant arterial stenosis in the lower extremities compared to subtracted 3D fast spin echo MRA and was also found to provide higher image quality and diagnostic accuracy in the abdominal and pelvic regions [19].

While the majority of initial QISS MRA studies were performed at 1.5T [9, 11, 12], QISS MRA has also shown good diagnostic accuracy at higher field strength. 3T QISS MRA has high sensitivity (100%) in the presence of adequate image quality for the detection of peripheral artery stenosis when compared to the DSA as a reference standard [14]. Later studies have confirmed the feasibility of QISS MRA at 3T and reported high diagnostic performance and high image quality, especially in the distal segments [20-22].

Conclusion

Past studies have shown that QISS MRA provides high diagnostic accuracy for the detection of hemodynamically significant arterial stenosis of the lower extremities at both 1.5 and 3T. QISS MRA seems to be a feasible alternative for patients in whom contrast media administration is contraindicated, especially in the light of the new ACR guidelines widening the population considered at risk for NSF to patients with eGFR <40 ml/min/1.73m^2 [23]. Furthermore, QISS MRA may avoid the timing-related difficulties of contrast-enhanced CTA and better visualize heavily calcified arteries. Finally, its relative insensitivity to blood-flow and patient motion simplifies the patient workflow by requiring minimal user input during the acquisition.

References

1 Hiatt WR, Hoag S, Hamman RF. Effect of diagnostic criteria on the prevalence of peripheral arterial disease. The San Luis Valley Diabetes Study. Circulation. 1995;91(5):1472-9.

2 Expert Panel on Vascular Imaging, Dill KE, Rybicki FJ, et al. ACR Appropriateness Criteria® Claudication - Suspected Vascular Etiology. Available at https://acsearch.acr.org/docs/69411/Narrative/. American College of Radiology. Accessed 10/19/2015.

3 Norgren L, Hiatt WR, Dormandy JA, et al. Inter-society consensus for the management of peripheral arterial disease. Int Angiol. 2007;26(2):81-157.

4 Davenport MS, Khalatbari S, Cohan RH, Dillman JR, Myles JD, Ellis JH. Contrast material-induced nephrotoxicity and intravenous low-osmolality iodinated contrast material: risk stratification by using estimated glomerular filtration rate. Radiology. 2013;268(3):719-28.

5 Kuo PH, Kanal E, Abu-Alfa AK, Cowper SE. Gadolinium-based MR contrast agents and nephrogenic systemic fibrosis. Radiology. 2007;242(3):647-9.

6 Miyazaki M, Lee VS. Nonenhanced MR angiography. Radiology. 2008;248(1):20-43.

7 Lim RP, Hecht EM, Xu J, et al. 3D nongadolinium-enhanced ECG-gated MRA of the distal lower extremities: preliminary clinical experience. J Magn Reson Imaging. 2008;28(1):181-9.

8 Haneder S, Attenberger UI, Riffel P, Henzler T, Schoenberg SO, Michaely HJ. Magnetic resonance angiography (MRA) of the calf station at 3.0 T: intraindividual

Case 2

A 65-year-old man was referred for evaluation and treatment of intermittent claudication. Relevant past medical history included hyperlipidemia, hypertension, carotid artery disease, subclavian artery disease, and PAD. Physical examination was remarkable for normal femoral pulses, diminished popliteal pulses and Dopplerable posterior tibial and dorsalis pedis pulses bilaterally. The patient's ABI in the right leg (0.72) was consistent with moderate ischemia, while ABI in the left leg (0.95) was within normal limits at rest. The patient was referred for a lower extremity CTA to plan for revascularization. This demonstrated occluded right superficial femoral, popliteal, anterior tibial, and peroneal arteries and left popliteal, peroneal, anterior tibial, and posterior tibial arteries. Complete lumen visibility was limited due to the presence of heavy calcification, especially in the superficial femoral arteries. As a result, the length of the occlusion could not be determined. Non-contrast QISS MRA (1.5T MAGNETOM Avanto) was performed and was able to sufficiently visualize the entire lower extremity runoff including the heavily calcified segments. QISS MRA provided superior image quality in the calves, visualizing the three vessel runoff in the right calf and the proximal total occlusion of all three left calf vessels filling via collaterals. QISS MRA findings were confirmed with subsequent DSA results.

comparison of non-enhanced ECG-gated flow-dependent MRA, continuous table movement MRA and time-resolved MRA. Eur Radiol. 2011;21(7):1452-61.
9 Edelman RR, Sheehan JJ, Dunkle E, Schindler N, Carr J, Koktzoglou I. Quiescent-interval single-shot unenhanced magnetic resonance angiography of peripheral vascular disease: Technical considerations and clinical feasibility. Magn Reson Med. 2010;63(4):951-8.
10 Offerman EJ, Hodnett PA, Edelman RR, Koktzoglou I. Nonenhanced methods for lower-extremity MRA: a phantom study examining the effects of stenosis and pathologic flow waveforms at 1.5T. J Magn Reson Imaging. 2011;33(2):401-8.
11 Hodnett PA, Koktzoglou I, Davarpanah AH, et al. Evaluation of peripheral arterial disease with nonenhanced quiescent-interval single-shot MR angiography. Radiology. 2011;260(1):282-93.
12 Hodnett PA, Ward EV, Davarpanah AH, et al. Peripheral arterial disease in a symptomatic diabetic population: prospective comparison of rapid unenhanced MR angiography (MRA) with contrast-enhanced MRA. AJR Am J Roentgenol. 2011;197(6):1466-73.
13 Klasen J, Blondin D, Schmitt P, et al. Nonenhanced ECG-gated quiescent-interval single-shot MRA (QISS-MRA) of the lower extremities: comparison with contrast-enhanced MRA. Clin Radiol. 2012;67(5):441-6.
14 Hansmann J, Morelli JN, Michaely HJ, et al. Nonenhanced ECG-gated quiescent-interval single shot MRA: Image quality and stenosis assessment at 3 tesla compared with contrast-enhanced MRA and digital subtraction angiography. J Magn Reson Imaging. 2014;39(6):1486-93.
15 Offerman EJ, Koktzoglou I, Glielmi C, Sen A, Edelman RR. Prospective self-gated nonenhanced magnetic resonance angiography of the peripheral arteries. Magn Reson Med. 2013;69(1):158-62.
16 Edelman RR, Giri S, Dunkle E, Galizia M, Amin P, Koktzoglou I. Quiescent-inflow single-shot magnetic resonance angiography using a highly undersampled radial k-space trajectory. Magn Reson Med. 2013;70(6):1662-8.
17 Thierfelder KM, Meimarakis G, Nikolaou K, et al. Non-contrast-enhanced MR angiography at 3 Tesla in patients with advanced peripheral arterial occlusive disease. PLoS One. 2014;9(3):e91078.
18 Koktzoglou I, Murphy IG, Giri S, Edelman RR. Quiescent interval low angle shot magnetic resonance angiography of the extracranial carotid arteries. Magn Reson Med. 2015.
19 Ward EV, Galizia MS, Usman A, Popescu AR, Dunkle E, Edelman RR. Comparison of quiescent inflow single-shot and native space for nonenhanced peripheral MR angiography. J Magn Reson Imaging. 2013;38(6):1531-8.
20 Knobloch G, Gielen M, Lauff MT, et al. ECG-gated quiescent-interval single-shot MR angiography of the lower extremities: initial experience at 3 T. Clin Radiol. 2014;69(5):485-91.
21 Amin P, Collins JD, Koktzoglou I, et al. Evaluating peripheral arterial disease with unenhanced quiescent-interval single-shot MR angiography at 3 T. AJR Am J Roentgenol. 2014;202(4):886-93.
22 Wagner M, Knobloch G, Gielen M, et al. Nonenhanced peripheral MR-angiography (MRA) at 3 Tesla: evaluation of quiescent-interval single-shot MRA in patients undergoing digital subtraction angiography. Int J Cardiovasc Imaging. 2015;31(4):841-50.
23 ACR Committee on Drugs and Contrast Media. ACR Manual on Contrast Media. Version 10.1. 2015.

Contact

Akos Varga-Szemes, M.D., Ph.D.
Division of Cardiovascular Imaging
Department of Radiology and Radiological Science
Medical University of South Carolina
25 Courtenay Drive, MSC 226
Charleston, SC 29425, USA
Phone +1 843-876-0097
Fax +1 843-876-3157
vargaasz@musc.edu

ESMRMB
European Society for Magnetic Resonance in Medicine and Biology

Lectures on MR 2016

Educational courses, exercises, and practical demonstrations on MR physics and engineering

Simultaneous multi-slice/ multiband imaging
January 18–20, Nijmegen/NL

Acquisition strategies for hyperpolarised spin systems: Spectral, spatial and temporal
February 24–26, Munich/DE

Quantitative MRI for characterising brain tissue microstructure NEW!
June 6–8, Leipzig/DE

Create your own echo: How to generate, calculate and manipulate echoes
June 20–22, Tübingen/DE

RF coils: Design, build and characterise your own
June 21–23, L'Aquila/IT

Non-Cartesian MRI: Implementation and application NEW!
August 25–28, Würzburg/DE

RF pulses: Design and applications
September 8–10, Krakow/PL

In vivo MR spectroscopy: From basics to advanced methods NEW!
September 26–28, Vienna/AT

www.esmrmb.org

Case Report: QISS MRA at 3T

Anna-Maria Lydon, PgDip MRI, DCR(R)[1]; Associate Professor Andrew Holden, MBChB, FRANZCR[2]; Dr. Jacobus Kritzinger, MBChB, FRCPC[2]

[1] Centre for Advanced MRI, Faculty of Medical & Health Sciences, University of Auckland; New Zealand
[2] Auckland City Hospital, New Zealand

Quiescent Interval Single-Shot (QISS) MR Angiography (MRA) has been shown to be a robust technique for non-contrast MRA of the peripheral vasculature at 1.5T. At 3T, early versions of the sequence offered greater signal-to-noise ratio (SNR) than at 1.5T, but were occasionally compromised by inversion pulse insufficiency due to B_1 inhomogeneities. This gave rise to poor venous suppression particularly in the abdominal and pelvic region. We had the opportunity to try a WIP version of the QISS MRA sequence with a modified FOCI pulse which was hoped to overcome aforementioned B_1 inhomogeneities and improve venous suppression whilst maintaining small vessel visualisation on 3T.

We present a case of a 69-year-old male who was referred with short distance left leg claudication, and reduced left femoral pulse, query iliac artery disease. He had a history of smoking 10 cigarettes per day. The patient was imaged on the 3T MAGNETOM Skyra (Siemens Healthcare, Erlangen, Germany) using the peripheral matrix coil in combination with the spine and body matrix coils. ECG gating was achieved using the Siemens wireless PMU.

At the time of imaging the patient had a heart rate of 68 bpm and a recent eGfr of 70 ml/min / 1.73 m^2.

QISS MRA sequences using TrueFISP readout were acquired as a vessel scout technique as this provides an excellent overview for planning subsequent contrast-enhanced (CE) MRA imaging. The standard QISS MRA was used which consists of 1 x 1 x 3 mm contiguous axial slices, single slice per RR interval, flip angle 90°, iPat 3, 40 slices per station. We acquired the abdominal stations during quiet respiration as we found our elderly population cope with this better than with breath-holds and there is no time penalty between techniques.

As per our standard protocol subsequent CE-MRA imaging was performed using diluted 20 ml Multihance (Gadobenate dimeglumine) + 10 ml 0.9% NaCl, followed by 0.9% NaCl flush. A test bolus of 1.5 ml contrast @ 2 ml/s followed by 20 ml 0.9% NaCl was sampled using a dynamic 2D FLASH single

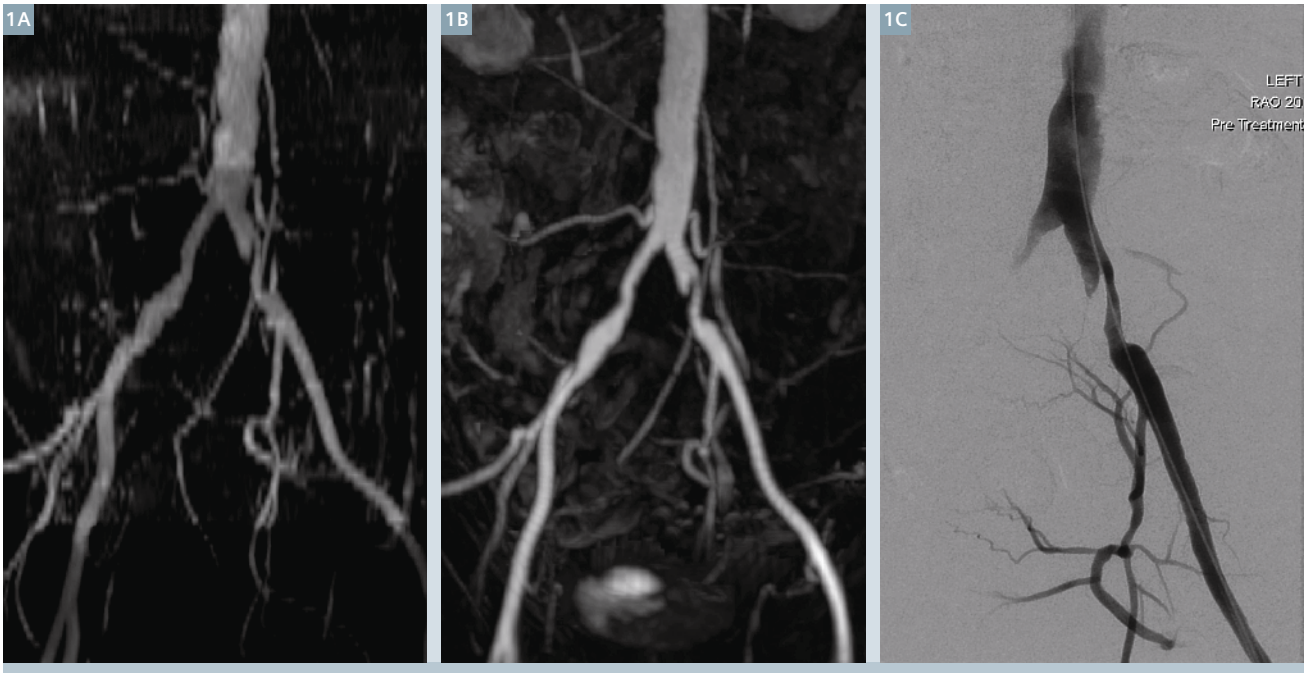

1 QISS MRA CE-MRA DSA

Reprinted from MAGNETOM Flash 3/2015

slice positioned at the level of the aortic bifurcation to determine the arrival time of the contrast in the abdominal aorta. Next the tibial arteries were imaged using time-resolved TWIST MRA sequence using 4 ml diluted contrast and a 20 ml NaCl flush delivered @ 2 ml/s. Finally, the full peripheral arterial tree is imaged from above the renal arteries to the pedal arteries using 22-23 ml diluted contrast delivered as follows:

Dual-phase contrast injection:
10 ml @ 2 ml/s, followed by
13 ml @ 1.5 ml/s then an NaCl flush of 20 ml @ 1 ml/s.

Findings included a high-grade stenosis of the mid left common iliac artery. There was also a mild-moderate stenosis of the proximal right common iliac artery. Femoral and popliteal arteries were of normal calibre. There was three vessel run-off to each calf, with severe disease of the left anterior tibial artery and vessel occlusion by mid-calf.

Follow-up DSA confirmed QISS MRA and CE-MRA findings, and the left common iliac artery lesion was treated by angioplasty and stenting with an 8 x 40 mm self-expanding stent, post dilated to 7 mm.

In this case QISS images correlated excellently with the CE-MRA images and subsequent DSA imaging as seen below. We have found that the optimized FOCI pulse is particularly effective in the aorto-iliac region and this case demonstrates very nicely how this new version of the sequence (now product) performs compared to CE-MRA and also DSA.

Acknowledgements

We would like to thank Dr Robert Edelman (Northwestern University, Chicago, IL, USA) and Shivraman Giri (Siemens Healthcare, USA) for providing us with this version of the WIP for evaluation. We would also like to thank Benjamin Schmitt (Siemens Healthcare, Australia) for his support.

Contact

Anna-Maria Patricia Lydon, PgDip MRI, DCR(R)
Charge MRI Technologist
The University of Auckland
Centre for Advanced MRI
Private Bag 92019
Auckland 1142, New Zealand
Phone: +64 9 923 9512
a.lydon@auckland.ac.nz

Learn more!

Quantification and speed. What else drives CMR into broader clinical use? Don't miss the talks of experienced and renowned experts at:

www.siemens.com/magnetom-world

Emerging Contributions of CMR in Cardiology

Dudley Pennell

Royal Brompton & Harefield (London, UK)

Need for Speed in CMR

James Carr

Northwestern Memorial Hospital (Chicago, IL, USA)

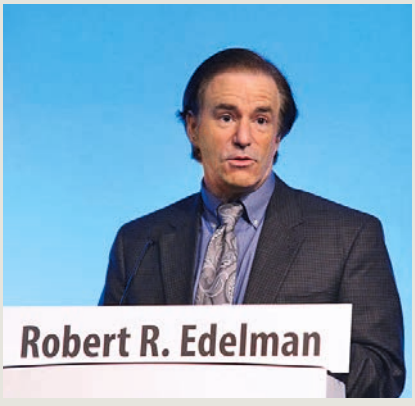

Advances in Non-CE MR Angiography

Robert R. Edelman

NorthShore University HealthSystem (Evanston, IL, USA)

Cardiac Diffusion Tensor MRI Using Simultaneous Multi-Slice Acquisition with a Blipped-CAIPIRINHA Readout

Choukri Mekkaoui[1]; Timothy G. Reese[1]; Marcel P. Jackowski[2]; Himanshu Bhat[3]; David E. Sosnovik[1,4]

[1] Athinoula A. Martinos Center for Biomedical Imaging, Department of Radiology, Massachusetts General Hospital, Harvard Medical School, Boston, MA, USA
[2] Department of Computer Science, Institute of Mathematics and Statistics, University of São Paulo, São Paulo, Brazil
[3] Siemens Healthcare, Charlestown, MA, USA
[4] Cardiovascular Research Center, Cardiology Division, Massachusetts General Hospital, Harvard Medical School, Boston, MA, USA

Background

Heart muscle is highly anisotropic with an intricate microstructure, well suited to characterization with diffusion tensor imaging (DTI) [1]. The most widely used measure of fiber organization in the myocardium is the helix angle (HA), simply defined as the inclination of the myofiber out of the local short-axis plane. Myofibers in the subendocardium have a positive HA, while those in the subepicardium have a negative HA [1, 2]. These myofibers are further arranged into laminar sheets, which slide against each other allowing the myocardium to thicken during systole [3, 4]. Alterations of this microstructure due to heart disease affect its mechanical efficiency and also could contribute to arrhythmias [5, 6]. These microstructural changes can precede symptoms and thus a non-invasive evaluation could be of significant clinical value.

The motion of the heart is five orders of magnitude greater than the self-diffusion of water. Therefore, approaches that are sensitive to the microscopic diffusion of water, but not to cardiac motion and strain, are needed for successful *in vivo* imaging [7-9]. One approach to enable *in vivo* DTI uses a diffusion-encoded stimulated echo (STE) sequence (Fig. 1), which can be implemented on most clinical scanners [10, 11]. The diffusion-encoded STE sequence is played out over two successive heartbeats. The first and second 90° excitation pulses are applied in the first heartbeat, and the third excitation pulse in the second heartbeat. The diffusion-encoding gradients are monopolar and placed immediately after the first and third excitation pulses. The main appeal of the STE approach is its conceptual immunity to cardiac motion. Ideally, each monopolar diffusion gradient occurs at exactly the same time in two sequential R-R intervals. Hence, not only is the phase due to the diffusion-encoding gradient unwound, but the influence of cardiac motion on the phase of the magnetization also is unwound.

The use of a STE sequence, however, introduces a high degree of inefficiency into the acquisition due to the dual-gated acquisition. Additionally, the STE is half the amplitude of a spin-echo. Consequently most investigators have used ~8 averages per slice in order to achieve sufficient signal-to-noise (SNR) during diffusion-encoded STE acquisitions, taking 5-7 minutes per slice [12]. The inefficiency of the STE approach frequently requires the anatomical coverage of the acquisition to be compromised. For instance, only 3 short-axis slices can be imaged in ~15 minutes, which covers only 25% of the myocardium [12]. New approaches to improve anatomical coverage and reduce scan time are thus sorely needed. The development of simultaneous multi-slice (SMS) acquisition using a blipped Controlled Aliasing in Parallel Imaging (blipped-CAIPIRINHA) readout holds great promise [13, 14], and could play a key role in facilitating the more widespread use of cardiac DTI.

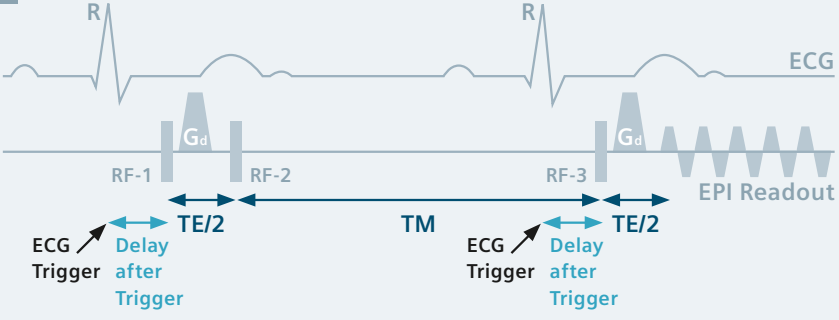

1 Dual gated stimulated echo (STE) sequence. Three 90° excitation pulses (RF) are applied over two successive heartbeats. The excitation (RF-1), refocusing (RF-3), and diffusion dephase and rephrase occur at the same time in the R-R intervals, thereby exploiting periodicity of heart motion to rewind motion related dephasing. Additionally, the long diffusion time (including TM), allows a sufficient b-value to be produced on clinical scanners without the need for an excessively long TE.

Reprinted from MAGNETOM Flash 3/2015

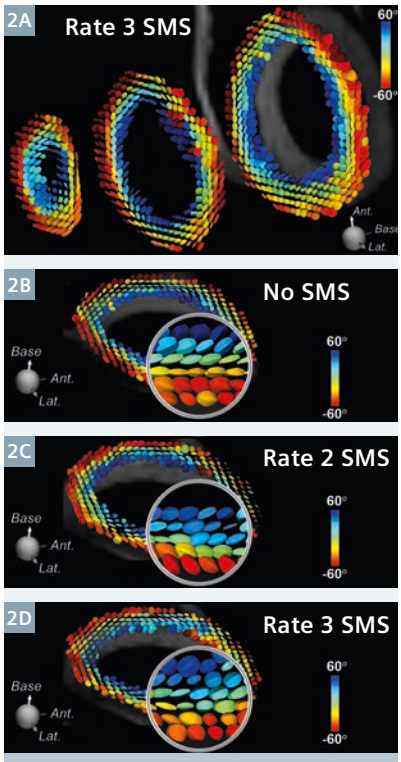

2 **(2A)** Simultaneous acquisition of 3 slices with rate 3 SMS. The gap between the slices is 500% of slice thickness. The tensor field is represented by supertoroids color-coded by HA. Supertoroid fields resulting from no SMS **(2B)**, rate 2 **(2C)**, and rate 3 **(2D)** SMS acquisitions of the same mid-ventricular slice are consistent with the transmural change in HA from positive in the subendocardium to negative in the subepicardium.

Implementation

The technical details of SMS excitation using blipped-CAIPIRINHA are described in detail in the SMS Supplement of MAGNETOM Flash (63) 3/2015. The technique has been used extensively in the brain [13, 14], and preliminary experience with it in the heart appears promising [15]. In the current article, we describe our experience with this technique for cardiac DTI in healthy volunteers.

Breath-hold DTI was performed on a clinical 3T scanner (MAGNETOM Skyra, Siemens Healthcare, Erlangen, Germany) with a 34-element receive coil[1] (18 anterior and 16 posterior elements). Images were acquired with a diffusion-encoded STE sequence, which was volume-selected in the phase-encode axis using a slab selective radiofrequency (RF) pulse. Acquisition parameters included: FOV 360 x 180 mm, resolution 2.5 x 2.5 x 8 mm^3, in-plane GRAPPA rate 2, TE 34 ms, b-value 500 s/mm^2, 10 diffusion-encoding directions, and 8 averages. Twelve short-axis slices were acquired in the systolic sweet spot of the cardiac cycle to mitigate strain effects [11, 16]. Imaging was performed with no SMS, and rates 2 and 3 SMS. HA was derived from the diffusion tensor, which was estimated from the diffusion-weighted images. Fiber tracts were constructed by integrating the primary eigenvector field into streamlines using an adaptive 5th order Runge-Kutta approach [5].

Results and impact

With no SMS, 96 breath-holds were required to cover the entire LV. Using rate 2 SMS, this was reduced to 48 breath-holds, and with rate 3 SMS to 32. With rate 3 SMS, the acquisition time was approximately 20 minutes for whole-heart coverage. Image quality was well preserved using both rates 2 and 3 SMS. This is demonstrated in Figure 2, where the diffusion tensor in each voxel is represented by the supertoroidal model [17]. The glyphs are parameterized by the magnitude and orientation derived from the diffusion tensor and color-coded by HA. The transmural evolution in HA from positive in the subendocardium to negative in the subepicardium is well resolved in all 3 slices with rate 3 SMS. Glyph fields using rates 2 and 3 SMS of a mid-ventricular slice compare favorably with those acquired with no SMS, and are consistent with expected transmural evolution in HA.

Tractography of the heart has previously been performed over a small anatomical range (3-5 slices) or with

[1] The product is still under development and not commercially available yet. Its future availability cannot be ensured.

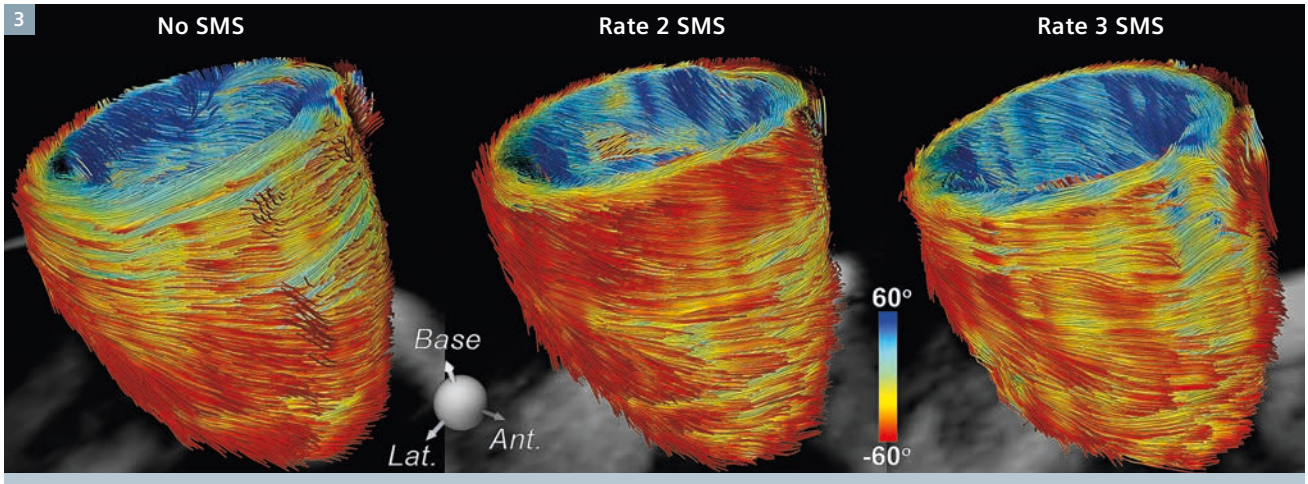

3 Tractography of the entire LV, color-coded by HA, of the same subject imaged with no SMS, and rates 2 and 3 SMS. Tracts obtained using rates 2 and 3 SMS compare favorably and are in agreement with those obtained with no SMS.

very large slice gaps. Meaningful tractography requires the entire heart to be imaged without any slice gaps. With no SMS, this takes over 60 minutes to acquire. However, as shown in Figure 3, fiber tracts of the entire LV were successfully obtained with rates 2 and 3 SMS, and are qualitatively comparable with those obtained with no SMS.

Discussion

DTI of the heart has the potential to improve the understanding, diagnosis and management of a range of cardiovascular diseases. However, the main limitation is long scan times. With current techniques, the acquisition of 3 short-axis slices takes ~20 minutes. We demonstrated that using SMS, scan time was reduced by 3-fold. The simultaneous acquisition of 3 slices (basal, medial, and apical), as shown in Figure 2, takes ~5 minutes. While imaging only 3 slices yields limited coverage of the LV, the utility of this approach has been demonstrated in first-pass perfusion studies of the heart [18]. The additional acquisition of DTI images in the same 3 short-axis slices would add little time to a clinical study and could be of substantial value.

DTI of the entire heart, while more demanding, could provide a unique way to evaluate myocardial microstructure. SMS combined with further technical advances may facilitate the clinical translation of whole-heart DTI, enabling the reliable characterization of myocardial structure in a wide range of patients with cardiac diseases.

References

1 Streeter DD, Jr., Spotnitz HM, Patel DP, Ross J, Jr., Sonnenblick EH. Fiber orientation in the canine left ventricle during diastole and systole. Circ Res. 1969;24(3):339-47.

2 Scollan DF, Holmes A, Winslow R, Forder J. Histological validation of myocardial microstructure obtained from diffusion tensor magnetic resonance imaging. Am J Physiol. 1998;275(6 Pt 2):H2308-18.

3 LeGrice IJ, Smaill BH, Chai LZ, Edgar SG, Gavin JB, Hunter PJ. Laminar structure of the heart: ventricular myocyte arrangement and connective tissue architecture in the dog. Am J Physiol. 1995;269(2 Pt 2):H571-82.

4 Dou J, Tseng WY, Reese TG, Wedeen VJ. Combined diffusion and strain MRI reveals structure and function of human myocardial laminar sheets in vivo. Magn Reson Med. 2003;50(1):107-13.

5 Mekkaoui C, Huang S, Chen HH, Dai G, Reese TG, Kostis WJ et al. Fiber architecture in remodeled myocardium revealed with a quantitative diffusion CMR tractography framework and histological validation. J Cardiovasc Magn Reson. 2012;14:70.

6 Trayanova NA. Whole-heart modeling: applications to cardiac electrophysiology and electromechanics. Circ Res. 2011;108(1):113-28.

7 Sosnovik DE, Wang R, Dai G, Reese TG, Wedeen VJ. Diffusion MR tractography of the heart. J Cardiovasc Magn Reson. 2009;11:47.

8 Nguyen C, Fan Z, Sharif B, He Y, Dharmakumar R, Berman DS et al. In vivo three-dimensional high resolution cardiac diffusion-weighted MRI: a motion compensated diffusion-prepared balanced steady-state free precession approach. Magn Reson Med. 2014;72(5):1257-67. doi:10.1002/mrm.25038.

9 Gamper U, Boesiger P, Kozerke S. Diffusion imaging of the in vivo heart using spin echoes--considerations on bulk motion sensitivity. Magn Reson Med. 2007;57(2):331-7. doi:10.1002/mrm.21127.

10 Reese TG, Weisskoff RM, Smith RN, Rosen BR, Dinsmore RE, Wedeen VJ. Imaging myocardial fiber architecture in vivo with magnetic resonance. Magn Reson Med. 1995;34(6):786-91.

11 Tseng WY, Reese TG, Weisskoff RM, Wedeen VJ. Cardiac diffusion tensor MRI in vivo without strain correction. Magn Reson Med. 1999;42(2):393-403.

12 Nielles-Vallespin S, Mekkaoui C, Gatehouse P, Reese TG, Keegan J, Ferreira PF et al. In vivo diffusion tensor MRI of the human heart: reproducibility of breath-hold and navigator-based approaches. Magn Reson Med. 2013;70(2):454-65.

13 Setsompop K, Cohen-Adad J, Gagoski BA, Raij T, Yendiki A, Keil B et al. Improving diffusion MRI using simultaneous multi-slice echo planar imaging. NeuroImage. 2012;63(1):569-80. doi:10.1016/j.neuroimage.2012.06.033.

14 Setsompop K, Gagoski BA, Polimeni JR, Witzel T, Wedeen VJ, Wald LL. Blipped-controlled aliasing in parallel imaging for simultaneous multislice echo planar imaging with reduced g-factor penalty. Magn Reson Med. 2012;67(5):1210-24. doi:10.1002/mrm.23097.

15 Lau AZ, Tunnicliffe EM, Frost R, Koopmans PJ, Tyler DJ, Robson MD. Accelerated human cardiac diffusion tensor imaging using simultaneous multislice imaging. Magn Reson Med. 2015;73(3):995-1004. doi:10.1002/mrm.25200.

16 Stoeck CT, Kalinowska A, von Deuster C, Harmer J, Chan RW, Niemann M et al. Dual-phase cardiac diffusion tensor imaging with strain correction. PLoS One. 2014;9(9):e107159. doi:10.1371/journal.pone.0107159.

17 Mekkaoui C, Chen IY, Chen HH, Kostis WJ, Pereira F, Jackowski MP et al. Differential response of the left and right ventricles to pressure overload revealed with diffusion tensor MRI tractography of the heart in vivo. Journal of Cardiovascular Magnetic Resonance. 2015;17(Suppl 1):O3-O. doi:10.1186/1532-429X-17-S1-O3.

18 Stab D, Wech T, Breuer FA, Weng AM, Ritter CO, Hahn D et al. High resolution myocardial first-pass perfusion imaging with extended anatomic coverage. J Magn Reson Imaging. 2014;39(6):1575-87. doi:10.1002/jmri.24303.

Timothy G. Reese

Choukri Mekkaoui

Contact

Choukri Mekkaoui
Athinoula A. Martinos Center for Biomedical Imaging
149 13th Street
Charlestown, MA 02129, USA
Phone: +1 617 724-3407
Fax: 617 726-7422
mekkaoui@nmr.mgh.harvard.edu

Self-Navigated Free-Breathing High-Resolution 3D Cardiac Imaging: A New Sequence for Assessing Cardiovascular Congenital Malformations

Pierre Monney, M.D.[1]; Davide Piccini[2]; Grégoire Berchier[1]; Tobias Rutz, M.D.[1]; Gabriella Vincenti[1]; Milan Prša, M.D.[3]; Nicole Sekarski, M.D.[3]; Matthias Stuber, Ph.D.[4]; Juerg Schwitter, M.D.[1]

[1] Division of Cardiology and Cardiac MR Center, University Hospital of Lausanne (CHUV), Lausanne, Switzerland
[2] Advanced Clinical Imaging Technology, Siemens Healthcare IM BM PI, Lausanne, Switzerland
[3] Unit of Pediatric Cardiology, Department of Pediatrics, University Hospital Lausanne (CHUV), Lausanne, Switzerland
[4] Department of Radiology, University Hospital (CHUV) and University of Lausanne (UNIL) / Center for Biomedical Imaging, (CIBM), Lausanne, Switzerland

Introduction

Congenital cardiac malformations occur in 9.1 per 1,000 live births [1] and range from simple defects including bicuspid aortic valve or isolated restrictive ventricular septal defect, to complex malformations requiring surgical correction or palliation early in life. While the neonatal mortality with such complex malformations remained stable, an important increase in life expectancy has been achieved with the advances in surgical treatment and the majority of the patients can nowadays reach adulthood [2].

As a consequence of this increase in life expectancy, the population of adult patients with congenital heart disease is growing [3]. Despite an optimal surgical correction or palliation, a regular follow-up of these patients is mandatory as they remain at higher risk for long-term cardiac complications including arrhythmia and heart failure [4, 5]. Cardiac imaging plays an important role in the follow-up of these patients to assess the morphology and function of the cardiac chambers and the valves, and to assess the integrity of any surgically implanted material. While echo-cardiography is used as the first-line imaging modality for initial diagnosis and follow-up assessments, cardiac magnetic resonance (CMR) is the modality of choice for the assessment of

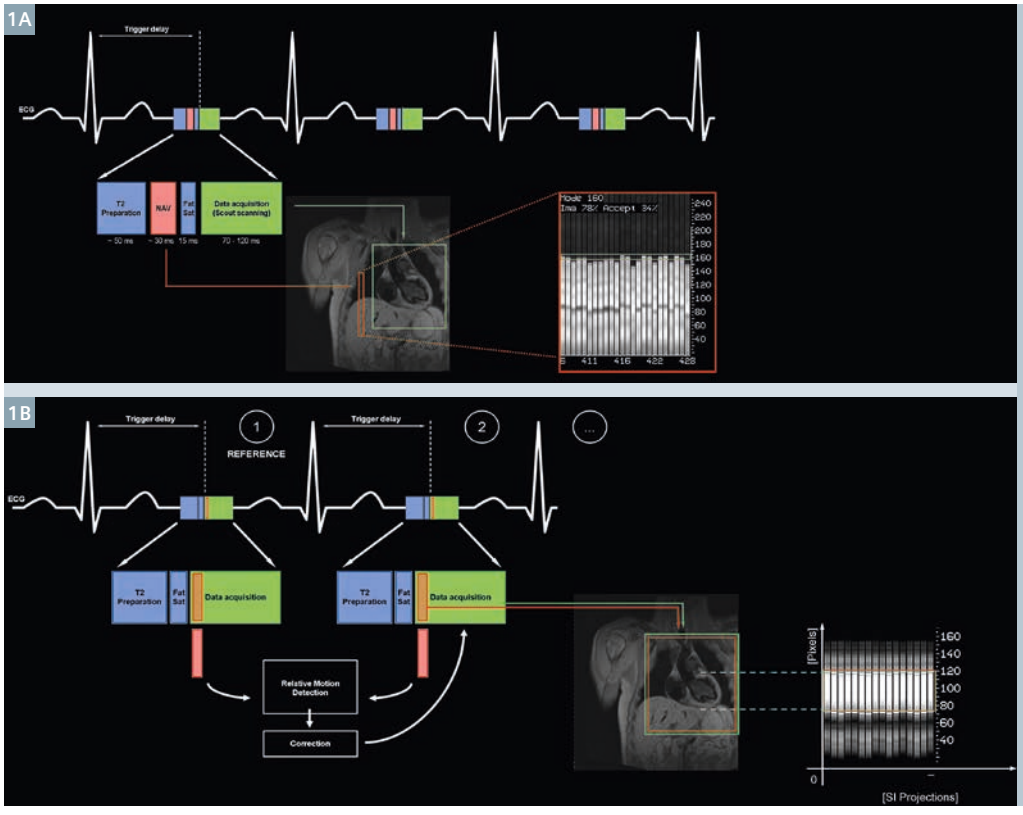

1 (**1A**) To consistently acquire data at the same respiratory position, a narrow acceptance window is defined, corresponding to the end-expiration, and only data acquired within this window are utilized in the final image reconstruction, while all other data segments are rejected and reacquired later during the scan. (**1B**) The position of the heart at the beginning of each data segment is compared with a reference position, i.e. the position of the ventricular blood-pool at the very first data segment, and automatically corrected for respiratory motion before the data are sent to the reconstruction pipeline.

the right ventricle, the pulmonary arteries and veins, and for imaging extracardiac shunts or conduits [5].

Several consensus papers from scientific societies provide recommendations for standard CMR protocols adapted to the different cardiac malformations [6-9]. Three-dimensional whole-heart acquisitions are now routinely performed, especially for more complex malformations, as they allow the acquisition of a full volume of data during one single imaging sequence, including the heart and the intra-thoracic vessels. This volume of data can be explored freely and specific 2D images can be extracted in any plane orientation during post-processing.

As CMR acquisitions are relatively slow and a high spatial resolution is required, the acquisition has to be segmented over several heartbeats. Additionally, the amount of data is so large that it cannot be acquired during one single breath-hold and respiratory motion compensation is needed for an adequate data acquisition during free-breathing.

Self-navigation: a new concept for respiratory motion compensation

Initially developed for coronary artery visualization, three-dimensional whole-heart navigator-based acquisitions have been used for over a decade to also assess the complex anatomy of congenital cardiac malformations [10]. These sequences rely on diaphragmatic respiratory navigation, where a pencil-beam navigator, usually placed on the dome of the right hemi-diaphragm, detects the respiratory position of the liver-lung interface along the superior-inferior direction for every heartbeat [11]. To consistently acquire data at the same respiratory position, a narrow acceptance window is defined, corresponding to the end-expiration, and only data acquired within this window are utilized in the final image reconstruction, while all other data segments are rejected and reacquired later during the scan (Fig. 1A). However, respiratory motion of the right hemidiaphragm and the heart are not tightly coupled, in particular during irregular breathing, when this correlation changes. As a result, data quality, especially during longer scans, can be inadequate if patients start to breath irregularly. In addition, with the navigator approach, acquisition duration is unpredictable and scan efficiency is typically in the order of 40% [12].

In order to address these limitations, respiratory self-navigation has been developed for coronary artery imaging [13-15]. With this strategy, the position of the heart itself is monitored over time and this approach should therefore also be robust in cases of irregular breathing. In addition, the respiratory motion information is extracted directly from the ventricular blood-pool signal throughout the respiratory cycle, so that navigator placement is not needed [13]. The prototype imaging sequence consists of a segmented 3D radial acquisition, intrinsically robust against motion, undersampling and foldover artifacts, with T2 and fat-saturation pre-pulses, and a balanced Steady-State Free Precessing (bSSFP) readout. The arrangement of the radial lines in *k*-space follows a spiral phyllotaxis pattern [16], with the first radial line of each acquired data segment (at each heartbeat) being consistently oriented in the superior-inferior direction, allowing for a 1D-detection of the cardiac displacement during the respiratory cycle. The position of the heart at the beginning of each data segment is thus compared with a reference position, i.e. the position of the ventricular blood-pool at the very first data segment, and automatically corrected for respiratory motion before the data are sent to the reconstruction pipeline (Fig. 1B). With this acquisition scheme, the respiratory motion correction reliably tracks the heart position and scan efficiency is typically 100%.

Characteristics of the sequence and planning strategy

With the current version of this prototype sequence[1], a cubic field-of-view of 180-240 mm³ is acquired with a 3D isotropic spatial resolution of 0.9-1.15 mm³. Other important imaging parameters are TR 3.1 ms, TE 1.65 ms, matrix size (192)³, receiver bandwidth 898 Hz/pixel, and RF excitation angle of 90°-115°. The trigger delay is selected to match one of the quiescent periods of the cardiac cycle – either mid-diastole or end-systole – previously identified on a standard four-chamber cine acquisition of the heart. The temporal resolution is adapted to the duration of the quiescent cardiac period, and may range from 18 to over 100 ms. A higher temporal resolution (= a lower number of lines per segment) has to be compensated by a higher number of heartbeats (= a higher number of shots) to ensure an adequate filling of the *k*-space. As a rule of thumb, we made sure that a minimum of 20% of the Nyquist sampling of *k*-space lines (= number of shots x number of lines per segment) were acquired, corresponding to a 6 to 12-minute scan duration, depending on the heart rate of the patient. The Nyquist undersampling ratio can be easily assessed by a tooltip that pops up when hovering the mouse pointer over the 'Radial Views' parameter in the Resolution tab.

The self-navigated 3D whole-heart acquisition is easy to use, as it avoids the placement of a pencil-beam navigator on the right hemi-diaphragm. The planning of the sequence is performed in two steps: 1) the *coil-localizer sequence* (allowing an automated selection of the receiver coils that will best detect the blood-pool signal for respiratory navigation) [17], and 2) the *data acquisition sequence*. The coil-localizer sequence is first selected, and the planning is simply using the axial, sagittal and coronal localizers. On each of these orthogonal planes, the cubic volume of acquisition is displayed as a square field-of-view, which has to be centered on the left ventricular blood-pool. A saturation band is placed on the anterior thoracic fat to reduce striking artifacts (Fig. 2). The coil-localizer sequence is

[1] The product is still under development and not commercially available yet. Its future availability cannot be ensured.

Reprinted from MAGNETOM Flash 3/2015

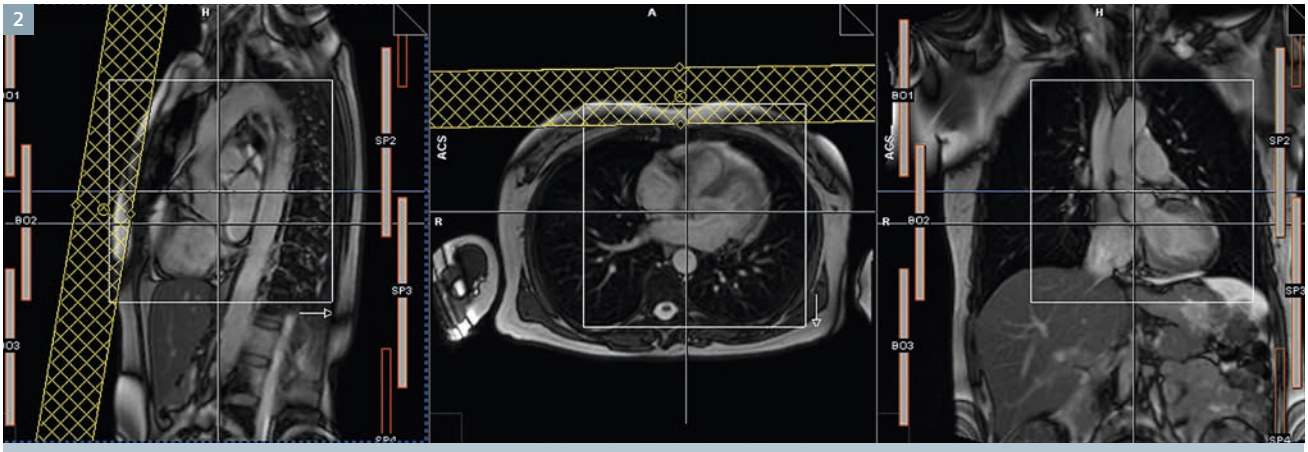

2 The cubic field-of-view is simply placed on the heart, while keeping the left ventricular blood-pool roughly in the center. A saturation band is placed on the anterior thoracic fat to reduce striking artifacts.

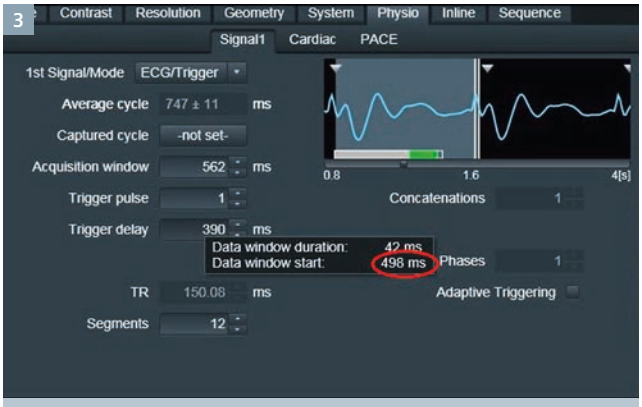

3 The trigger delay is selected, such that the data window start matches the onset of the quiescent period previously identified.

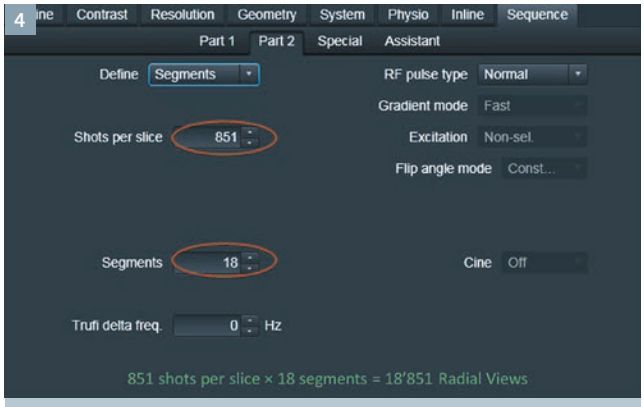

4 Depending on the duration of the quiescent period, the duration of the acquisition window can be modified, together with the number of heartbeats of acquisition (shots per slice), in order to keep the number of acquired *k*-space profiles over the above mentioned 20% of the Nyquist limit.

started without a breath-hold, typically lasting a total of about 10 sec. The data acquisition sequence is then opened, and the positions of the acquisition volume and of the saturation band are simply copied from the coil-localizer sequence. The trigger delay is selected, such that the data window start matches the onset of the quiescent period previously identified (Fig. 3). Depending on the duration of the quiescent period, the duration of the acquisition window can be modified, together with the number of heartbeats of acquisition (shots per slice), in order to keep the number of acquired *k*-space profiles over the above mentioned 20% of the Nyquist limit (Fig. 4). The sequence is then started during free-breathing, and the quality of respiratory tracking can be checked in real time throughout the data acquisition, using the inline monitor (Fig. 5).

Experience in patients with congenital heart disease

Early experience with 3D self-navigated cardiac imaging was gained from small series of volunteers aiming at the visualization of the coronary arteries [13-15]. These early studies reported a good performance of the sequence with an image quality that was equal or better than that obtained with

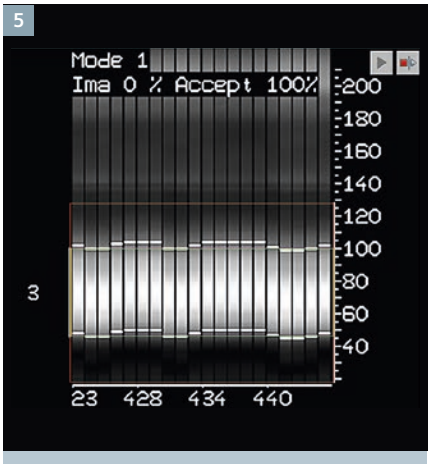

5 The quality of respiratory tracking can be checked in real time throughout the data acquisition, using the inline monitor.

conventional diaphragm navigation [13]. The first single-center experience on patients was also reported for coronary artery assessment [14]. 78 patients were included, and the self-navigated 3D sequence was used with a spatial resolution of 1.15 x 1.15 x 1.15 mm^3. The proximal segments of the coronary arteries were visualized in 92% of cases and the distal segments in 56%. When compared to invasive coronary angiography (available for comparison in 31 patients), the sensitivity and specificity for the detection of a significant coronary artery stenosis were 65% and 85%, respectively.

The first experience using the sequence for the characterization of congenital heart malformations was recently reported in a single-center series of 105 patients [18]. All examinations were performed on a 1.5T MAGNETOM Aera (Siemens Healthcare, Erlangen, Germany). The cohort included patients with ages ranging from 2 to 56 years (55% were males), and 44% had a complex cardiac malformation. The majority of the datasets (87%) were acquired after intravenous contrast injection (Gadovist, Bayer Schering Pharma, Zurich, Switzerland). While no direct head-to-head comparison with the conventional 3D whole-heart imaging sequence using diaphragm navigation was performed, this study aimed to assess the diagnostic performance and the image quality obtained with the new self-navigated sequence.

Using the 3D whole-heart self-navigated sequence alone, the systematic segmental anatomy of the heart and great vessels was correctly described in 93% to 96% of cases (by two different readers) and 93% to 95% of the residual uncorrected defects were correctly identified. Images were of diagnostic quality in 90% of cases and 70% were of good to excellent quality. Injection of intravenous contrast before image acquisition was associated with an improvement in image quality, resulting in a diagnostic image quality in 94% and a good to excellent image quality in 77% of the contrast-enhanced datasets. The origin and proximal course of the coronary arteries were visualized in 93%, 87% and 98% of the cases for the left anterior descending, left circumflex and right coronary artery, respectively, and all four patients of the cohort with an abnormal course of the coronary arteries were correctly identified. Finally, the measurement of the great arteries' diameters were very robust with a high intra-observer (coefficient of variation 3.5%) and inter-observer (coefficient of variation 5.0%) agreement.

27% of the patients were of pediatric[2] age (age <16) and the performance of the self-navigated 3D sequence also showed good results in this population. Despite the fact that fewer datasets were of good to excellent quality in children, a diagnostic image quality was obtained as frequently as in adult patients. This slight reduction in image quality might be attributed to a shorter quiescent period of the cardiac cycle with higher heart rates, or to the fact that dephasing artifacts, which may occur with high-velocity flows, more severely obscured the small vascular structures of pediatric patients.

Figure 6 shows 2D images reconstructed from a 3D whole-heart dataset acquired with self-navigation in a 47-year-old man with unoperated pulmonary atresia with a ventricular septal defect (VSD). 6A shows a large anterior mal-alignment VSD (*) with an overriding aorta. The branch pulmonary arteries are hypoplastic (6B) and there is fibrous atresia of the main pulmonary artery, located immediately behind the left atrial appendage (arrow on 6C).

Another example of complex cardiac anatomy is presented in Figure 7. This 27-year-old patient was born with

[2] MR scanning has not been established as safe for imaging fetuses and infants under two years of age. The responsible physician must evaluate the benefit of the MRI examination in comparison to other imaging procedures.

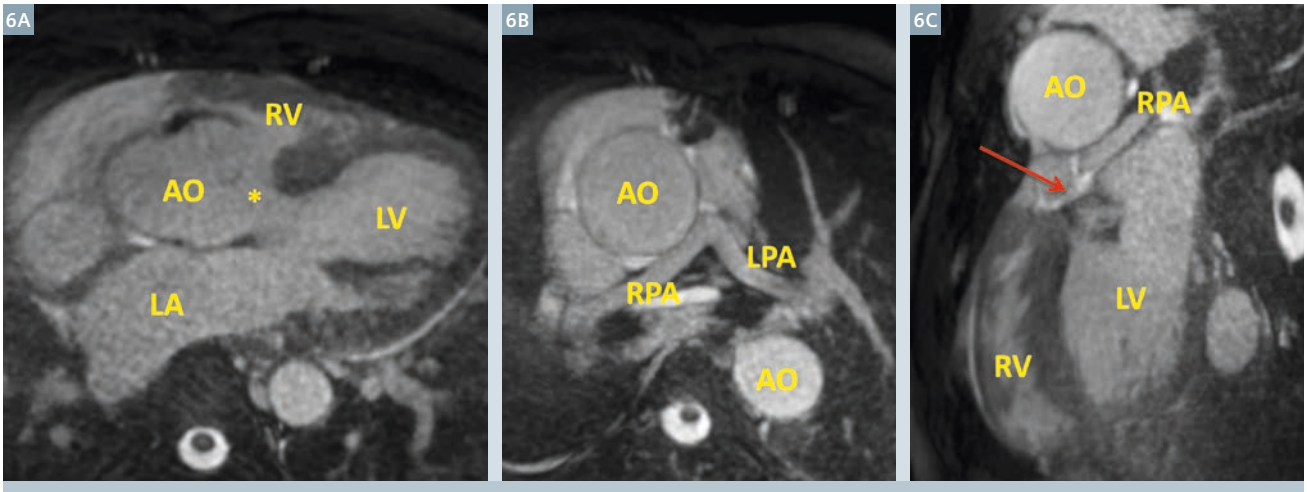

6 2D images reconstructed from a 3D whole-heart dataset acquired with self-navigation in a 47-year-old man with unoperated pulmonary atresia with a ventricular septal defect (VSD). **6A** shows a large anterior mal-alignment VSD (*) with an overriding aorta. The branch pulmonary arteries are hypoplastic (**6B**) and there is fibrous atresia of the main pulmonary artery, located immediately behind the left atrial appendage (arrow on **6C**).

right atrial isomerism, complete atrioventricular septal defect, total anomalous pulmonary venous return (TAPVR) and a single ventricle of right ventricular morphology. He underwent surgical correction of the TAPVR, followed by a bilateral Glenn operation and an extracardiac Fontan operation. 7A shows a large central liver and no spleen. The inferior vena cava (IVC) is located anterior to the descending aorta (AO). 7B shows the single ventricle with the typical characteristics of a right ventricle, connected to the ascending aorta. The systemic venous return is presented on 7C: both the right-sided superior vena cava (SVC) and the persistent left SVC are connected to the pulmonary arteries (bilateral Glenn), whereas the IVC is connected to the left pulmonary artery through an extracardiac conduit. 7D shows the normal-sized branch pulmonary arteries.

Good performance of the 3D self-navigated cardiac sequence is also demonstrated in children [18], as shown in the example presented in Figure 8. This 6-year-old patient, born with d-transposition of the great arteries, underwent an arterial switch operation. To connect the aorta to the left ventricle and the pulmonary artery to the right ventricle, the main pulmonary artery has to be displaced anteriorly to the ascending aorta by the surgeon. 8A shows the typical anterior

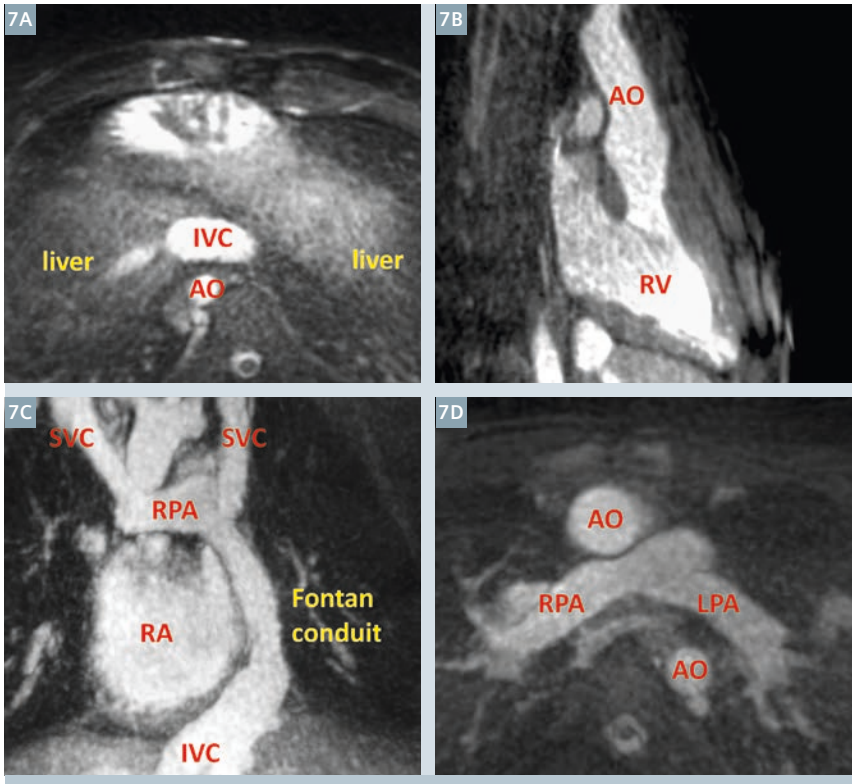

7 This 27-year-old patient was born with right atrial isomerism, complete atrioventricular septal defect, total anomalous pulmonary venous return (TAPVR) and a single ventricle of right ventricular morphology. He underwent surgical correction of the TAPVR, followed by a bilateral Glenn operation and an extracardiac Fontan operation. **7A** shows a large central liver and no spleen. The inferior vena cava (IVC) is located anterior to the descending aorta (AO). **7B** shows the single ventricle with the typical characteristics of a right ventricle, connected to the ascending aorta. The systemic venous return is presented on **7C**: both the right-sided superior vena cava (SVC) and the persistent left SVC are connected to the pulmonary arteries (bilateral Glenn), whereas the IVC is connected to the left pulmonary artery through an extracardiac conduit. **7D** shows the normal-sized branch pulmonary arteries.

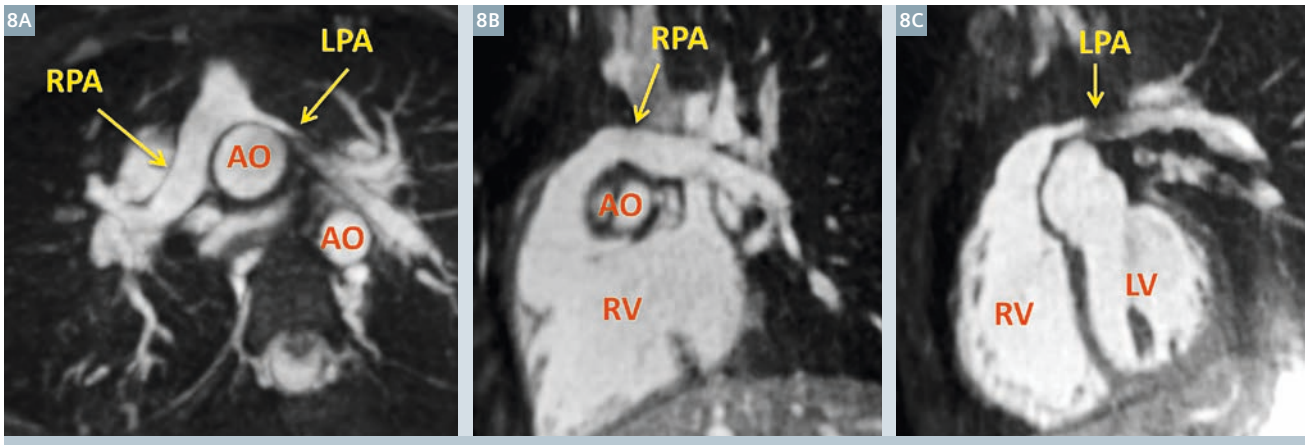

8 This 6-year-old patient, born with d-transposition of the great arteries, underwent an arterial switch operation. To connect the aorta to the left ventricle and the pulmonary artery to the right ventricle, the main pulmonary artery has to be displaced anteriorly to the ascending aorta by the surgeon. **8A** shows the typical anterior position of the main pulmonary artery with the branch pulmonary arteries running on either side of the aorta. In this patient, the right pulmonary artery is of normal size (**8B**) while the left pulmonary artery appears compressed by the ascending aorta. Flow acceleration in the LPA induces dephasing of the spins and appears as a low-signal artifact in the vessel (**8C**).

position of the main pulmonary artery with the branch pulmonary arteries running on either side of the aorta. In this patient, the right pulmonary artery is of normal size (8B) while the left pulmonary artery appears compressed by the ascending aorta. Flow acceleration in the LPA induces dephasing of the spins and appears as a low-signal artifact in the vessel (8C).

Abnormal origin or course of the coronary arteries can be successfully detected with this sequence, as shown in Figure 9. This 4-year-old patient is known for a surgically corrected tetralogy of Fallot, associated with a coronary abnormality. As shown on 9A, all 3 coronary arteries originate from a single main stem connected to the right coronary sinus of the aortic root. On 9B, the course of the left anterior descending artery (LAD) is anterior to the main pulmonary artery. The left circumflex artery (LCx) has a proximal course between the aorta and the atria (9C), while the right coronary artery (RCA) has a normal course around the tricuspid annulus (9D). Such morphology – especially the presence of a LAD running anterior to the main pulmonary artery, is associated with a risk of coronary artery damage during the surgical correction of the right ventricular outflow tract obstruction. A precise identification of the coronary anatomy in these patients is therefore essential.

Discussion and conclusion

The self-navigated 3D cardiac imaging sequence is characterized by a great ease of use and a low operator interaction. The radial acquisition scheme renders the sequence immune to foldover artifacts and a high isotropic resolution is obtained over a relatively large field-of-view. The temporal resolution can be individually adapted to the heart rate, i.e. the duration of the quiescent period of the cardiac cycle, resulting in a 6 to 12 min acquisition duration, which can be known *a priori*.

With these characteristics, the sequence can be easily added to the standard imaging protocol of patients with congenital cardiac malformations. The performance of the sequence was considered very good in this population with a diagnostic image quality obtained in 94% of contrast-enhanced datasets and 93 to 96% of residual defects correctly detected. Despite the fact that very young children <2 years old were not included in the reported study, the performance of this sequence was good in the pediatric population[2] as well [18].

Further improvements are likely to be implemented to this sequence in the future, including the development of 3D rather than 1D respiratory motion compensation algorithms [19, 20], or strategies to selectively remove *k*-space lines associated with extreme respiratory positions [21], which were shown to further improve image quality.

In conclusion, the 3D self-navigated cardiac imaging sequence is characterized by its high robustness while providing high temporal and high isotropic spatial resolution. It may serve as an attractive tool for the three-dimensional assessment of congenital heart malformations in adults and children.

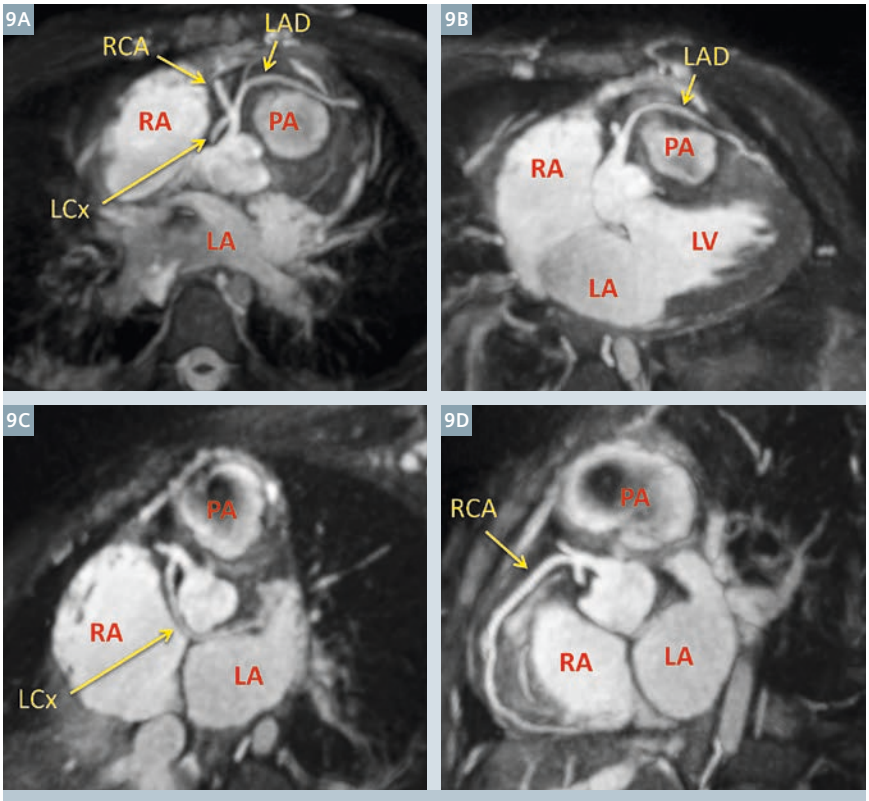

9 This 4-year-old patient has surgically corrected tetralogy of Fallot, associated with a coronary abnormality. As shown on **9A**, all 3 coronary arteries originate from a single main stem connected to the right coronary sinus of the aortic root. On **9B**, the course of the left anterior descending artery (LAD) is anterior to the main pulmonary artery. The left circumflex artery (LCx) has a proximal course between the aorta and the atria (**9C**), while the right coronary artery (RCA) has a normal course around the tricuspid annulus (**9D**).

Acknowledgement

The authors would like to thank all the members of the Center for Cardiac Magnetic Resonance of the CHUV (CRMC, Prof Juerg Schwitter MD) and of the Center for Cardiovascular MR Research (CVMR, Prof Matthias Stuber PhD), as well as the

[2] MR scanning has not been established as safe for imaging fetuses and infants under two years of age. The responsible physician must evaluate the benefit of the MRI examination in comparison to other imaging procedures.

MR technologists team at the CHUV for their active and excellent collaboration during this study. An important acknowledgement also goes to our colleagues from the pediatric cardiology unit and from the adult congenital heart disease clinic at the CHUV, Lausanne. Finally, we want to thank the Siemens Healthcare MR Cardio team of Edgar Müller in Erlangen.

References

1 van der Linde D, Konings EE, Slager MA, et al. Birth prevalence of congenital heart disease worldwide: a systematic review and meta-analysis. Journal of the American College of Cardiology 2011;58:2241-7.

2 Wren C, O'Sullivan JJ. Survival with congenital heart disease and need for follow up in adult life. Heart 2001;85:438-43.

3 Marelli AJ, Mackie AS, Ionescu-Ittu R, Rahme E, Pilote L. Congenital heart disease in the general population: changing prevalence and age distribution. Circulation 2007;115:163-72.

4 Bouchardy J, Therrien J, Pilote L, et al. Atrial arrhythmias in adults with congenital heart disease. Circulation 2009;120:1679-86.

5 Baumgartner H, Bonhoeffer P, De Groot NM, et al. ESC Guidelines for the management of grown-up congenital heart disease (new version 2010). European heart journal 2010;31:2915-57.

6 Kilner PJ, Geva T, Kaemmerer H, Trindade PT, Schwitter J, Webb GD. Recommendations for cardiovascular magnetic resonance in adults with congenital heart disease from the respective working groups of the European Society of Cardiology. European heart journal 2010;31:794-805.

7 Kilner P, Valsangiacomo Buechel E, Schwitter J. Congenital Heart Diseases in Adults. In: Schwitter J, ed. CMR Update. 2. Edition ed. Lausanne, Switzerland: Schwitter, J. www.herz-mri.ch; 2012:136-55.

8 Fratz S, Chung T, Greil GF, et al. Guidelines and protocols for cardiovascular magnetic resonance in children and adults with congenital heart disease: SCMR expert consensus group on congenital heart disease. Journal of cardiovascular magnetic resonance : official journal of the Society for Cardiovascular Magnetic Resonance 2013;15:51.

9 Valsangiacomo Buechel ER, Grosse-Wortmann L, Fratz S, et al. Indications for cardiovascular magnetic resonance in children with congenital and acquired heart disease: an expert consensus paper of the Imaging Working Group of the AEPC and the Cardiovascular Magnetic Resonance Section of the EACVI. European heart journal cardiovascular Imaging 2015;16:281-97.

10 Sorensen TS, Korperich H, Greil GF, et al. Operator-independent isotropic three-dimensional magnetic resonance imaging for morphology in congenital heart disease: a validation study. Circulation 2004;110:163-9.

11 Wang Y, Rossman PJ, Grimm RC, Riederer SJ, Ehman RL. Navigator-echo-based real-time respiratory gating and triggering for reduction of respiration effects in three-dimensional coronary MR angiography. Radiology 1996;198:55-60.

12 Kato S, Kitagawa K, Ishida N, et al. Assessment of coronary artery disease using magnetic resonance coronary angiography: a national multicenter trial. J Am Coll Cardiol 2010;56:983-91.

13 Piccini D, Littmann A, Nielles-Vallespin S, Zenge MO. Respiratory self-navigation for whole-heart bright-blood coronary MRI: methods for robust isolation and automatic segmentation of the blood pool. Magnetic resonance in medicine 2012;68:571-9.

14 Piccini D, Monney P, Sierro C, et al. Respiratory self-navigated postcontrast whole-heart coronary MR angiography: initial experience in patients. Radiology 2014;270:378-86.

15 Stehning C, Bornert P, Nehrke K, Eggers H, Stuber M. Free-breathing whole-heart coronary MRA with 3D radial SSFP and self-navigated image reconstruction. Magnetic resonance in medicine 2005;54:476-80.

16 Piccini D, Littmann A, Nielles-Vallespin S, Zenge MO. Spiral phyllotaxis: the natural way to construct a 3D radial trajectory in MRI. Magnetic resonance in medicine 2011;66:1049-56.

17 Piccini D, Marechal B, Coppo S, et al. Automated and Subject-Specific Coil Selection for Respiratory Self-Navigation in Coronary MRA. Proc Intl Soc Mag Reson Med. Milan2014:2503.

18 Monney P, Piccini D, Rutz T, et al. Single centre experience of the application of self navigated 3D whole heart cardiovascular magnetic resonance for the assessment of cardiac anatomy in congenital heart disease. Journal of cardiovascular magnetic resonance : official journal of the Society for Cardiovascular Magnetic Resonance 2015;17:55.

19 Henningsson M, Prieto C, Chiribiri A, Vaillant G, Razavi R, Botnar RM. Whole-heart coronary MRA with 3D affine motion correction using 3D image-based navigation. Magnetic resonance in medicine 2014;71:173-81.

20 Pang J, Sharif B, Arsanjani R, et al. Accelerated whole-heart coronary MRA using motion-corrected sensitivity encoding with three-dimensional projection reconstruction. Magnetic resonance in medicine 2014.

21 Chaptinel J, Piccini D, Coppo S, Bonanno G, Schwitter J, Stuber M. Optimized Data Selection for 3D Radial Self-Navigated Whole-Heart Coronary MRA. MRA Club; 2013; New York City, New York, USA.

Further reading

For more images and quantitative analyses on this study, please refer to the newly published paper in Reference 18.

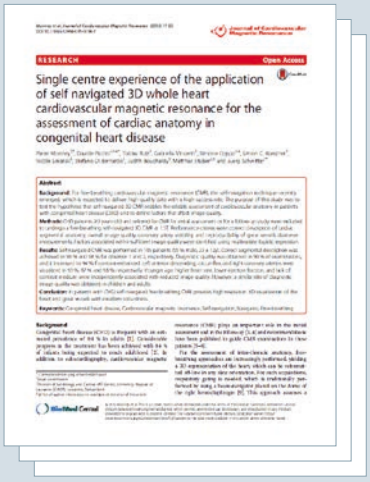

Pierre Monney

Juerg Schwitter

Contact

Professor Juerg Schwitter
Médecin Chef Cardiologie
Directeur du Centre de la RM Cardiaque du CHUV
Centre Hospitalier Universitaire Vaudois – CHUV
Rue du Bugnon 46, 1011 Lausanne, Switzerland
Phone: +41 21 314 0012
jurg.schwitter@chuv.ch
www.cardiologie.chuv.ch

Utility of Delayed Enhanced Cardiac MRI in the Assessment of Cardiomyopathies

Mohamad G. Ghosn, Ph.D.[1]; Kongkiat Chaikriangkrai, M.D.[1]; Itamar Birnbaum, M.D.[2]; Gary McNeal, MS (BME)[3]; Dipan J. Shah, M.D.[1]

[1] Houston Methodist Hospital, Houston, TX, USA
[2] Baylor College of Medicine, Houston, TX, USA
[3] Siemens Healthcare, Malvern, PA, USA

Introduction

Heart failure (HF) is a major public health problem in the United States, with over 5 million individuals afflicted, and well over 600,000 new cases diagnosed each year resulting in a direct and indirect cost in the United States of nearly $35 billion annually [1]. While coronary artery disease (CAD) is the leading cause of left ventricular (LV) dysfunction, anywhere from a third to a half of all patients have LV dysfunction in the absence of significant epicardial CAD [2]. Most of these patients are labeled with the general diagnosis of idiopathic non-ischemic cardiomyopathy (NICMP), as no direct discernable etiology of their myocardial dysfunction is evident. Identification of the specific etiology of HF in these patients with NICMP can have important prognostic implications [3]. However the traditional imaging modalities such as echocardiography, nuclear scintigraphy, or coronary angiography are limited in their ability to specifically evaluate the myocardium and to perform tissue characterization. In fact even the utility of endomyocardial biopsy is uncertain because of frequent non-specific findings, and the inherent invasiveness and small but finite risk of the procedure [4].

In recent years, delayed contrast enhancement (DE) cardiac magnetic resonance (CMR) has emerged as a powerful non-invasive technique for direct assessment of myocardial structure and tissue characterization. Studies have demonstrated its ability to detect both irreversible acute ischemic injury and chronic myocardial infarction (MI) with a high level of accuracy [5-8]. Using this same technique in patients with NICMP has enabled the detection of unique patterns of myocardial scarring which aid in identifying a specific etiology of NICMP and therefore help provide additional prognostic information and occasionally drastically alter patient management. The focus of this article will be to describe the potential role of DE-CMR in assessment of patients with cardiomyopathy.

Idiopathic dilated cardiomyopathy

An early study by McCrohon et al. [9] studied a population of 90 patients with heart failure and LV dysfunction consisting of 63 with idiopathic dilated cardiomyopathy and 27 with ischemic cardiomyopathy. Of the 27 patients with ischemic cardiomyopathy, all had a history of myocardial infarction and all had a myocardial hyperenhancement pattern involving the subendocardium. Of the 63 patients with idiopathic dilated cardiomyopathy, 59% had no hyperenhancement, 13% had hyperenhancement involving the subendocardium (similar to that found in ischemic cardiomyopathy) and 28% had hyperenhancement in

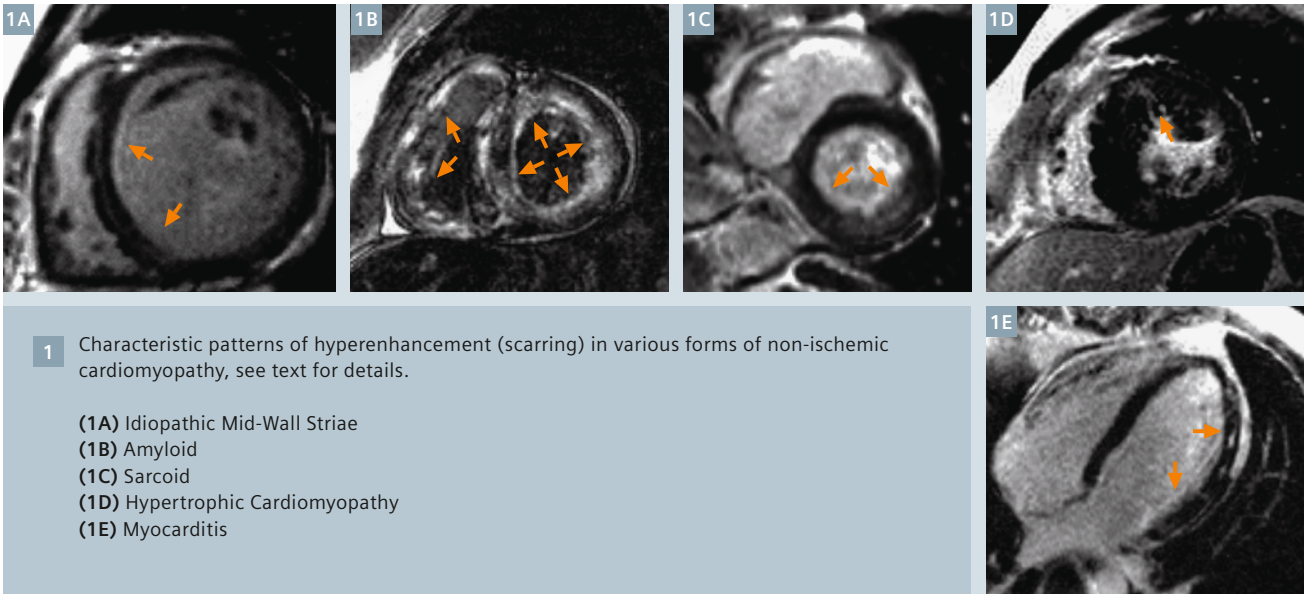

1 Characteristic patterns of hyperenhancement (scarring) in various forms of non-ischemic cardiomyopathy, see text for details.

(1A) Idiopathic Mid-Wall Striae
(1B) Amyloid
(1C) Sarcoid
(1D) Hypertrophic Cardiomyopathy
(1E) Myocarditis

Reprinted from MAGNETOM Flash 3/2015

an unusual pattern, primarily involving the ventricular midwall with subendocardial sparing.

In a recent study we evaluated 45 patients with symptomatic heart failure and evidence of significant LV systolic dysfunction (LVEF < 35% on invasive ventriculography or echocardiography). 28 patients had ischemic cardiomyopathy and 17 had idiopathic dilated cardiomyopathy. In this study, hyperenhancement patterns consistent with prior myocardial infarction were identified; linear midwall striae with increased image intensity were not scored as hyperenhanced regions. Interestingly, the findings demonstrated that all patients with ischemic cardiomyopathy had hyperenhancement, whereas only 12% of patients with idiopathic dilated cardiomyopathy had hyperenhancement. When we tested clinical parameters for their utility in distinguishing ischemic from non-ischemic cardiomyopathy, we found that the best discriminator was the presence of hyperenhancement on DE-MRI which had a 100% sensitivity, 88% specificity, and 96% overall accuracy for the detection of ischemic disease.

In this study, 100% of patients with ischemic cardiomyopathy had evidence of hyperenhancement, despite the fact that only 50% had clinical history of myocardial infarction. This finding is consistent with necropsy studies that have demonstrated that virtually all patients with congestive heart failure and significant coronary artery disease have gross myocardial scarring at autopsy, even in those without clinical history of MI, angina, or Q-waves [10, 11]. Conversely, we observed in patients with idiopathic dilated cardiomyopathy that hyperenhancement was uncommon. This finding is also consistent with previous studies. Roberts et al. [12] found grossly visible scars at cardiac necropsy in 14% of patients with idiopathic dilated cardiomyopathy. Uretsky et al. [13] evaluated chronic heart failure patients at autopsy and found old infarcts in 12% of patients without coronary artery disease. A number of mechanisms may be responsible for myocardial infarction in patients without coronary artery disease, including coronary vasospasm, thrombosis with spontaneous lysis superimposed on minimal atherosclerosis, or coronary emboli. Regardless of the mechanism, myocardial infarction in the absence of coronary artery disease is rare, and the findings in this study suggest that DE-MRI may be useful in distinguishing ischemic from non-ischemic cardiomyopathy non-invasively. One caveat, however, should be noted. The non-CAD cohort in the study by McCrohon [9] included only patients with idiopathic dilated cardiomyopathy, as patients with other forms of non-ischemic cardiomyopathy, such as hypertrophic cardiomyopathy, myocarditis, and infiltrative cardiomyopathy, were excluded at the time of enrollment.

Hypertrophic cardiomyopathy

Hypertrophic cardiomyopathy (HCM) is the most frequently occurring genetic cardiomyopathy [14]. Several studies have described DE-MRI findings in patients with hypertrophic cardiomyopathy (HCM). Choudhury et al. [15] enrolled 21 patients who were thought to be representative of the majority of community patients with HCM, since they were identified by routine outpatient screening procedures and were generally asymptomatic or minimally symptomatic. Patients with concomitant CAD were excluded. In this study, cine MRI demonstrated that the maximum LV end-diastolic wall thickness averaged 25 ± 8 mm, and the LV ejection fraction was preserved (70 ± 11%). DE-MRI demonstrated that hyperenhancement was found in the majority of patients (81%), and hyperenhancement mass was on average 8 ± 9% of the left ventricular mass. The pattern of hyperenhancement, however, was peculiar. Hyperenhancement occurred only in hypertrophied regions, was patchy with multiple foci, and predominately involved the middle third of the ventricular wall. Additionally, all patients with hyperenhancement had involvement at the junctions of the interventricular septum and the RV free wall. On a regional basis, there was a modest correlation between the extent of hyperenhancement and end-diastolic wall thickness ($r = 0.36$, $p < 0.0001$). No region with end-diastolic wall thickness < 10 mm had any hyperenhancement. There was also a significant but inverse correlation between the extent of hyperenhancement and systolic wall thickening ($r = -0.21$, $p < 0.0001$).

Although a number of pathophysiological processes are evident in hypertrophic cardiomyopathy, Choudhury et al. interpreted hyperenhancement in HCM as specifically representing myocardial scarring. The rationale for this assumption is discussed at length in an editorial [16] and data by Moon et al. [17] suggests that this assumption is valid. In a patient that underwent heart transplantation after *in vivo* DE-MRI, followed by detailed histological analysis of the explanted heart, there was a significant relationship, regionally, between the extent of hyperenhancement and the amount of myocardial fibrosis ($r = 0.7$, $p < 0.0001$) but not disarray.

Moon et al. [18] performed DE-MRI in 53 patients selected from a dedicated HCM clinic. Overall, hyperenhancement was found in 79% of patients, a figure quite similar to that found by Choudhury et al. This study, however, also compared DE-MRI findings to the presence of clinical risk factors for sudden death in HCM (e.g. non-sustained ventricular tachycardia, syncope, family history of premature cardiac death, etc.), and to progressive adverse LV remodeling. Interestingly, the authors observed that there was a greater extent of hyperenhancement in patients with two or more risk factors for sudden death (15.7% vs. 8.6%, $p = 0.02$) and in patients with progressive remodeling (28.5% vs. 8.7% of LV mass, $p < 0.001$).

Since hyperenhancement was observed in approximately 80% of patients in both the study by Choudhury et al. and Moon et al., the presence of hyperenhancement in itself cannot be indicative of an adverse prognosis. However, it is possible that the amount of hyperenhancement – indicative of the amount of

scarring – may be an important prognostic determinant. This hypothesis is currently being tested in observational clinical trials.

Myocarditis

Clinical manifestation of myocarditis or inflammatory cardiomyopathy varies with a broad spectrum of symptoms ranging from asymptomatic signs to myocardial infarction and cardiogenic shock. Myocarditis can occasionally lead to sudden death and may progress to dilated cardiomyopathy in up to 10% of patients [19]. Endomyocardial biopsy is considered as gold standard for diagnosis. It is an invasive procedure and has limited sensitivity and specificity. A noninvasive and effective diagnostic imaging modality is CMR. Cine imaging shows wall motion abnormalities that are matched by areas of scar on DE-CMR. The scar pattern frequently involves the epicardial myocardium of the lateral wall.

Mahrholdt et al. [19] performed DE-MRI in 32 patients who were diagnosed with myocarditis by clinical criteria. Hyperenhancement was found in 28 of 32 patients (88%). Of the 21 patients in whom myocardial biopsy was obtained from the region of hyperenhancement, histopathological analysis revealed active myocarditis in 19. Hyperenhancement was usually observed in a patchy distribution originating primarily from the epicardial quartile of the wall with one or several foci with a predilection for the lateral free wall. The pattern and distribution of hyperenhancement found in this study are consistent with that of myocardial lesions found in postmortem evaluations in patients with myocarditis [20]. The potential mechanism for hyperenhancement in myocarditis was postulated to be similar to that for coronary artery disease: either acute necrosis with cell membrane rupture for acute lesions, or myocardial scarring and fibrosis for chronic lesions. If true, this mechanism would imply that the presence, location, and total extent of irreversible myocardial damage that occurs in a patient with myocarditis could be determined noninvasively by DE-MRI.

Amyloid

Cardiac involvement is seen with primary amyloidosis (AL) and is an example of infiltrative cardiomyopathy [24]. Cardiac amyloid is associated with a poor prognosis with a median survival of 6 months [24, 25]. Diagnosis of cardiac involvement requires multiple endomyocardial biopsies, each biopsy specimen has a 55% sensitivity for the detection of amyloid protein [26]. CMR is a noninvasive diagnostic tool that can identify patients and guide biopsies to areas of scarring for improved sensitivity. Cine CMR shows a restrictive morphology. DE-CMR shows early diffuse heterogeneous enhancement and this proves difficult to null the myocardial signal at standard inversion time (TI). This leads to difficulty in distinguishing normal from abnormal myocardium. Inversion time scout images are obtained over a range of TI times to identify the TI time corresponding to the null point of the blood-pool and the myocardium. Amyloid protein deposits in the intercellular spaces and this plays a major role in the pattern of hyperenhancement seen on DE-CMR. According to Maceira et al. there was 97% concordance in diagnosis of cardiac amyloid by combining the presence of late gadolinium enhancement and an optimized T1 threshold (191 ms at 4 minutes) between myocardium and blood. DE-CMR pattern shows scar in the subendocardium and mid wall distributions [27].

Sarcoidosis

Myocardial involvement is evident in about 5% of patients with sarcoidosis, however, autopsy studies have shown up to 50% of cases of noncaseating granulomas in fatal sarcoidosis [28]. In one study by Smedema et al. CMR was performed for evaluation of cardiac sarcoidosis in 58 patients with biopsy proven pulmonary sarcoidosis and it showed a DE-CMR pattern mostly involving basal and lateral segments in 19 patients [29]. In 8 of the 19 patients patchy scar was present. The sensitivity and specificity of CMR were 100% and 78%, and the positive and negative predictive values were 55% and 100%, respectively, with an overall accuracy of 83%. Sudden cardiac death is a leading cause of mortality in this population [30]. We hypothesize that the presence and extent of hyperenhancement on DE-CMR may be directly related to the risk of sudden cardiac death in this population.

Risk stratification for sudden death

Scarred myocardium is an established anatomical and electrophysiological substrate for the occurrence of ventricular tachyarrhythmias and sudden death in patients with CAD [31]. The ability of DE-MRI to accurately detect the presence and extent of scarred myocardium may make it uniquely suited to noninvasively identify individuals with substrate for sudden death. Some recent pilot data comparing DE-MRI findings to results at electrophysiological study (EPS) suggests that this hypothesis is valid [32]. For example, of the total of 58 patients studied, 18 were determined to be at high risk for sudden death by EPS (inducible monomorphic ventricular tachycardia), and all 18 had myocardial scarring on DE-MRI. Conversely, none of the 22 patients without scarring had inducible monomorphic VT. On multivariate analysis, scar size by DE-MRI was found be the best independent predictor of inducibility at EPS.

Earlier in this section, we noted that hyperenhancement can be observed in patients with non-ischemic cardiomyopathy, particularly in those with hypertrophic and infiltrative forms of disease. Although there is currently less evidence linking scarred myocardium to sudden death in patients without CAD, there is reason to believe that scar tissue can serve as substrate for malignant ventricular tachyarrhythmias in these patients as well [16]. Therefore, we hypothesize that DE-MRI will provide important prognostic information for patients with a wide range of myocardial disorders. Studies are currently underway to evaluate for a relationship between sudden cardiac death and the presence, extent, or morphology of myocardial scar.

Conclusion

Delayed enhancement CMR is proving to be an invaluable tool in the evaluation of patients with cardiomyopathy. Although a number of studies have been performed in the past decade, significant work still remains to be done. The utility of CMR on evaluation of cardiomyopathies is yet to be fully explored; the authors speculate that CMR will be an integral part of the evaluation of these patients for years to come.

References

1 Rosamond, W., et al., Heart Disease and Stroke Statistics 2008 Update. A Report From the American Heart Association Statistics Committee and Stroke Statistics Subcommittee. Circulation, 2007.

2 Fox, K.F., et al., Coronary artery disease as the cause of incident heart failure in the population. Eur Heart J, 2001. 22(3): p. 228-36.

3 Felker, G.M., et al., Underlying causes and long-term survival in patients with initially unexplained cardiomyopathy. N Engl J Med, 2000. 342(15): p. 1077-84.

4 Hunt, S.A., et al., ACC/AHA 2005 Guideline Update for the Diagnosis and Management of Chronic Heart Failure in the Adult: a report of the American College of Cardiology/American Heart Association Task Force on Practice Guidelines (Writing Committee to Update the 2001 Guidelines for the Evaluation and Management of Heart Failure): developed in collaboration with the American College of Chest Physicians and the International Society for Heart and Lung Transplantation: endorsed by the Heart Rhythm Society. Circulation, 2005. 112(12): p. e154-235.

5 Kim, R.J., et al., Relationship of MRI delayed contrast enhancement to irreversible injury, infarct age, and contractile function. Circulation, 1999. 100(19): p. 1992-2002.

6 Fieno, D.S., et al., Contrast-enhanced magnetic resonance imaging of myocardium at risk: distinction between reversible and irreversible injury throughout infarct healing. J Am Coll Cardiol, 2000. 36(6): p. 1985-91.

7 Hillenbrand, H.B., et al., Early assessment of myocardial salvage by contrast-enhanced magnetic resonance imaging. Circulation, 2000. 102(14): p. 1678-83.

8 Kim, R.J., et al., The use of contrast-enhanced magnetic resonance imaging to identify reversible myocardial dysfunction. N Engl J Med, 2000. 343(20): p. 1445-53.

9 McCrohon, J.A., et al., Differentiation of heart failure related to dilated cardiomyopathy and coronary artery disease using gadolinium-enhanced cardiovascular magnetic resonance. Circulation, 2003. 108(1): p. 54-9.

10 Schuster, E.H. and B.H. Bulkley, Ischemic cardiomyopathy: a clinicopathologic study of fourteen patients. Am Heart J, 1980. 100(4): p. 506-12.

11 Boucher, C.A., et al., Cardiomyopathic syndrome caused by coronary artery disease. III: Prospective clinicopathological study of its prevalence among patients with clinically unexplained chronic heart failure. Br Heart J, 1979. 41(5): p. 613-20.

12 Roberts, W.C., R.J. Siegel, and B.M.n. McManus, Idiopathic dilated cardiomyopathy: analysis of 152 necropsy patients. Am J Cardiol, 1987. 60(16): p. 1340-55.

13 Uretsky, B.F., et al., Acute coronary findings at autopsy in heart failure patients with sudden death: results from the assessment of treatment with lisinopril and survival (ATLAS) trial. Circulation, 2000. 102(6): p. 611-6.

14 Maron, B.J., Hypertrophic cardiomyopathy: a systematic review. JAMA, 2002. 287(10): p. 1308-20.

15 Choudhury, L., et al., Myocardial scarring in asymptomatic or mildly symptomatic patients with hypertrophic cardiomyopathy. J Am Coll Cardiol, 2002. 40(12): p. 2156-64.

16 Kim, R.J. and R.M. Judd, Gadolinium-enhanced magnetic resonance imaging in hypertrophic cardiomyopathy: in vivo imaging of the pathologic substrate for premature cardiac death? J Am Coll Cardiol, 2003. 41(9): p. 1568-72.

17 Moon, J.C., et al., The histologic basis of late gadolinium enhancement cardiovascular magnetic resonance in hypertrophic cardiomyopathy. J Am Coll Cardiol, 2004. 43(12): p. 2260-4.

18 Moon, J.C., et al., Toward clinical risk assessment in hypertrophic cardiomyopathy with gadolinium cardiovascular magnetic resonance. J Am Coll Cardiol, 2003. 41(9): p. 1561-7.

19 Mahrholdt, H., et al., Cardiovascular magnetic resonance assessment of human myocarditis: a comparison to histology and molecular pathology. Circulation, 2004. 109(10): p. 1250-8.

20 Shirani, J., L.J. Freant, and W.C.n. Roberts, Gross and semiquantitative histologic findings in mononuclear cell myocarditis causing sudden death, and implications for endomyocardial biopsy. Am J Cardiol, 1993. 72(12): p. 952-7.

21 Moon, J.C., et al., Gadolinium enhanced cardiovascular magnetic resonance in Anderson-Fabry disease. Evidence for a disease specific abnormality of the myocardial interstitium. Eur Heart J, 2003. 24(23): p. 2151-5.

22 Moon, J.C., et al., The histological basis of late gadolinium enhancement cardiovascular magnetic resonance in a patient with Anderson-Fabry disease. J Cardiovasc Magn Reson, 2006. 8(3): p. 479-82.

23 Beer, M., et al., Impact of enzyme replacement therapy on cardiac morphology and function and late enhancement in Fabry's cardiomyopathy. Am J Cardiol, 2006. 97(10): p. 1515-8.

24 Falk, R.H., R.L. Comenzo, and M. Skinner, The systemic amyloidoses. N Engl J Med, 1997. 337(13): p. 898-909.

25 Falk, R.H., Diagnosis and management of the cardiac amyloidoses. Circulation, 2005. 112(13): p. 2047-60.

26 Pellikka, P.A., et al., Endomyocardial biopsy in 30 patients with primary amyloidosis and suspected cardiac involvement. Arch Intern Med, 1988. 148(3): p. 662-6.

27 Maceira, A.M., et al., Cardiovascular magnetic resonance in cardiac amyloidosis. Circulation, 2005. 111(2): p. 186-93.

28 Sharma, O.P., A. Maheshwari, and K. Thaker, Myocardial sarcoidosis. Chest, 1993. 103(1): p. 253-8.

29 Smedema, J.P., et al., The additional value of gadolinium-enhanced MRI to standard assessment for cardiac involvement in patients with pulmonary sarcoidosis. Chest, 2005. 128(3): p. 1629-37.

30 Virmani, R., J.C. Bures, and W.C. Roberts, Cardiac sarcoidosis; a major cause of sudden death in young individuals. Chest, 1980. 77(3): p. 423-8.

31 Hurwitz, J.L. and M.E.n. Josephson, Sudden cardiac death in patients with chronic coronary heart disease. Circulation, 1992. 85(1 Suppl): p. I43-9.

32 Klem, I., et al., The utility of contrast enhanced MRI for screening patients at risk for malignant ventricular tachyarrhythmias. J Cardiovasc Magn Reson, 2004. 6(1): p. 84.

Mohamad G. Ghosn

Dipan J. Shah

Contact

Dipan J. Shah, M.D., FACC
Associate Professor
The Methodist Hospital Research Institute
Director, Cardiac Magnetic Resonance Imaging
Methodist DeBakey Heart and Vascular Center
The Methodist Hospital
6565 Fannin St
Houston, TX 77030, USA
Phone: +1 713-332-2539
DJShah@HoustonMethodist.org

MOLLI T1 Mapping Sequence: the Best Approach for Delayed Enhancement (DE) CMR?

Magalie Viallon[1]; Thomas Troalen[2]; Bruce Spottiswoode[3]; Pierre Croisille[1]

[1] CREATIS UMR CNRS 5220 INSERM U1040, University of Lyon, France
CHU de Saint Etienne, Université Jean Monnet, France
[2] Siemens Healthcare, Saint-Priest, France
[3] Siemens Healthcare, Chicago, IL, USA

In the field of cardiac magnetic resonance imaging (CMR), there is a growing interest in tissue characterization and quantification of lesion size, especially myocardial infarct (MI) size. Infarct size is a crucial determinant for patient prognosis and follow-up, and delayed enhancement (DE) gadolinium sequences are established techniques for detecting myocardial infarction and focal myocardial scarring of non-ischemic origin [1, 2].

Nevertheless, since DE-CMR is based on T1-weighted inversion recovery imaging, it intrinsically entails visual interpretation of relative signal intensities in relation to healthy myocardium, and relies on adequate prospective setting of inversion-time during the acquisition. This introduces a user-dependency on the final image quality and achieved contrast-to-noise ratio (CNR) between MI and healthy tissue in the DE-CMR images. This remains true whatever the kernel type used for the acquisition (TrueFISP, FLASH or signal polarity (PSIR, MAGIR)) [3]. PSIR techniques introduced by Kellman et al. [4] undoubtedly alleviate most ambiguities caused by magnitude reconstruction by always warranting a positive contrast of MI lesions related to normal myocardium, but do not ensure an optimized CNR between the two compartments. When relaxation times between lesions and surrounding tissues (blood and myocardium) are similar, lesion detection may remain ambiguous especially in the case of endocardial or papillary lesions.

Synthetic IR reconstructions can provide optimal contrast DE-CMR images

Since MOLLI has the ability to calculate T1 in each pixel of the image, synthetic MAGnitude Inversion-Recovery (MAGIR) or Phase Sensitive Inversion-Recovery (PSIR) images can retrospectively be calculated using the following simple equations:

$$SI(TI)_{PSIR} = 1 - 2x \exp(TI/T1) \quad \text{Eq. 1}$$

and

$$SI(TI)_{MagIR} = |SI(TI)_{PSIR}| \quad \text{Eq. 2}$$

Using a small increment in TI, e.g. 10 ms, allows physicians to systematically retrospectively screen a wide range of contrast, for instance between 200 ms and 500 ms, and hence to retrospectively choose the optimal contrast-of-interest between two tissue components best suited to his diagnosis without acquisition time loss, and without requiring additional acquisitions with different TI settings. This approach has first been proposed by Varga-Szemes and co-authors [5].

Figures 1 to 3 show an example acquired in a 65-year-old male patient with an inaugural ST elevation myocardial infarction with left anterior descending artery occlusion reperfused H+1h30. CMR was performed 4 days after reperfusion. Native synthetic MAGIR reconstructions (Fig. 1) showed increased signal related to edema in reperfused anteroseptal injured myocardium. Post-gadolinium injection synthetic MAGIR reconstructions performed 10 min after bolus injection (Fig. 2), showed in the same mid slice level the extent of acute anteroseptal necrosis.

Figures 4 to 6 show images acquired in a patient suspected of cardiac amyloidosis with a concentric hypertrophic cardiomyopathy (HCM). Both native and post-contrast injection MAGIR reconstructions allow for intra-myocardial focal lesions in the inferior wall to be identified with confidence, more clearly delineated after injection, with a subtle involvement of the anterior papillary muscle and anterolateral subendocardium.

Figure 7 shows a 67-year-old patient with a dilated cardiomyopathy (DCM) that clearly shows after gadolinium injection the extent of a post-ischemic subendocardial scar spread in the anterior wall and extended to anteroseptal and lateral walls, with a partial involvement of the anterior papillary muscle but with an islet of preserved muscle here clearly depicted. Note the existence of a mid-wall fibrosis in the inferoseptal segment raising discussion of the association with a non-ischemic mechanism. All these findings are strengthened by the visual analysis of the contrast

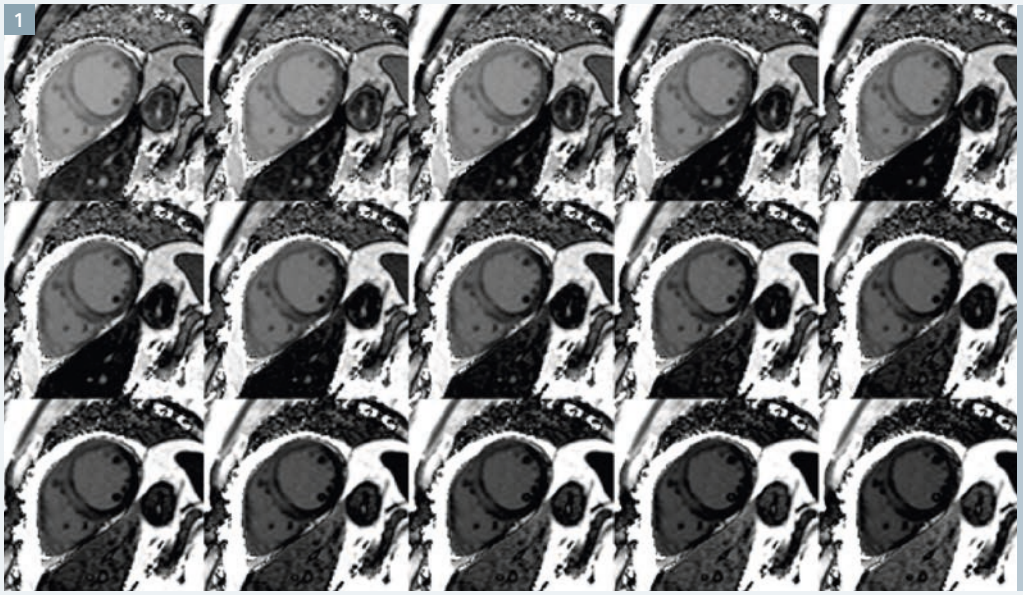

1 15 out of 40 synthetic native MAGIR images in an anterior acute myocardial infarction (AMI) patient. Reconstructed images are TI shifted every 10 ms in a 200 to 500 ms range (1.5T MAGNETOM Aera, *syngo* MR D13).

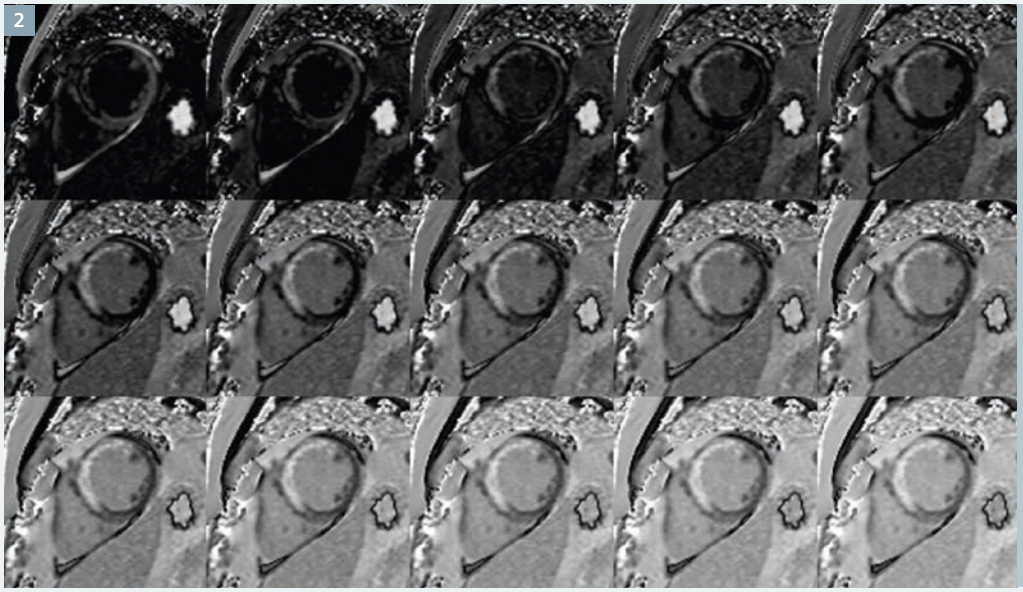

2 15 out of 40 synthetic post-gadolinium injection (0.02 mmol.kg^{-1}) MAGIR images in the same AMI patient. Reconstructed images are TI shifted every 10 ms in a 200 to 500 ms range.

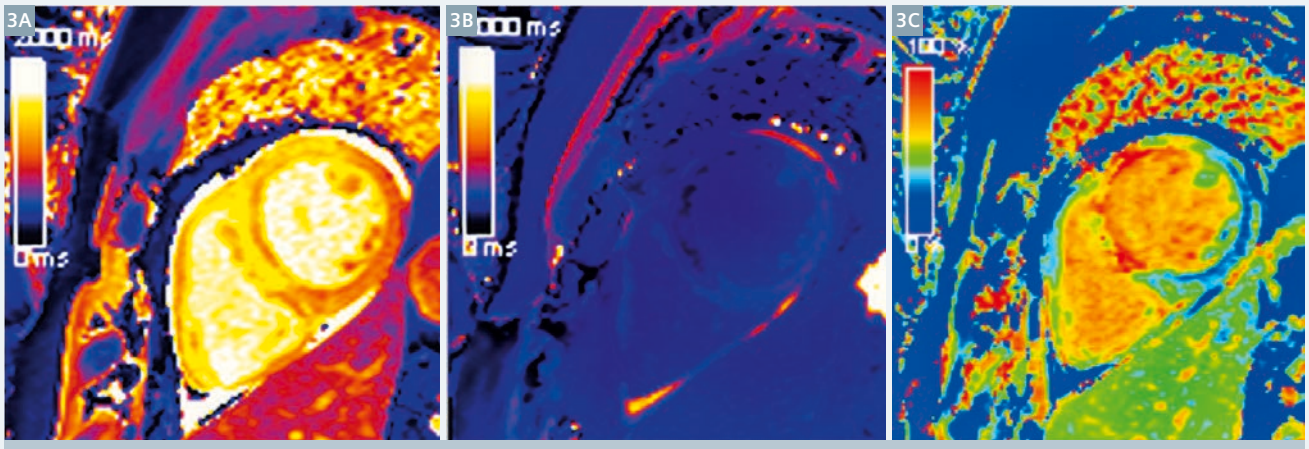

3 Corresponding: **(3A)** Pre-contrast (native) T1 map, **(3B)** post-contrast T1 map and **(3C)** ECV map in the same AMI patient.

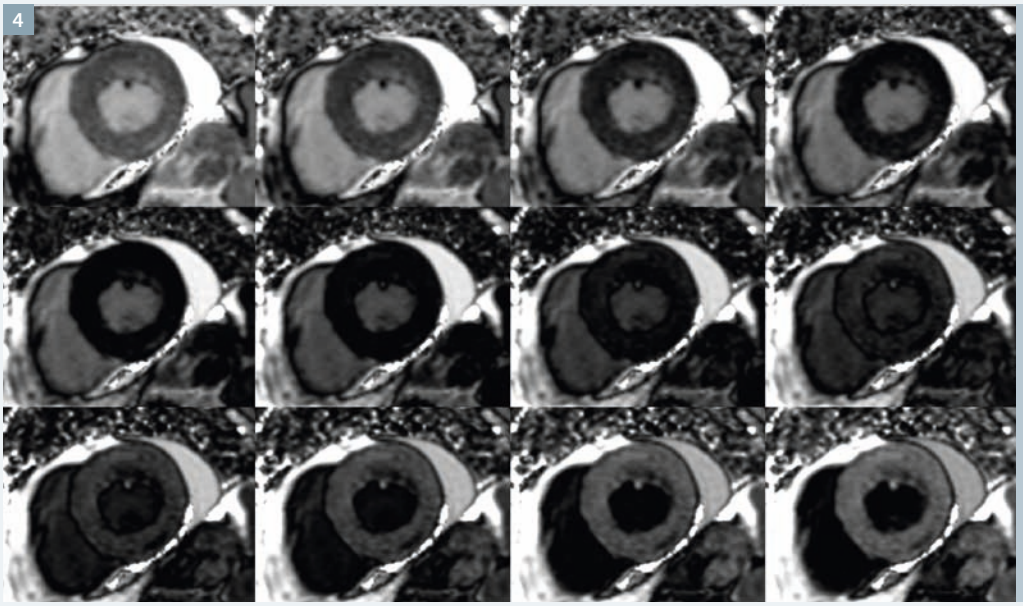

4 12 out of 40 synthetic native MAGIR images in an HCM patient. Reconstructed images are TI shifted every 10 ms in a 200 to 500 ms range (1.5T MAGNETOM Aera, *syngo* MR D13).

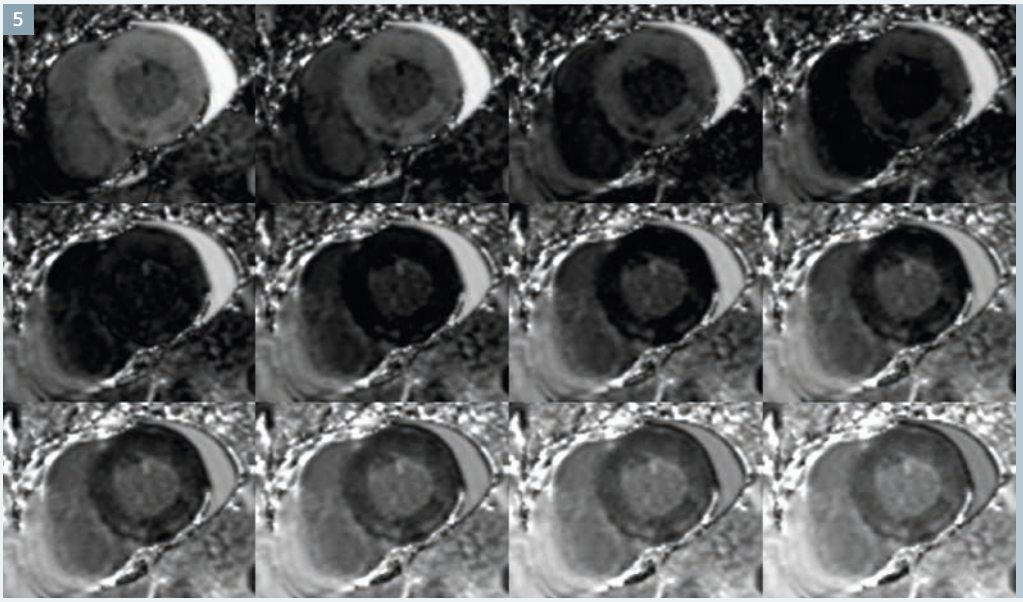

5 12 out of 40 synthetic post-gadolinium injection (0.02 $mmol.kg^{-1}$) MAGIR images in the same HCM patient. Reconstructed images are TI shifted every 10 ms in a 200 to 500 ms range.

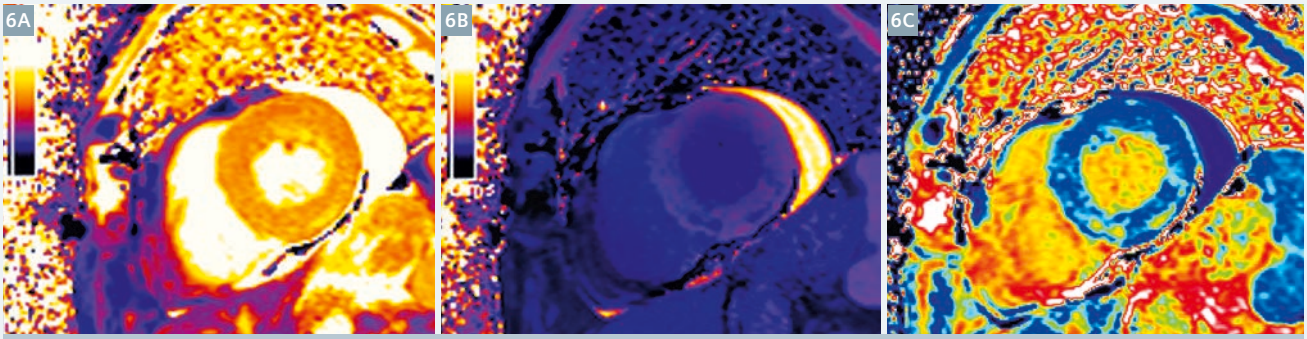

6 Corresponding: **(6A)** Native T1 map, **(6B)** post-contrast T1 map and **(6C)** ECV map in the same patient.

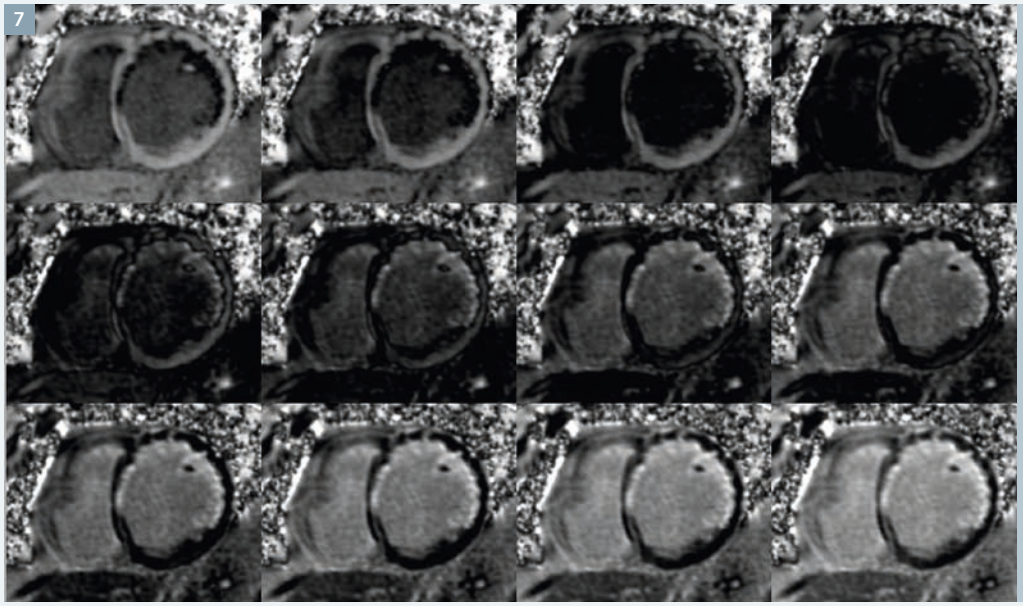

7 12 out of 40 synthetic post-gadolinium injection (0.02 mmol.kg^{-1}) MAGIR images in the same post-ischemic DCM patient. Reconstructed images are TI shifted every 10 ms in a 200 to 500 ms range (3T MAGNETOM Prisma, *syngo* MR E11).

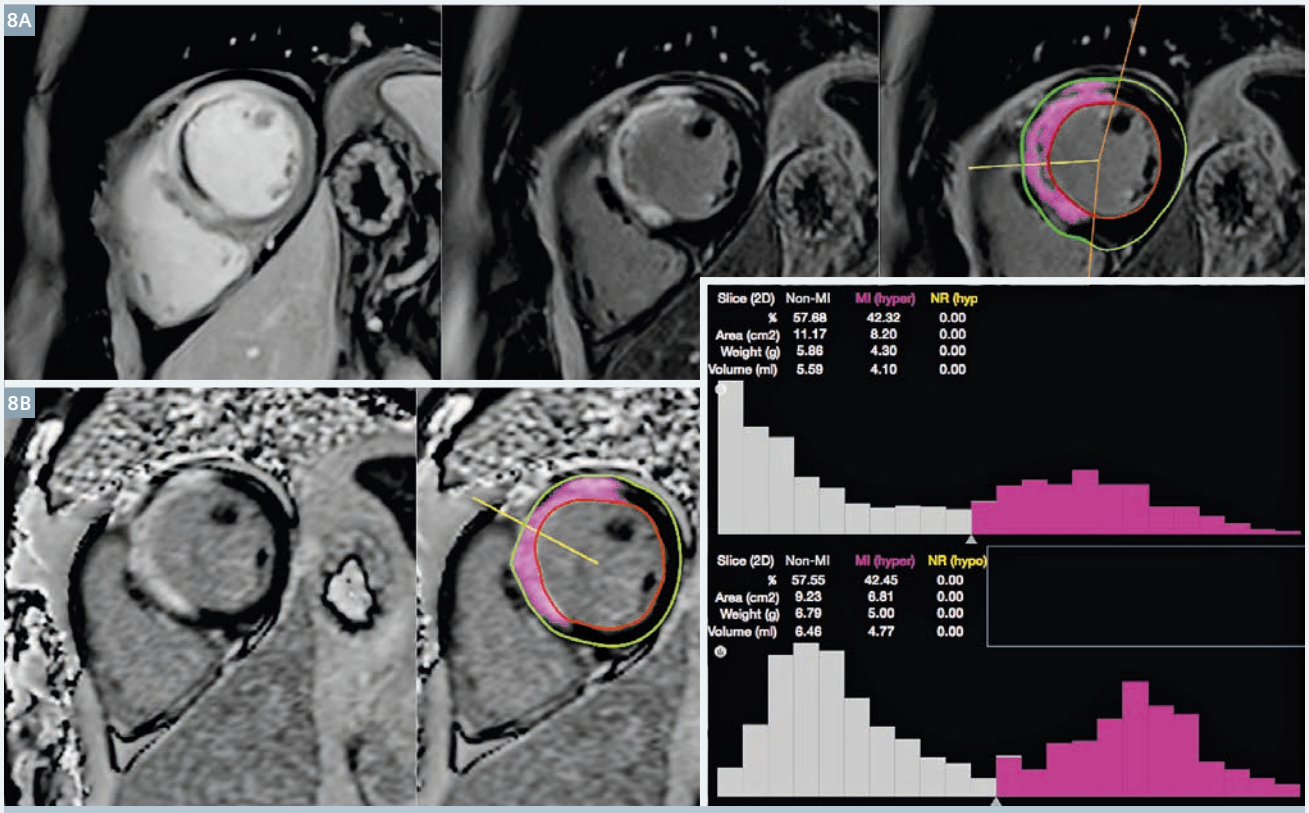

8 Short axis images obtained using 3D IR-GRE: **(8A)** Early gadolinium enhancement and **(8B)** late gadolinium enhancement and corresponding LGE MAGIR and PSIR synthetic images. Calculated histogram of pixel intensity in the myocardium, in the MAGIR optimal contrast as compared to original LGE images. Pink overlay corresponds to the area of delayed enhancement after 10 min post-injection using a Full Width at Half Maximum (FWHM) algorithm (CMRSegTools plugin (CREATIS) with OsiriX, Pixmeo, Geneva).

dynamics across the entire series of TI values that may be determinant in sub-endocardial regions, more difficult to differentiate from the enhanced cavity, especially at 3T, with again an additional information at no additional acquisition time cost.

Taken together, the capability to generate synthetic images and existing T1-mapping and ECV-mapping possibility, the MOLLI acquisitions represent a powerful diagnostic tool in CMR offering a three-in-one advanced tissue characterization technique: Highest capacity to highlight and detect abnormalities while offering quantitative measures of T1 and ECV in absolute units. T1 mapping together with optional synthetic reconstructions therefore provides a unique capacity for objective determination of the severity of disease with integration into clinical routine without extra-acquisition time. It also reinforces robustness of CMR.

Synthetic reconstruction for improved automatic segmentation of MI size

Several histogram-based methods have been proposed for the measurement of DE-CMR infarct size from the simple (manual or semi-automatic thresholding) to the more advanced, including the finite Gaussian mixture (FGM) model where Gaussian likelihood distribution is assumed [6].

These are widely used models in segmentation because they are mathematically simple. Unfortunately, variable CNR, and artifacts limit the performance of histogram-based algorithms that in turn present pitfalls which, under clinical conditions, lead to unreliable results. By eliminating the need for patient-based prospective TI adjustments, synthetic IR images based on T1 mapping offer a satisfactory answer to one of the most significant downsides of conventional DE-CMR acquisition. This technique could potentially offer a unique way to standardize lesion size measurements for multicenter clinical trials.

Of course, other downsides to the automatic segmentation of MI infarct, such as partial volume effects, motivates for high resolution images and thinner slice thickness offered with well optimized 3D IR-GRE sequences, although these come at the cost of the longer acquisition times that most patients are unable to tolerate.

In conclusion, the all-in-one MOLLI including optional synthetic reconstructions reinforces the unique capability of CMR to provide additional information. This in turn may lead to improved diagnostic confidence, increased diagnostic accuracy and improved robustness, alleviating user-dependent adjustments during acquisition, and resulting in the most advanced, and shortest post-gadolinium tissue characterization MR protocol.

References

1 Simonetti OP, Kim RJ, Fieno DS, Hillenbrand HB, Wu E, Bundy JM, Finn JP, Judd RM. An improved MR imaging technique for the visualization of myocardial infarction. Radiology 2001;218:215–223. doi: 10.1148/radiology.218.1.r01ja50215.

2 Kim RJ, Fieno DS, Parrish TB, Harris K, Chen E-L, Simonetti O, Bundy J, Finn JP, Klocke FJ, Judd RM. Relationship of MRI Delayed Contrast Enhancement to Irreversible Injury, Infarct Age, and Contractile Function. Circulation 1999;100:1992–2002. doi: 10.1161/01.CIR.100.19.1992.

3 Viallon M, Jacquier A, Rotaru C, Delattre BMA, Mewton N, Vincent F, Croisille P. Head-to-head comparison of eight late gadolinium-enhanced cardiac MR (LGE CMR) sequences at 1.5 tesla: from bench to bedside. J Magn Reson Imaging 2011;34:1374–1387. doi: 10.1002/jmri.22783.

4 Kellman P, Arai AE, McVeigh ER, Aletras AH. Phase-sensitive inversion recovery for detecting myocardial infarction using gadolinium-delayed hyperenhancement. Magn Reson Med 2002;47:372–383. doi: 10.1002/mrm.10051.

5 Varga-Szemes A, van der Geest RJ, Spottiswoode BS, Muscogiuri G, De Cecco CN, Suranyi P, Rehwald WG, Schoepf JU. Quantification of myocardial late gadolinium enhancement using synthetic inversion recovery imaging. Journal of Cardiovascular Magnetic Resonance 2015;17(Suppl 1):O8.

6 Kim HW, Farzaneh-Far A, Kim RJ. Cardiovascular Magnetic Resonance in Patients with Myocardial Infarction. Journal of the American College of Cardiology 2010;55. doi:10.1016/j.jacc.2009.06.059.

Pierre Croisille

Magalie Viallon

Contact

Magalie Viallon, Ph.D.
CREATIS, UMR CNRS 5220 – INSERM U1044
Service de Radiologie Hôpital Nord
Université J.Monnet Saint-Etienne
Pôle de Recherche et d'Enseignement Supérieur (PRES)
Université de Lyon, France
Phone:+33 4 77 82 84 36
magalie.viallon@creatis.insa-lyon.fr
http://www.creatis.insa-lyon.fr

syngo.MR Cardiac 4D Ventricular Function

Bernd J. Wintersperger, M.D. EBCR FAHA[1]; Arne Littmann, Ph.D.[2]

[1] Department of Medical Imaging, University Health Network, University of Toronto, Canada
[2] Siemens Healthcare, Erlangen, Germany

Objectives and definitions

Cardiac MRI background

In developed countries, approximately 2% of adults present with heart failure and in the elderly population (>65), this increases to 6–10%. [1, 2]

Cardiac MRI is considered as the gold standard with respect to accuracy and reproducibility of volumes, mass, and wall motion. [3]

Cardiac MRI primarily aims to assess cardiac morphology and functional parameters such as ventricular volumes, ejection fraction, mass and regional wall motion. Furthermore, cardiac MRI provides an even more detailed evaluation of the myocardial tissue including the evaluation of ischemia, myocardial viability and scar, as well as potential edematous changes which may be important aspects towards therapy guidance. In a large variety of cardiac diseases, patient prognosis is closely related to the left ventricular ejection fraction (LVEF), with a low ejection fraction being related to higher morbidity and mortality.

By definition, the ventricular ejection fraction (EF) is the percentage of blood that is being 'ejected' from the maximally filled ventricle during systole of each heartbeat (Fig. 1). Mathematically, cardiac volumes and ejection fraction are related by the following equation:

$$EF = \frac{EDV - ESV}{EDV} \times 100$$

Where:

- EDV (End-diastolic volume) relates to the maximum volume of the ventricle at the end of the filling phase of the cardiac cycle (diastole) with all valves closed just prior to the ventricular ejection.
- ESV (End-systolic volume) relates to the minimum volume of the ventricle at the end of the ejection period (systole) with all valves closed just before ventricular filling.

Measuring volumes

To calculate LVEF, the volume of the ventricular cavity needs to be assessed at two different specific time points within the cardiac cycle, at end-diastole and at end-systole.

In order to do so, imaging data is acquired using cine techniques (typically SSFP techniques) in a series of multiple parallel short axis slices with additional long axis orientations, sampling the entire left ventricle as illustrated in Figure 2.

On a broad outline, during post-processing, contouring of the endocardial border on every single short axis slice allows computing the slice area contained within the endocardial contours. By incorporating the knowledge about the slice extension along the ventricular long axis, the volume represented by this contour at a specific phase can be calculated. The sum of all volumes/slices at end diastole and end systole then results in EDV and ESV, respectively.

Besides these basic operations an important additional aspect needs to be considered: the physiologic shortening and elongation of the ventricle along its long axis over the cardiac cycle.

1

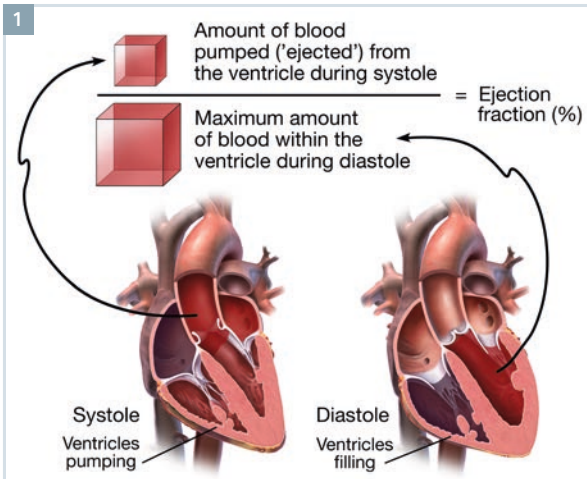

1 Schematic explanation of left ventricular (LV) ejection fraction (EF). *Reprodcued with permission from medmovie.com.*

2

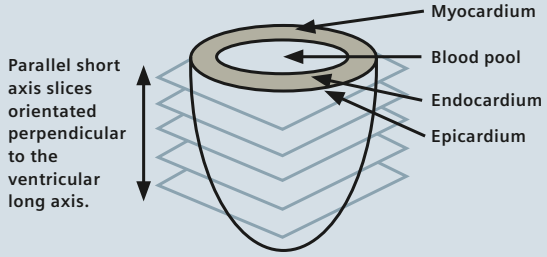

2 Stack of short axis slices sampling the left ventricle.

Through plane motion and base representation

General illustration

During myocardial contraction and relaxation throughout the cardiac cycle, the entire heart demonstrates significant deformation and motion, including translation, rigid body rotation, regional twist, and most importantly a change in long axis dimension.

This change in the long axis dimension is characterized by a ventricular shortening with a physiologic excursion of the basal plane towards the apex during systole (basal descent) while the apex remains relatively stationary (Fig. 3). This through plane motion has been well documented and averages to a max. systolic excursion of ~13 mm in healthy subjects while it is known to generally be reduced in disease [4].

Related to the fact that the LV cross sectional area is at its largest at the base of the heart, the potential error related to through plane motion is generally significant. This may lead to possible inclusion of atrial volume into the LV volume calculation and thus potentially resulting in an overestimation of the LV volume in systole (ESV) with subsequent underestimation of EF [5].

Spatial orientation and position of base plane

The accuracy of the estimated volume of an object is substantially dependent on the way this specific object is spatially sampled by the input images.

In cardiac MRI, the ventricles are typically sampled by a set of parallel short axis 2D slices, where the slice distance and the slice thickness are relatively large in comparison to the in-plane resolution. If all slices are acquired parallel to each other, it is difficult to accurately capture through plane motion with such a sampling pattern. This is especially true if the upper and/or lower boundary of the object of interest may not be entirely parallel to the slice orientation.

3

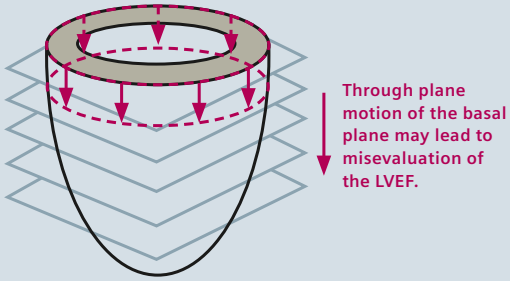

3 Simple illustration of the through plane motion based on a stack of short axis slices.

4

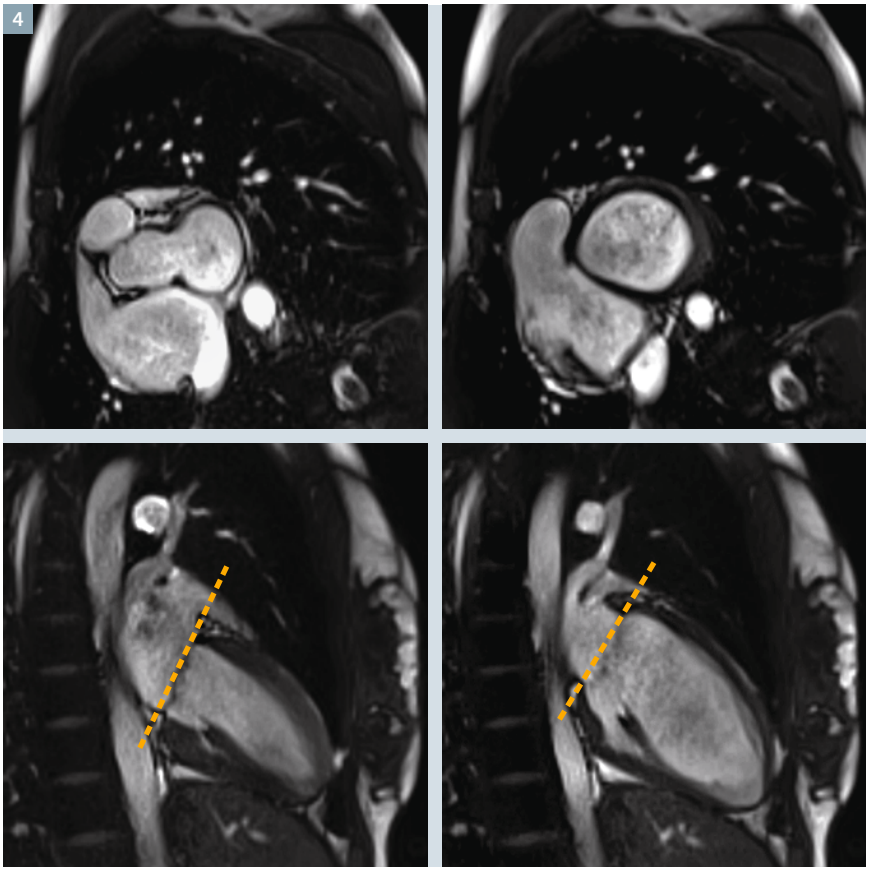

Taking a closer look at Figure 4, it becomes obvious that both these conditions are often true for the delineation of the atrio-ventricular (AV) valve (mitral valve in case of the left ventricle) plane: Neither remains it parallel to the short axis over the entire cardiac cycle, nor is the complex through plane motion entirely parallel to the short axis slice orientation (which is represented by the dashed yellow line in the two chamber view).

As illustrated in Figure 4, the exact position of the mitral valve plane and its change over the cardiac cycle are best captured on long axis slices such as the two-chamber view.

Traditional approach to determine LV volume in cardiac MRI

Traditionally, LV volumes in cardiac MRI were determined solely based on a stack of short axis slices. As illustrated in the previous paragraph, the mitral valve and its motion

5

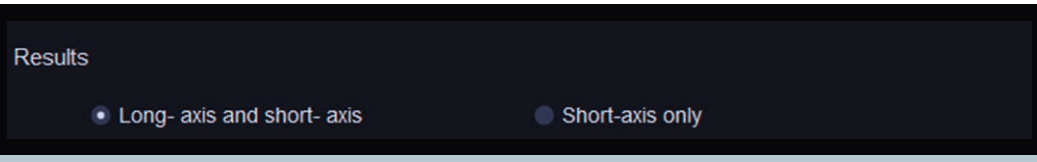

5 Finding Details Dialog in *syngo*.via allows to choose the requested method

6A

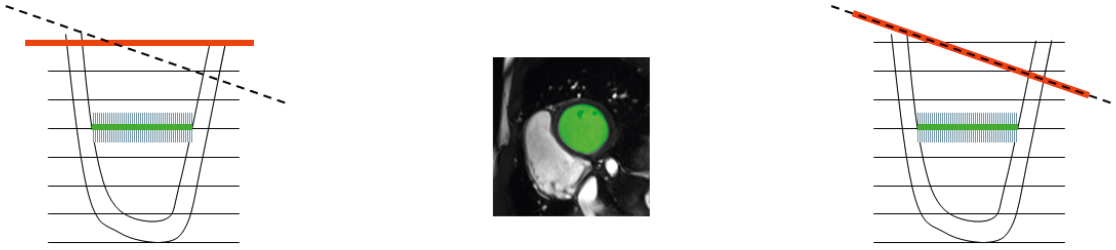

6B

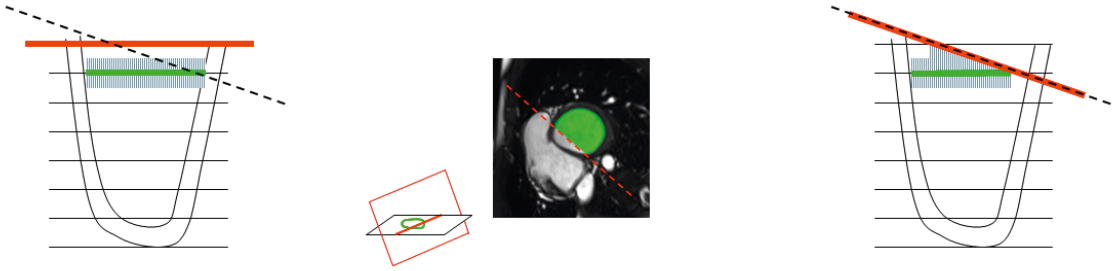

6C

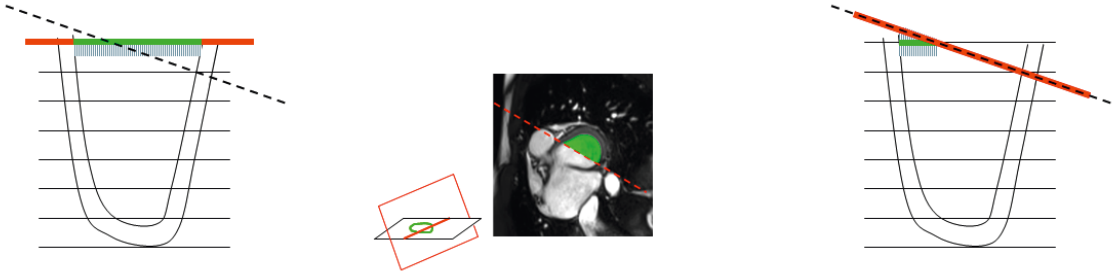

6D

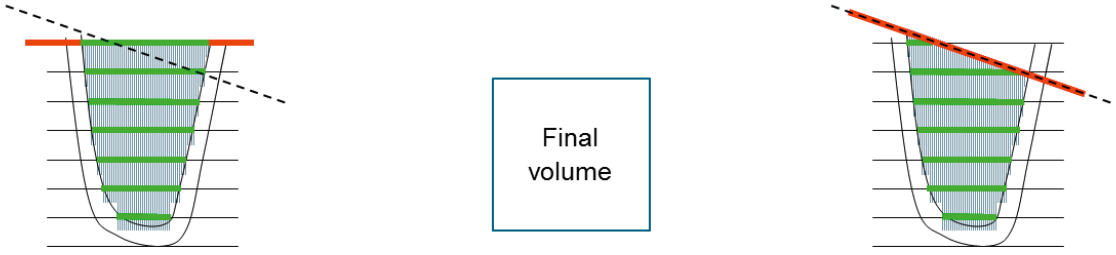

— Model of the mitral valve plane
--- Anatomical position of the mitral valve plane

6 Comparison of two possible approaches and the corresponding final volumes (left: short axis only, right: long axis and short axis). The principle is described on a mid-ventricular slice **(6A)**, a basal slice intersecting with the mitral valve plane **(6B)** and the most basal slice **(6C)**. The representation of the final volume is shown in **(6D)**. When the mitral valve plane intersects the contours, only the portion on the ventricular side of the valvular plane is considered for volumetric calculations until the contours fully reach the mitral valve plane.

towards the ventricular apex from ED to ES is not adequately visualized in the short axis slices. Consequently, this approach requires special care with regard to inclusion of basal slices in order not to include atrial volume in the LV volumetric evaluation.

In an attempt to at least consistently overcome the short-coming of this "short axis only approach", it is a generally accepted convention to only include basal slices into the LV volumetric evaluation if at least 50% (180 degree) of the LV blood volume is surrounded by ventricular myocardium.

Argus VF Analysis represents an approach for this traditional way to determine ventricular volume which has been in use for decades.

syngo.MR Cardiac 4D Ventricular Function

syngo.MR Cardiac 4D Ventricular Function provides two approaches to compute LV volumes and LV function:

1. "Short axis only" approach: Only short axis slices are used (Argus-like)

- The position of the mitral valve plane in ED and ES is defined by the position of the blood pool point in ED and ES.
- The orientation of the mitral valve plane is by definition parallel to the short axis slices.

2. "Long axis and short axis" approach: Both short axis and long axis are taken into consideration

- The position of the mitral valve plane in ED and ES is defined on the long axis slice(s) by setting "valve points" in ED and ES.
- The orientation of the mitral valve plane is matching the anatomical orientation (which may be not parallel to the short axis slice orientation).

The user can switch between both variants by selecting the desired option in the Finding Details Dialog (Fig. 5).

Both approaches are schematically illustrated in Figure 6.

Conclusion

The described differences in the methodical approach clearly result in variations of quantitative results. Affection of both phases, EDV and ESV, may not necessarily result in a relevant difference in LVEF when compared to the "short axis only" approach. As the orientation of the mitral valve plane and its change over the cardiac cycle is patient specific, there is no simple relationship of both approaches to each other and therefore it is not possible to mathematically convert the volumes computed with the two described approaches.

As illustrated, the "Long-axis and short-axis" approach allows to accurately model any orientation of the mitral valve plane seen on the acquired long axis slices. Since it also allows defining the mitral valve plane independently in ED and in ES, this approach enables the user to also accurately model the apically directed motion of the mitral valve plane from ED to ES. Due to this advantage over the traditional "Short-axis only" approach, the "Long-axis and short-axis" approach is selected as default in *syngo*.MR Cardiac 4D Ventricular Function. It has however to be kept in mind that such an approach requires an adequate cross-reference of short axis and long axis slices in a patients data set and as such consistent breath-holding levels.

References

1 McMurray JJ, Pfeffer MA (2005). "Heart failure". Lancet 365 (9474): 1877–89.
2 Dickstein K;Eur. Heart J. 29 (19): 2388–442.
3 McMurray-EurJHeartFail-14-803.
4 Walter et al; Circulation 1991; 84:721-731.
5 Berkovic et al.; European Journal of Radiology 73 (2010) 260–265.

Further Reading

- Hammon M. et al.; Pediatric Radiology, Volume 45, Issue 5, pp 651-657.
- Hammon M. et al.; Poster ECR: Cardiac MRI in pediatric patients with surgically treated right-sided congenital heart disease: Automated left ventricular volumes and function analysis and effects of different manual adjustments.

Contact

Bernd J. Wintersperger, M.D. EBCR FAHA
Professor of Radiology
University of Toronto
Department of Medical Imaging
Director of Cardiac Imaging Operations
University Health Network
Mount Sinai Hospital and Women's College Hospital
585 University Avenue
Toronto, Ontario, M5G 2N2
Canada
Bernd.Wintersperger@uhn.ca

The entire editorial staff at DZHK Centre for Cardiovascular Imaging and at Siemens Healthcare extends their appreciation to all the radiologists, technologists, physicists, experts and scholars who donate their time and energy – without payment – in order to share their expertise with the readers of MAGNETOM Flash.

MAGNETOM Flash – Imprint

Publisher:
Siemens Healthcare GmbH
Magnetic Resonance,
Karl-Schall-Straße 6, D-91052 Erlangen, Germany

Guest Editor:
Prof. Eike Nagel, MD, PhD, FESC, FACC, FRCR, Director of the Institute for Experimental and Translational Cardiovascular Imaging, DZHK Centre for Cardiovascular Imaging, Head of Interdisciplinary Cardiovascular Imaging, University Hospital Frankfurt/Main, Germany

Editor-in-chief:
Antje Hellwich
(antje.hellwich@siemens.com)

Editorial Board:
Reto Merges; Wellesley Were;
Sunil Kumar S.L., Ph.D.;
Gary R. McNeal, MS (BME);
Peter Kreisler, Ph.D.

Review Board:
Lars Drüppel, Ph.D.; Shivraman Giri, Ph.D.; Matthias Lichy, M.D., M.Sc.; Edgar Müller; Christian Schuster, Ph.D.; Bruce Spottiswoode, Ph.D.; Susanne von Vietinghoff; Heike Weh

Production:
Norbert Moser,
Siemens Healthcare GmbH

Layout:
Agentur Baumgärtner,
Friedrichstraße 4, D-90762 Fürth, Germany

Printer:
Rotaplan Offset Kammann Druck GmbH,
Hofer Straße 1, D-93057 Regensburg, Germany

We welcome your questions and comments about the editorial content of MAGNETOM Flash. Please contact us at magnetomworld.med@siemens.com.

Manuscripts as well as suggestions, proposals and information are always welcome; they are carefully examined and submitted to the editorial board for attention. MAGNETOM Flash is not responsible for loss, damage, or any other injury to unsolicited manuscripts or other materials. We reserve the right to edit for clarity, accuracy, and space. Include your name, address, and phone number and send to the editors, address above.

MAGNETOM Flash is also available online:

www.siemens.com/magnetom-world

Please enter your business address

Institution

Department

Function

Title

Name

Street

Postal Code

City

State

Country

MR system used

Please include me in your mailing list for the following Siemens Healthcare customer magazine(s):

☐ Medical Solutions

☐ MAGNETOM Flash

☐ SOMATOM Sessions

☐ AXIOM Innovations

Stay up to date with the latest information

Register for:

E-mail

☐ Yes, I consent to the above information being used for future contact regarding product updates and other important news from Siemens.

☐ unsubscribe from info service

Please print clearly!

→Visit www.siemens.com/magnetom-world for case reports, clinical methods, application tips, talks and much more clinical information.

SUBSCRIBE NOW!

– and get your free copy of future MAGNETOM Flash! Interesting information from the world of magnetic resonance – gratis to your desk. Send us this postcard, or subscribe online at www.siemens.com/MAGNETOM-World

Siemens Healthcare GmbH
Antje Hellwich
HC DI MR CRM SCI
Karl-Schall-Straße 6
91052 Erlangen
Germany

MAGNETOM Flash

On account of certain regional limitations of sales rights and service availability, we cannot guarantee that all products included in this brochure are available through the Siemens sales organization worldwide. Availability and packaging may vary by country and is subject to change without prior notice. Some/All of the features and products described herein may not be available in the United States.

The information in this document contains general technical descriptions of specifications and options as well as standard and optional features which do not always have to be present in individual cases, and which may not be commercially available in all countries. Due to regulatory reasons their future availability cannot be guaranteed. Please contact your local Siemens organization for further details.

Siemens reserves the right to modify the design, packaging, specifications, and options described herein without prior notice. Please contact your local Siemens sales representative for the most current information.

Note: Any technical data contained in this document may vary within defined tolerances. Original images always lose a certain amount of detail when reproduced.

Not for distribution in the US

Siemens Healthcare Headquarters
Siemens Healthcare GmbH
Henkestraße 127
91052 Erlangen
Germany
Phone: +49 9131 84-0
siemens.com/healthcare

Order No. A91MR-1000-118M-7600 | Printed in Germany | CC MR 3534 12151.5 | © Siemens Healthcare GmbH, 2015

siemens.com/magnetom-world